ISSN 0038-531X

Russian Original Vol. 55, No. 6, December, 1983

June, 1984

SATEAZ 55(6) 797-904 (1983)

SOVIET ATOMIC ENERGY

АТОМНАЯ ЭНЕРГИЯ
(ATOMNAYA ÉNERGIYA)

TRANSLATED FROM RUSSIAN

c/b CONSULTANTS BUREAU, NEW YORK

SOVIET ATOMIC ENERGY

Soviet Atomic Energy is abstracted or indexed in *Chemical Abstracts, Chemical Titles, Pollution Abstracts, Science Research Abstracts, Parts A and B, Safety Science Abstracts Journal, Current Contents, Energy Research Abstracts,* and *Engineering Index.*

Soviet Atomic Energy is a translation of *Atomnaya Énergiya,* a publication of the Academy of Sciences of the USSR.

An agreement with the Copyright Agency of the USSR (VAAP) makes available both advance copies of the Russian journal and original glossy photographs and artwork. This serves to decrease the necessary time lag between publication of the original and publication of the translation and helps to improve the quality of the latter. The translation began with the first issue of the Russian journal.

Consultants Bureau journals appear about six months after the publication of the original Russian issue. For bibliographic accuracy, the English issue published by Consultants Bureau carries the same number and date as the original Russian from which it was translated. For example, a Russian issue published in December will appear in a Consultants Bureau English translation about the following June, but the translation issue will carry the December date. When ordering any volume or particular issue of a Consultants Bureau journal, please specify the date and, where applicable, the volume and issue numbers of the original Russian. The material you will receive will be a translation of that Russian volume or issue.

Subscription (2 volumes per year)
Vols. 54 & 55: $500 (domestic); $555 (foreign)
Vols. 56 & 57: $560 (domestic); $621 (foreign)

Single Issue: $100
Single Article: $7.50

CONSULTANTS BUREAU, NEW YORK AND LONDON

c/b
233 Spring Street
New York, New York 10013

Published monthly. Second-class postage paid at Jamaica, New York 11431.

Mailed in the USA by Publications Expediting, Inc., 200 Meacham Avenue, Elmont, NY 11003.

POSTMASTER: Send address changes to *Soviet Atomic Energy,* Plenum Publishing Corporation, 233 Spring Street, New York, NY 10013.

SOVIET ATOMIC ENERGY

A translation of *Atomnaya Énergiya*

June, 1984

Volume 55, Number 6 December, 1983

CONTENTS

CONTENTS

(continued)

The Russian press date (podpisano k pechati) of this issue was 11/25/1983. Publication therefore did not occur prior to this date, but must be assumed to have taken place reasonably soon thereafter.

ESCAPE OF RADIOACTIVE FISSION PRODUCTS FROM LEAKING FUEL ELEMENTS INTO AN ORGANIC COOLANT

E. I. Shkokov, V. V. Konyashov, Yu. G. Simonov, Yu. V. Chechetkin, A. D. Yurchenko, and E. K. Yakshin

UDC 621.039.548

Investigations and experience in the operation of reactors show that the physicochemical properties of the coolants used (water, boiling water, sodium) considerably affect the escape of radioactive fission products from leaking fuel elements. This applies also to an organic coolant, the radiation-thermal decomposition of which with the formation of deposits on the cladding and under the cladding of leaking fuel elements, suppresses the escape of fission products. At the same time, data about the escape of fission products are particularly important for reactors with organic coolants, as the inherent activity of an organic coolant is very low (lower by 3-4 orders than the activity, for example, of the water of water-cooled/water-moderated reactors (VVÉR) [1]). Therefore, for a correct calculation of the biological shielding of the pipelines and plant of the primary circuit, it is necessary to take account of the contribution of fission products to the coolant activity.

The coolant is ditolylmethane (DTM); its temperature is 410-450°K and its pressure is 0.5-0.8 MPa. Fuel elements with a length of 1100 mm and with an outside diameter of 9.8 mm were tested. The fuel pellets, of sintered UO_2 with a density of 10.2 g/cm^3 and with a ^{235}U enrichment of 3%, had an outside diameter of 7.6 mm and an axial opening with a diameter of 1.4 mm.

The escape of fission products from fuel elements with damaged cans was studied for a fuel burnup of 10^{17}-$1.7\cdot10^{20}$ fissions/cm (4-7000 MW·days/ton U), a fission intensity of $6\cdot10^{9}$-$9\cdot10^{18}$ fissions/cm^3·sec (specific power 0.18-28 W/g) and a maximum fuel temperature of 450-1300°K.

The escape of fission products was monitored by the activity of the radionuclides in the coolant. The value of the escape of the i-th radionuclide from the leaking fuel elements (K_i), equal to the ratio of the number of atoms formed in the fuel element (R_i), was determined by the total activity of the radionuclide in the loop circuit (B_i). Samples of the coolant and gas from the volume compensator were taken periodically, and samples of the deposits from the inner surfaces of the plant and loop were taken at the end of each experiment. The activity of the radionuclides in the samples was measured on a γ-spectrometer with a Ge(Li)-detector; the relative statistical error of the measurements was up to 10%, and the total error of the determination of the escape was about 30%.

In all the experiments, in the initial period of irradiation of the fuel elements, a reduction of the escape of fission products with increase of the fuel burnup occurred (Fig. 1), well known from experiments with oxide fuel [2-5] at a temperature below 1300°K. The escape of gaseous fission products (GFP) depended on the intensity of the fissions in the fuel (Fig. 2).

The dependence of the escape of GFP from fuel or leaking fuel elements on the radioactive decay λ_i is assumed to be characterized by the power index n in the relation $K_i \sim \lambda_i^{-n}$. In the range of fission intensities from $6\cdot10^{10}$ to $9\cdot10^{12}$ fissions/cm^3·sec, the value of n in the investigations carried out varied from 0 to 0.3. With a fission intensity in the fuel of $6\cdot10^{10}$ fissions/cm^3·sec, the yield of GFP from the leaking elements was almost independent of λ_i. Consequently, the migration time of the GFP beneath the cladding of the fuel elements investigated was significantly less than the half-life of the short-lived radio-

Translated from Atomnaya Énergiya, Vol. 55, No. 6, pp. 359-362, December, 1983. Original article submitted February 7, 1983.

0038-531X/83/5506-0797$07.50

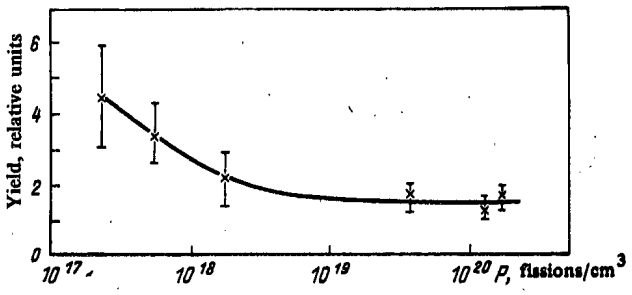

Fig. 1. Dependence of the escape of ^{133}Xe from leaking fuel elements on the fuel burn-up (fission intensity $9 \cdot 10^{12}$ fissions/cm^3·sec).

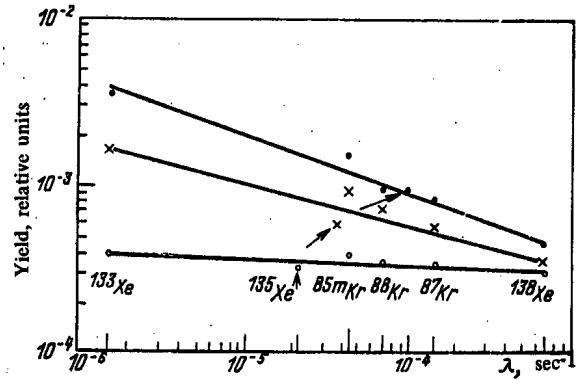

Fig. 2. Escape of gaseous fission products from leaking fuel elements versus the decay constant (burnup $5 \cdot 10^{17}$ fissions/cm^3, fission intensity, fissions/cm^3·sec: ○) $6 \cdot 10^{10}$; ×) $1 \cdot 10^{12}$, ●) $9 \cdot 10^{12}$; for ^{135}Xe, the burnup in the neutron flux is taken into account).

nuclide ^{138}Xe (17 min). The escape of GFP also did not vary with increase of the opening in the fuel element cladding from 0.01 to 1.2 mm^2.

Before the coolant flows in beneath the cladding, the change of the GFP escape within the measurement limits studied of the fission intensity, was due mainly to the nature and parameters of the processes taking place in the oxide fuel. The escape of GFP, defined by the value of n = 0 and obtained at a low fission intensity in the fuel ($6 \cdot 10^{10}$ fissions/cm^3·sec), corresponds either to a recoil mechanism of the fission products from the fuel or to a "self-expulsion" mechanism [6]. An estimate showed that satisfactory coincidence with experiments is given by a calculation based on the recoil mechanism, in which it was assumed that those fission fragments escape from the fuel which had completely lost their energy in the gas void between the fuel and the cladding, and also in the gas space of open pores. The calculated value of the GFP escape from the fuel, found by the self-expulsion mechanism, is a factor of 5 lower than the measured value.

With increase of the fission intensity in the fuel from $6 \cdot 10^{10}$ to $(1\text{-}9) \cdot 10^{12}$ fissions/cm^3·sec, the value of n was increased up to 0.2-0.3. The GFP escape, characterizing n = 0.2-0.3, is typical for uranium dioxide at a low temperature [2, 3, 5-7] and confirms the significant contribution to the total escape of the GFP from the fuel at least of one further mechanism of release, besides the recoil mechanism. Subtracting from the yields measured for a fission intensity of $(1\text{-}9) \cdot 10^{12}$ fissions/cm^3·sec the yields measured for $6 \cdot 10^{10}$ fissions/cm^3·sec (contribution of the recoil mechanism), the following dependence of the escape of GFP on the radioactive decay and fission intensity f is obtained:

$$K_i \sim \lambda_i^{-0.5} f^{0.5}.$$

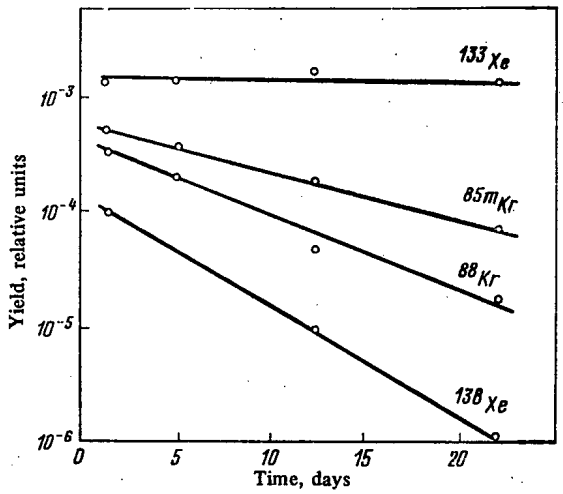

Fig. 3. Variation of the escape from a leaking fuel element versus time, in the case of the formation of deposits on its cladding.

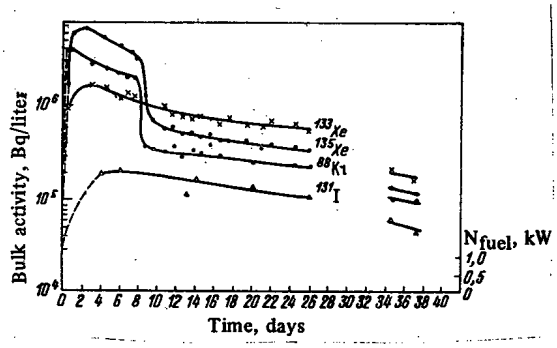

Fig. 4. Change of bulk activity of the fission products in the coolant during irradiation of a leaking fuel element (N_{fuel} is the power of the fuel element during irradiation).

It is characteristic for the mechanism of radiation-stimulated diffusion, well known from [8-10]. The results of the calculation of the GFP escape from the fuel according to this mechanism, coincide with the experimental data obtained with an error of $\pm$30%. The radiation-stimulated diffusion coefficient is taken from [10].

We note that the calculation by the thermal diffusion mechanism gives underestimated values by comparison with experiment. According to the data of [8, 11], at a temperature of the oxide fuel below 1300°K, radiation-stimulated diffusion predominates over thermal diffusion.

The escape of iodine radioisotopes from the fuel elements investigated into the organic coolant was a factor of 5 less than the escape of GFP at the start of irradiation, and a factor of 300 less than for a fuel burnup of $(0.5\text{-}1.7)\cdot10^{20}$ fissions/cm^3·sec. The escape of iodine radioisotopes, less by a factor of 10 by comparison with the escape of GFP, is obtained also in boiling water reactors; in this case, the marked difference is explained by the sorption of iodine on the inside surface of the fuel-element claddings [12-14]. It can be postulated that the same mechanism is valid also for the leaking fuel elements with aluminum cladding operating in the organic coolant. This supposition is based on the results of investigations of the sorption of iodine on the surface of metals from a gaseous medium [15].

In the operating conditions of the fuel elements in the organic coolant, the formation on the claddings of deposits of radiation-thermal cracking products (RTCP) of the coolant is

characteristic [1]. An increase of the RTCP of DTM, taking place during irradiation of the fuel element and in regions of damage, leads to a reduction of the escape of GFP from the fuel element (Fig. 3). The rate of reduction of the escape of radionuclides is approximately proportional to the radioactive decay constant. It is probable that this is due to an increase of the migration time of the radionuclides before their escape into the coolant, in particular by diffusion through the layer of deposits. The rate of reduction of the escape of iodine radionuclides was higher than for the GFP, which may be caused by the difference in the diffusion coefficients of the radionuclides in the RTCP. At the end of irradiation of the fuel elements, the yield of ^{131}I from them amounted in all to $2 \cdot 10^{-7}$.

During material-behavior investigations, radiation-thermal cracking products of DTM were detected not only outside but also beneath the cladding of leaking fuel elements. This is the consequence of the inflow of DTM under the cladding which probably occurs after shutdown of the reactor because of a reduction of the gas pressure under the cladding. Resumption of operation of the reactor leads to decomposition of the DTM which has flowed in, and to the formation of cokelike RTCP. The effect of these processes on the release of GFP is illustrated in Fig. 4. After the first reactor shutdown, the escape of GFP decreased by a factor of 5-7, with conservation of the escape of iodine radioisotopes. The phenomenon mentioned can be explained by the fact that the cokelike RTCP blocked the outflow of fission products from the major part of the fuel element. This led to a significant reduction of the escape of GFP but, at the same time, the escape of iodine radioisotopes was unchanged as, because of sorption on the inside surface of the fuel-element cladding, they entered the coolant only from the region of the fuel element close to the defect. After the second reactor shutdown (see Fig. 4), the escape of iodine radioisotopes was also reduced (scaled to nominal reactor power), which confirms the coking-up of the inside spaces of the fuel element in the vicinity of the defect.

In conclusion, it should be noted that the escape of fission products from defective oxide fuel elements into an organic coolant is significantly lower than the escape of fission products from leaking fuel elements in water-cooled/water-moderated reactors. According to the data of [13], with a linear loading of 11 kW/m, the escape of ^{133}Xe from leaking fuel elements of light-water reactors is equal to approximately 10^{-2}. This is almost a factor of 10 higher than the escape of ^{133}Xe from the fuel elements investigated into the organic coolant with the same linear loading and with a burnup of more than 10^{19} fissions/cm^3. The reason for this difference, as proposed in [13, 16, 17], lies in the increase of the diffusion coefficients of the fission products in oxide fuel by the action of water and steam penetrating under the cladding of the defective fuel element and increasing the stoichiometric ratio in the uranium dioxide.

LITERATURE CITED

1. V. A. Tsykanov, et al., At. Energ., 50, No. 6, 376 (1982).
2. R. Carroll et al., Nucl. Sci. Eng., 38, 143 (1969).
3. J. Findlay, J. Nucl. Mater., 35, 24 (1970).
4. P. Chenebault and R. Delmas, in: Behavior and Chemical State of Irradiated Ceramic Fuels, IAEA, Vienna, p. 337 (1974).
5. K. Shiba, et al., J. Nucl. Mater., 48, 253 (1973).
6. S. Yamagishi and T. Tanifuji, J. Nucl. Mater., 59, 243 (1976).
7. R. Soulhier, Nucl. Appl., 2, 138 (1966).
8. A. Höh and Hj. Matzke, J. Nucl. Mater., 48, 157 (1973).
9. O. Gautsch, J. Nucl. Mater., 35, 109 (1970).
10. N. Beatham, J. Nucl. Mater., 98, No. 2 (1981).
11. D. M. Skorov, Yu. F. Bychkov, and A. I. Dashkovskii, Reactor Material Behavior [in Russian], Atomizdat, Moscow (1979), p. 80.
12. G. Eigewilling and R. Hock, Trans. Am. Nucl. Soc., 23, 258 (1976).
13. E. Shuster et al., Nucl. Eng. Design, 64, 81 (1981).
14. A. V. Vasilishchuk et al., Preprint Scientific Research Institute of Nuclear Reactors, NIIAR-1 (26) [in Russian], Dimitrovgrad (1982).
15. M. Osborne, R. Briggs, and R. Wicher, Trans. Am. Nucl. Soc., 38, 463 (1981).
16. D. Cubieciotti, Nucl. Technol., 53, No. 1, 5 (1981).
17. B. Lastman, Radiation Phenomena in Uranium Dioxide [in Russian], Atomizdat, Moscow (1964).

THERMAL DESORPTION OF IMPLANTED HELIUM FROM AUSTENITIC STEELS OF 16-15 TYPE

V. S. Karasev and V. G. Kovyrshin

UDC 621.039.53:539.219.3

The accumulation of helium when a material is irradiated to a high fluence with fast neutrons and α particles has a substantial effect on embrittlement, swelling, the formation of surface flaws, and other processes that restrict the working life of the material in the first wall of a fusion reactor [1].

Austenitic stainless steels are considered [1] as the material for the first wall. The release of implanted helium has been examined for relatively low ion energies (up to some tens of keV) [2-5] and low concentrations (10^{-6}-10^{-2} at.%). However, the theoretical spectrum of a fusion reactor contains a high-energy helium-ion component (≥3.5 MeV) [1]. One needs data on the thermal desorption of helium at high temperatures after irradiation with ions of energy about 1 MeV, and also on the correlation of these processes with the change in properties in the material at high concentrations of implanted helium (up to 50 at.%).

Specimens of the austenitic stainless steels OKh16N15M3B and OKh16N15M3BR, which are similar in composition, were irradiated with the ÉSU-2 electrostatic accelerator at the Kharkov Technical Physics Institute of the Academy of Sciences of the Ukrainian SSR using helium ions of energy 0.5-1.6 MeV at doses in the range $5\cdot10^{16}$-1.6×10^{18} ion/cm² at about 50°C. Descriptions have previously been given [6-8] of the methods of irradiating the specimens and those used to examine the helium release and the surface changes during heating at a constant rate to 1300°C.

Effects of Radiation Dose. Two series of experiments were performed on irradiating OKh16N15M3B steel [6] in the dose range $5\cdot10^{16}$-1.2×10^{18} ion/cm² (energy of helium ions 0.8 MeV) and the same for OKh16N15M3BR in the range $5\cdot10^{16}$-1.6×10^{18} ion/cm² (helium-ion energies 0.5 and 0.8 MeV). The thermal desorption spectra for the OKh16N15M3BR specimens after irradiation at 0.5 and 0.8 MeV were identical and differed only in that the peaks were displaced by 20-30°C. The specimens were irradiated with normal incident monoenergetic beams.

Figures 1 and 2 show the temperature dependence of the relative release rate for three doses for each steel together with the background curves obtained under equivalent conditions without the specimens. In all cases, the spectra are for a heating rate of 0.25°C/sec.

The general trends are the same for the two steels. As the dose increases, the number of peaks rises from one to five, and the strengths of the peaks increase together with the amount of helium released in the first (low-temperature) peaks, while the temperature at which the release begins is lower, as is the formation of visible surface damage. The presence of several peaks indicates that there are various stages, each of which is associated with a particular migration mechanism. The values of the activation energy E_a (eV) as determined from the shifts in the peak temperatures T_{max} [9] with heating rates of about 0.1 to 0.25°C/sec are given in Figs. 1 and 2 at the tops of the corresponding peaks. At this heating rate, all the observable stages in the annealing were satisfactorily observed from the displacement of T_{max}, which was sufficient to give E_a. Some of the values of E_a have been revised in relation to earlier ones [6, 7]. The desorption characteristics and the surface-structure changes provide some conclusions on the mechanism for each stage.

The first stage, which is characteristic by the least release, is observed only after irradiation to a dose of about 10^{18} ion/cm². Here the activation energy is 0.4 ± 0.1 eV, which indicates the release of helium from surface layers. On heating, a transition structure is formed: swellings of irregular shape of size 100-300 μm (Fig. 3a); in the range 300-800°C in the first stage, these crack open (characteristic brief high-intensity pulses on curves I in Figs. 1 and 2). The resulting increase in the free surface favors the release of helium.

Translated from Atomnaya Énergiya, Vol. 55, No. 6, pp. 362-366, December, 1983. Original article submitted August 30, 1982.

0038-531X/83/5506-0801$07.50

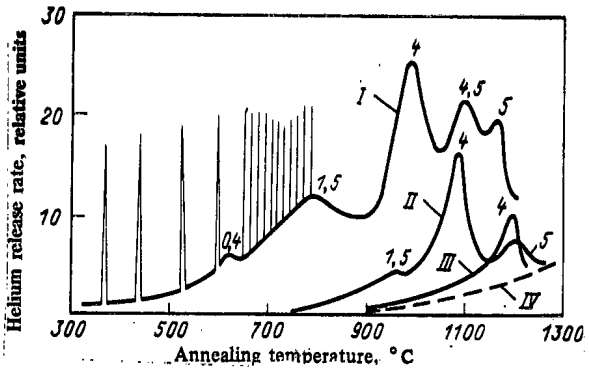

Fig. 1. Kinetic curves for the release of helium from OKh16N15M3B steel specimens irradiated by helium ions of energy 0.8 MeV: I) dose 1.2×10^{18} ion/cm^2; II) 4×10^{17} ion/cm^2; III) 1×10^{17} ion/cm^2; IV) background curve.

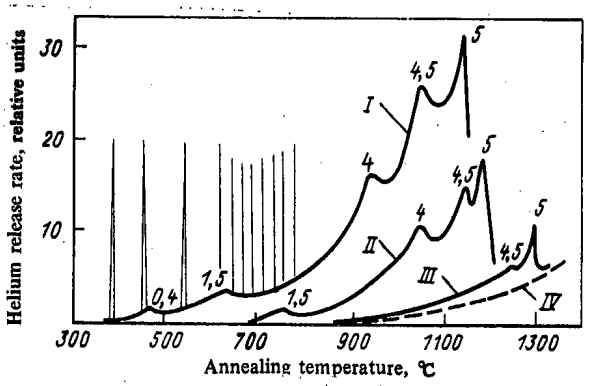

Fig. 2. Kinetic curves for the release of helium from OKh16N15M3BR steel specimens irradiated with helium ions of energy 0.5 MeV: I) dose 1.6×10^{18} ion/cm^2; II) 5×10^{17} ion/cm^2; III) 5×10^{16} ion/cm^2; IV) background curve.

Also, the desorption from the surface of OKh16N15M3B steel after reactor irradiation under conditions producing saturation with helium from the medium also occurs in the first stage [10].

The value $E_a = (1.5 \pm 0.2)$ eV for the next stage somewhat exceeds the activation energy for vacancy migration in austenitic steels (E = 1.3 eV [11]) and may include the energy of the binding of helium to vacancies, as well as the free-vacancy formation energy in the decomposition of point-defect clumps. No changes were observed in the surface structure in the temperature range for this stage.

The stage with $E_a = (4 \pm 0.4)$ eV controls a certain proportion of the released helium dependent on the type of steel and the dose. Desorption with an activation energy of about 4 eV is associated [12] with the formation, migration, coalescence, and emergence of helium bubbles at sinks, particularly at grain boundaries. The evidence on the surface-morphology change agrees with this. Amounts of about 10^{17} ion/cm^2 are insufficient to produce gas cavities of substantial size. Figure 1 shows that the desorption spectrum for OKh16N15M3B steel (dose $5 \cdot 10^{16}$–10^{17} ion/cm^2) is characterized by the release of helium only in one peak with $E_a = 4$ eV. On average, the grain size of the irradiated specimens remains at the initial level after heating to 1300°C (Figs. 3b and c, in the first of which the boundary between the irradiated and initial zones is seen). This indicates that helium emerges at the grain boundaries during heating, fixes them, and retards recrystallization [13], whereas in the unirradiated zone and on the outer side of the specimen (thickness 0.2 mm) there are

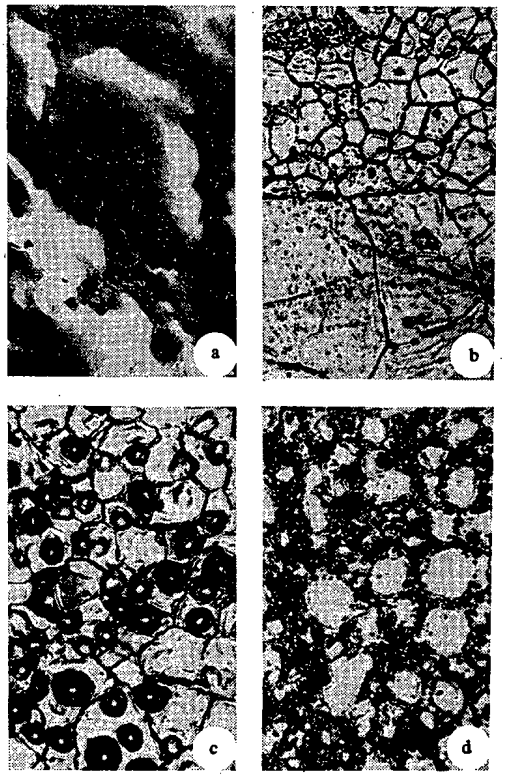

Fig. 3. Microstructures of the surfaces of irradiated specimens of 0Kh16N15M3B steel (a-c) and 0Kh16N15M3BR steel (d) after heating to 600°C (a) and 1300°C (b-d): a) dose 9×10^{17} ion/cm^2, ×300; b) 5×10^{16} ion/cm^2, ×450; c) 4×10^{11} ion/cm^2, ×450; d) 5×10^{17} ion/cm^2, ×450.

appreciable increases in grain size. We examined specimens that had received doses of $5 \cdot 10^{16}$-10^{17} ion/cm^2 after annealing and additional shallow etching, and this showed more clearly than does Fig. 3b that there are chains of pores of size 0.5-1 μm lying mainly at the grain boundaries but partly in the bodies.

At doses of over 2×10^{17} ion/cm^2, blistering occurs: a stage where bubbles arise at the surface (Fig. 3c). In the light of current concepts on the blistering mechanism [14], this is due to the fusion of gas bubbles and the growth of the blisters to critical sizes in the bulk of the grains. Helium is released from the blisters in a stage with $E_a = (4.5 \pm 0.5)$ eV, and also along the channels in the porous structure (pore diameter 0.5-1.5 μm, Fig. 3d) in the last stage with $E_a = (5 \pm 0.5)$ eV. The energy parameters for the last three stages are fairly close (4-5 eV) and characterize the formation and emergence of large helium accumulations.

Each of these stages involves a shift in the peak as the heating rate or dose is varied, which indicates thermal activation for the processes controlling the release. The characteristic changes in surface structure (Fig. 3b-d) and the high values of the activation energy show that the release is associated with microplastic deformation and failure. Such processes are also thermally activated [15] and are characterized by the corresponding values for the current activation energy.

The spectra show that the peaks shift to lower temperatures as the dose increases without change in the energy characteristics in a given stage. This applies for all peaks in both steels (Fig. 4). The dependence of T_{max} on the logarithm of the dose is linear. There is an appreciable difference in slope between curves 1 (1.5 eV) and 2-4 (4-5 eV), which may be associated with different migration mechanisms (single atoms of groups).

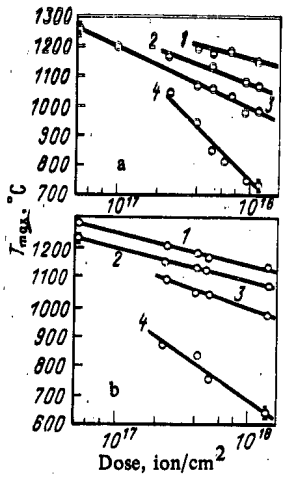

Fig. 4

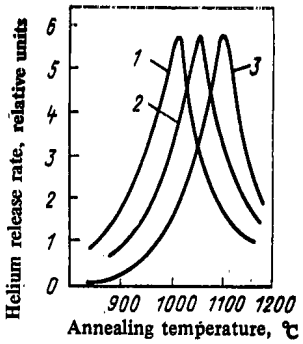

Fig. 5

Fig. 4. Dependence of T_{max} on dose for specimens of OKh16N15M3B steel at an ion energy of 0.8 MeV (a) and for OKh16N15M3BR steel at 0.5 MeV (b) and activation energies in eV of 5 (1); 4.5 (2); 4 (3); and 1.5 (4).

Fig. 5. Comparative desorption spectra for specimens of OKh16N15M3B steel irradiated to doses of 5×10^{17} ion/cm^2 at the following energies in MeV: 0.5 (1); 1 (2); 1.6 (3); and peak depths of 1.3, 2.1, and 3 μm correspondingly [16].

Effects of Ion Energy. As the energy increases, the surface damage changes substantially in character [16]: The blister diameter increases, while the density of them decreases, and the diameter distribution broadens. Results are available for ion energies of 0.5, 1, and 1.6 MeV as regards the effects on the peak positions on heating (dose 5×10^{17} ion/cm^2) for OKh16N15M3B specimens, which show that the temperature for the start of release increases with the energy (from 650 to 850°C), and also Fig. 5 shows that the peak temperature relates to the stage in which most of the helium is released. The other stages are now shown in Fig. 5, as substantially smaller proportions are released in these.

A similar shift in peak temperature with energy occurred in the release of helium from tungsten [17]. It has been determined analytically [18] that the peak positions are dependent on the radiation-defect concentration, which affects the migration conditions. According to these concepts, the shift in peak temperature is related to change in the depth of the helium at a constant activation energy (the effects of the energy are shown in Fig. 5), with further effects from the radiation-defect concentration (Fig. 4 shows the effect of dose), which agrees with our results.

Effects of Implantation Conditions. After irradiation to a given maximum concentration, the nature of the surface damage on subsequent heating is dependent on the conditions used (normal monoenergetic beam or a depth-scanning one) [8]. The implantation profiles are broadened and are similar to those expected for high-energy helium ions in a fusion reactor. The spectra were determined after irradiation with a scanning beam in which the angle of incidence of the ions varied from 0 to 74°. The maximum dose at the center of the target was 2.8×10^{18} ion/cm^2 and fell by about a factor 10 at a distance of 0.8 cm. The helium implantation profile varied correspondingly, as determined by Rutherford proton backscattering (Fig. 6a). There are reductions in the peak intensity (Fig. 6b) and in the area under the desorption curve (proportion of the least helium). Throughout the irradiation zone there was a single type of surface damage: pores of size 0.5-1.5 μm, while the desorption spectrum showed a single stage with $E_a = 5$ eV.

Figure 6b shows the shift in T_{max} produced by the implantation conditions, which is due to effects from factors acting in opposite senses. One the one hand, the implantation depth alters by about 0.6 μm from curve 3 to curve 1 (Fig. 6a), which should cause the peak to shift by about 40°C to higher temperatures (on change in the ion energy from 0.5 to 1.6 MeV,

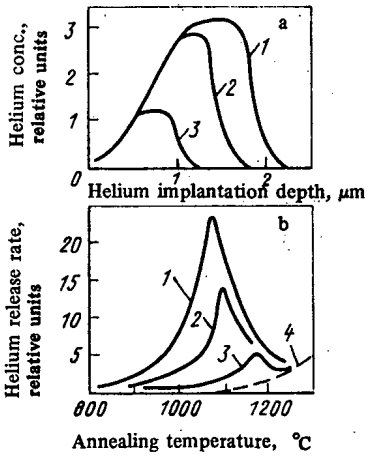

Fig. 6. Implantation profiles (a) and desorption spectra (b) for specimens of 0Kh16N15M3B steel irradiated by a depth-scanning beam of energy 1 MeV: 1) central zone; 2) at 0.4 cm from center; 3) at 0.8 cm from center; 4) background curve.

which alters the implantation depth by about 1.6 μm [16], the peak in Fig. 5 shifts by almost 100°C). On the other hand, an increase in the overall dose by a factor 10-15 has the reverse effect of shifting the peak by 150-200°C (Fig. 4a). The resultant shift from curve 3 to curve 1 (Fig. 6b) agrees with these estimates and shows that the dose (i.e., the radiation-defect concentration) has a substantial effect on the release during the formation of the porous structure.

Composition Effects. Although there are similarities between the desorption-kinetic curves for the two steels, there are certain differences, which are due to the presence of 0.005 at.% boron in 0Kh16N15M3BR steel designed to improve the physicomechanical properties, in particular the plasticity [19]. In this material, the main release process is the one with E_a = 5 eV at 5 × 10^{16} ion/cm^2 (Fig. 2, curve III), which is accompanied by the formation of a porous structure at the surface after annealing. The peaks with E_a = 5 eV also have the highest intensity for 0Kh16N15M3BR steel at higher doses, and the surface damage is characterized by a porous structure (Fig. 3d). The desorption and surface topography change for these steels under identical conditions of irradiation and annealing shows [7] that helium is retained in 0Kh16N15M3BR steel at higher temperatures than in 0Kh16N15M3B. Therefore, the release of helium through channels in the porous structure makes a contribution in 0Kh16N15M3BR steel. This may be due to the presence of boron compounds at the grain boundaries that hinder the emergence of helium bubbles, and therefore the release is reduced in the stage with activation energy 4 eV.

Conclusions. A study has been made of the effects of irradiation conditions on the thermal desorption of implanted helium from austenitic steels of 16-15 type. The energy parameters of the various release stages have been determined. There is a correlation between the desorption and the growth of the surface damage on heating. The peak positions and the temperature ranges for the corresponding stages are substantially dependent on the dose and ion energy. The results provide further insight into the behavior of helium in materials for the first wall of a fusion reactor under nonstationary conditions. The differences in release kinetics for two steels similar in composition indicate that it may be possible to make a suitable material by varying the additives.

We are indebted to G. D. Tolstolutskaya for providing the irradiated specimens and the data on the implantation profiles, and also for participating in the discussion of the results.

LITERATURE CITED

1. V. V. Orlov and I. V. Al'tovskii, Nuclear Science and Engineering, Series Physics of Radiation Damage and Radiation Materials Science [in Russian], Issue 1(15) (1981), p. 9.

2. D. Whitmel and R. Nelson, Rad. Effects, 14, 249 (1972).
3. W. Bauer and W. Wilson, "Radiation-induced voids in metals," AEC Symposium Series CONF-710601, Albany (1971), p. 230.
4. D. M. Skorov et al., Nuclear Science and Engineering, Series Physics of Radiation Damage and Radiation Materials Science [in Russian], Issue 1(1) (1974), p. 58.
5. D. M. Skorov et al., ibid., Issue 1(6) (1978), p. 46.
6. V. S. Karasev et al., ibid., Issue 2(13) (1980), p. 82.
7. V. S. Karasev et al., ibid., Issue 1(15) (1981), p. 52.
8. V. V. Gann et al., At. Energ., 48, No. 4, 266 (1980).
9. V. S. Karasev et al., ibid., 34, No. 4, 251 (1973).
10. V. S. Karasev et al., Nuclear Science and Engineering, Series Physics of Radiation Damage and Radiation Materials Science [in Russian], Issue 2(10) (1979), p. 48.
11. S. Harkness and Che-Yu-Li, in: Radiation Damage in Reactor Materials, Proc. Symposium IAEA, Vol. 2, Vienna (1969), p. 289.
12. D. Reed et al., Vacuum, 24, No. 4, 179 (1974).
13. A. S. Nikiforov et al., At. Energ., 53, No. 1, 3 (1982).
14. M. I. Guseva, Yu. V. Martynenko, and V. F. Rybalko, Nuclear Science and Engineering, Series Physics of Radiation Damage and Radiation Materials Science [in Russian], Issue 4(18) (1981), p. 35.
15. F. Garofalo, Creep and Long-Term Strength Laws for Metals [Russian translation], Metallurgiya, Moscow (1968).
16. G. D. Tolstolutskaya et al., Fiz. Khim. Obrab. Mater., No. 6, 29 (1979).
17. J. Pierre and D. Paulmier, C. R., 280, No. 2, B275 (1975).
18. S. Donnely and D. Ingram, Vacuum, 28, No. 2, 269 (1978).
19. N. P. Agapova et al., in: Peaceful Uses of Atomic Energy, Vol. 10, IAEA (1972), p. 3.

SYNERGIC EFFECT IN IRRADIATING GRAPHITE WITH H^+ IONS AND ELECTRONS

M. I. Guseva, S. M. Ivanov, and A. N. Mansurova

UDC 621.039.531:621.039.532.21

In some designs for fusion reactors, it is envisaged that there will be diaphragms made of graphite and sometimes also screens that are subject to radiation loads (with the exception of neutrons) and thermal loads. In particular, the diaphragm and screen will be irradiated by hydrogen ions and electrons. The screen material should be characterized by a small value of SZ^2 (S is the sputtering coefficient and Z is atomic number). The maximum sputtering coefficient for graphite produced by hydrogen ions is determined by the interaction that produces hydrocarbons at 300-700°C [1-3]. When the graphite is acted on simultaneously by atomic hydrogen from the gas phase and electrons of energy 100-600 eV, the chemical sputtering coefficient is much higher than that in the absence of electrons [4].

Here we examine the chemical sputtering of sintered carbon and MPG-8 graphite on parallel irradiation by H^+ ions of energy 10 keV and electrons or by hydrogen ions alone.

The irradiation was performed on the ILU-2 accelerator [5] in an irradiation device, in which the main elements were a planar graphite straight-channel oven with a system of screens and an electron gun with an indirectly heated cathode made of lanthanum hexaboride. The targets in the form of wafers of size 20 × 10 × 1 mm were mounted in the oven in special holders. The angles of incidence of the electrons and the H^+ ions on the target were correspondingly 30 and 0°. The MPG-8 graphite specimens were irradiated simultaneously by hydrogen ions and electrons at 100°C (E_e = 50-1500 eV) and 470°C (E_e = 400 eV), or by hydrogen ions alone at temperatures from 100 to 1600°C. The carbon-sinter specimens were

Translated from Atomnaya Énergiya, Vol. 55, No. 6, pp. 366-368, December, 1983. Original article submitted December 14, 1982.

 0038-531X/83/5506-0806$07.50

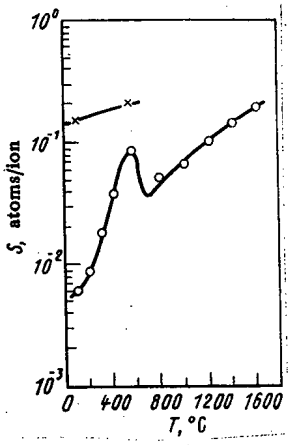

Fig. 1

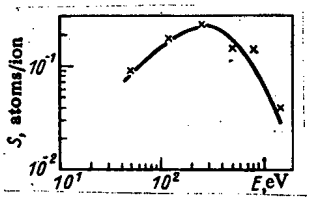

Fig. 2

Fig. 1. Temperature dependence of the sputtering coefficient for MPG-8 graphite by H^+ ions (○) at E = 10 keV and H^+ + e(×) at E_{H^+} = 10 keV, E_e = 400 eV.

Fig. 2. Dependence of the sputtering coefficient on electron energy for MPG-8 graphite to H^+ ions of energy 10 keV and also electrons (T_{irr} = 100°C).

irradiated simultaneously by H^+ ions and electrons at temperatures from 100 to 800°C (E_e = 400 eV) and by hydrogen ions alone at 100-1400°C. Before and after irradiation, the specimens were annealed at 1100°C for 1 h to outgas them. This heat treatment was performed for specimens irradiated at temperatures below 1100°C; for T_{irr} > 1100°C the specimens received only the preirradiation annealing at $T_{ann} = T_{irr}$. The target temperatures during irradiation and annealing were monitored with a tungsten–rhenium thermocouple. In most of the experiments, the H^+ dose was 3.6×10^{19} ion/cm^2, current density about 300 μA/cm^2, and ratio of the H^+ flux density to that of the electrons 1:20. The residual-gas pressure in the chamber was about 10^{-4} Pa, while the working pressure was about 10^{-3} Pa. Nitrogen traps were used to freeze out the oil vapor. The sputtering coefficient S was determined by weighing.

Figure 1 shows how the temperature affects the sputtering coefficient for MPG-8 graphite by H^+ ions. When the temperature is raised outside the limits stated in [1-3], there is a new sharp rise in the sputtering coefficient. To avoid any systematic error, check experiments were performed with the target heated to 1600°C in the absence of irradiation but at the same partial pressure of hydrogen in the chamber. The mass did not alter, which means that the mass reduction produced by H^+ bombardment is associated with sputtering.

Figure 1 shows that at 1600°C the sputtering coefficient is approximately two times S_{chem} in the region of the maximum for molecule formation at about 500°C. When the composition of the sputtered particles were examined, hydrocarbons were not detected, which indicates that there is no chemical sputtering at T_{irr} > 800°C. Further research is needed to interpret the accelerated sputtering of graphite at high temperatures.

Simultaneous bombardment by H^+ and electrons increases the sputtering coefficient by more than an order of magnitude even at 100°C, i.e., where there is no chemical sputtering in the absence of electron bombardment. In checks with the graphite bombarded by electrons, it was found that there was no change in the target mass, which means that a combination of H^+ and electrons clearly produces a synergic effect, whereas each form of bombardment separately does not produce chemical sputtering at this temperature.

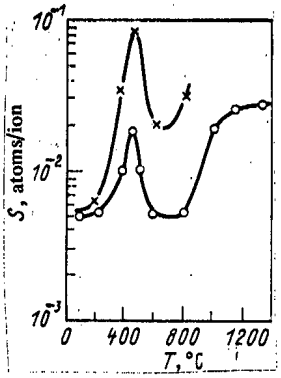

Fig. 3. Temperature dependence of the sputtering coefficient for USB-15 sintered carbon produced by H^+ ions (○) at E = 10 keV and by H^+ + e(×) or E_{H^+} = 10 keV, E_e = 400 eV.

The electron energies in our experiments were varied from 50 to 1500 eV. The sputtering coefficient varied most in the range 200-300 eV. Figure 2 shows that the electron energy has an appreciable effect on the sputtering rate produced by the hydrogen ions. The electron bombardment breaks the bonds between the carbon atoms and thus increases the probability that CH_4 molecules will be formed. Electrons of energy about 1500 eV penetrate a considerable distance into the graphite, while hydrocarbon molecules are produced by the H^+ only near the surface, so high-energy electrons have less effect on the sputtering coefficient. Also, the ionization cross section in electron impact has a maximum at about 300 eV. The synergic effect with MPG-8 graphite occurs also at about 500°C, which corresponds to the peak chemical sputtering by hydrogen ions. Parallel bombardment of MPG-8 graphite by hydrogen and electrons (E_e = 400 eV) increases S_{chem} by almost a factor 2.5, virtually up to the maximum possible value S_{max} = 0.25, which is realized if all the hydrogen atoms striking the target form escaping methane molecules.

Figure 3 shows how the temperature affects the sputtering coefficient for sintered carbon bombarded by H^+ and electrons together and for comparison by H^+ alone. There is a difference from fine-grained MPG-8 graphite in that at 100 and 200°C there is no synergic effect within the errors of experiment. There is no chemical sputtering of sintered carbon at temperatures up to 200°C, which indicates the exceptional chemical inertness of this variety of graphitized material. On the other hand, the synergic effect is prominent at T_{irr} = 400-800°C; at T_{irr} = 460°C, H^+ and electrons together increase the sputtering coefficient by about a factor of five. In that case, the chemical sputtering coefficients become comparable with those from MPG-8 graphite exposed to hydrogen ions alone. Therefore, the sputtering rate of sintered carbon in parallel irradiation at temperatures up to 200°C gives a value about 25 times less than that for ordinary fine-grained graphite, while the figure for $T_{irr} \approx$ 500°C is about a factor of two.

Sintered carbon at $T_{irr} \geqslant$ 1000°C (Fig. 3) resembles MPG-8 graphite in showing an increase in the sputtering coefficient with temperature. However, throughout the range, the value for the sintered carbon is much less than that for MPG-8 graphite.

These results show that it is necessary to consider synergic effects in choosing materials for the first wall of a fusion reactor. In particular, they show that it is hardly desirable to use graphite in a fusion reactor in devices that accumulate heat on account of thermal capacity, i.e., that operate by radiative cooling. On the other hand, our results show that sintered carbon can be used as the diaphragm if external cooling is provided, as in the PLT. Martynenko in 1977 [6] predicted a synergic effect from the combination of ions and electrons on the basis of concepts on the breakage of bonds for the surface atoms and thus reduction in the binding energy.

We are indebted to N. V. Pleshivtsev for constant interest.

LITERATURE CITED

1. N. P. Busharov et al., Fiz. Plazmy, 2, No. 4, 588 (1976).
2. M. I. Guseva, E. S. Ionova, and Yu. V. Martynenko, Preprint IAE-3225, Moscow (1979).
3. M. I. Guseva, et al., "Chemical sputtering of graphite by H^+ ions," Paper at the Soviet–American Seminar on Surface Effects in Fusion Equipment [in Russian], Moscow (1975).
4. C. Ashby and R. Rye, J. Nucl. Mater., 92, 141 (1980).
5. V. M. Gusev et al., Prib. Tekh. Eksp., No. 4, 19 (1969).
6. Yu. V. Martynenko, Preprint IAE-2815, Moscow (1977).

REPROCESSING AND THE SOLIDIFICATION OF NUCLEAR POWER STATION WASTES

A. S. Nikiforov, A. S. Polyakov, and
K. P. Zakharova

UDC 621.039.7

Nuclear power is making an increasing contribution to the production of electrical energy throughout the world [1] (Table 1), which makes more acute the question of power station safety, particularly a reliable system of rendering all forms of radioactive waste harmless. Power station operation leads to the accumulation of spent fuel, which contains 99.9% of the radionuclides formed by fission. The spent rods are held temporarily for 3-10 years at the stations in special basins and are then transported for reprocessing.

About 0.1% of the radionuclides formed in the reactor will pass to special equipment for processing before storage in the form of liquid, solid, and gaseous wastes. The safe disposal of liquid radioactive wastes LRW involves treating effluents to acceptable standards to enable them to be reused or discarded into open waterways, with the accumulation of the pollutants in a minimal volume isolated from the environment.

Two types of reactors form the basis of nuclear power in the USSR: the VVÉR and RBMK. There are some composition differences between the LRW from stations with VVÉR and RBMK reactors, but the processing schemes are essentially identical. All the homogeneous wastes are collected in receiving vessels, where they are mixed and averaged. The mixture is separated from the coarse suspensate and the pH is adjusted to about 10, after which the mixture is sent for evaporation, which is the main operation in purifying and concentrating LRW.

The evaporation is performed in two stages. The crude residue (concentrate) will contain 200-300 g/liter of salts, and this along with the slimes from spent filter materials (ion-exchange resins, filter pearlite containing precipitate, and activated charcoal) is sent to liquid-waste stores (concrete vessels of volume 400-3000 m^3 lined with stainless steel and designed to work for 20 years). After the lapse of 20 years, or in some cases earlier, the filled vessel must be emptied. The method of storing radioactive solutions and slimes in such vessels is temporary, since there is a potential hazard of leakage (due to corrosion of the materials) and radioactive contamination of the environment.

Major problems in LRW reprocessing are volume reduction and the salinity of the resulting wastes. Here improvements can come from advances in water-treatment technology and methods of decontaminating the loops, equipment, and buildings, together with the provision of sealed equipment during station operation and servicing.

Considerable importance attaches to differentiated collection of effluents differing in composition and radioactivity, which means that some of the water can be processed in the

Translated from Atomnaya Énergiya, Vol. 55, No. 6, pp. 368-372, December, 1983. Original article submitted June 23, 1983.

0038-531X/83/5506-0809$07.50

TABLE 1. Increase in the Overall Installed Power of All Stations and Nuclear Power Stations in the World in GW(el)

Year	All power stations	Nuclear power stations
1978	1830	106 (5,8) *
1979	1900	122 (6,4)
1980	2030	148 (7,3)
1985	2450—2850	290—350 (12)
2000	5230—6200	1030—1650 (20—27)

*In parentheses is the proportion of nuclear stations, %

most economical way or, if possible, discarded directly to external bodies.

Shower waters contain surfactants and have very low levels of radioactivity, and these should probably be collected separately from laundry waters and not processed if the level of radioactivity allows them to be discarded to the ordinary drainage. The scope for discarding various groups of laundry waters without processing will be determined not only by the radioelement contents but also by the concentrations of resistant surfactants type OP-7, SF-3K, and so on. At present, researches are in hand on treating laundry effluents by ultrafiltration, foam flotation, radiation-chemical destruction, etc. It is necessary to improve laundering processes to reduce the volumes of effluent and the contents of surfactants and salts in them. The progressive and more economical approach is to collect low-salt unorganized flows in special vessels and process them separately from salt solutions by ion-exchange treatment.

Filter materials (pearlites, ion-exchange resins, and activated charcoal) together with LRW concentrates will also be solidified for subsequent storage. The amount of spent pearlites sent every year to liquid-waste stores (per GW of installed electrical power) is 25-35 tons. The pearlites along with ion-exchange resins are transported hydraulically to the stores, while the decantation water along with trap water passes to reprocessing. The filter material sludges in the store consolidate, which complicates extracting them from the vessels for subsequent transfer to solidification.

One way of improving mechanical filtration of LRW in order to reduce the amount of pearlite in power station wastes is to use cermet filter elements that are regenerated by reverse flow, which are very widely used in various branches of industry in the USSR and are also employed at foreign nuclear power stations.

The volume of LWR can also be reduced by optimizing and automating the control systems for various processes, particularly coolant treatment, loop decontamination, and the cleaning of buildings and equipment, the regeneration of ion-exchange materials, and the processing of the resulting wastes, etc. A substantial reduction in the volume of wastes can be attained by improving methods of monitoring LRW and gaseous discharges, as well as sampling systems, together with automatic instrumental operation of analytical monitoring at power stations.

In the operation of a nuclear power station, there is the problem of eliminating ammonia. The usual alkali mode of evaporation for trap water leads to the distillation of the ammonia from the cubed residue and the accumulation of it in the ion-exchange filter, whence it passes with the regenerated material to evaporation again, i.e., there is no quantitative removal of ammonia in existing schemes for handling LRW. This leads to it accumulating in the system, which reduces the exchange capacity of the ion-exchange materials, shortens the filter cycle in the condensate treatment plant, and increases the amount of regeneration solution. To localize the ammonia one can best distill it, which utilizes its volatility in an alkaline medium and also the rectification effect.

It is also necessary to improve methods of removing traces of oil from effluents and reworking them. Removing oil from the distillate prevents the oil from entering the reactor loop and contaminating the ion-exchange filters, which thereby increases the working life of these. If the LRW contain oil, this should be distilled off with the steam. Development is

unfinished on methods of mechanical oil separation and sorption of residues on activated charcoal. It is necessary to increase the working life of carbon filters and the performance of the entire oil-purification system.

The final stage in LRW processing is to convert the concentrates to solid form for storage. Bitumening and cementing are the main methods of solidifying the LRW used abroad. Until recently, cementing was more widely used at lower stations, with bitumening used in nuclear centers. Since 1975, a cementing plant has been in operation at a nuclear power station in Sweden. In 1978, the equipment was reconstructed to improve the throughput and adapted for solidifying mixtures of ion-exchange materials containing boric acid [2].

Cementing is used also as a method of solidifying LRW in France (constructional hydraulic cements are employed), as well as in the Federal German Republic, Japan, and the USA [3-7]. In Britain, research is in hand on incorporating ion-exchange materials into a cement–vermiculite matrix [6], and in the USA studies are being performed on matrices based on cements with additives [8]. Although cementing technology is well developed, further efforts are being devoted in various countries to simplify and improve it to give stronger materials in which the radioactive nuclides have less tendency to leach out; much attention is also being given to reducing the volume of the products for storage. In particular, a method has been developed in the Federal German Republic for cementing previously dewatered wastes [5].

Studies have been made on the effects of sodium silicates, clay materials, and shales on the water resistance of materials formed by incorporating radioactive wastes into Portland cement, and this is being done not only in the USSR but also elsewhere. For example, studies in the Federal German Republic [8, 9] have shown that the addition of 20 mass % of Ca bentonite reduces the diffusion coefficient of ^{137}Cs by a factor of 6000-7000, which reduces the leaching rate by about a factor of 80. The leaching of strontium is reduced by increasing the density of the cement material.

Radionuclides are divided into three classes in accordance with the transformations that occur in cements [7]:

1) those that do not hydrolyze in the unsolidifed cement (pH about 12), for example ^{137}Cs, $^{51}Cr(VI)$, ^{131}I, and ^{3}H;

2) those that do not hydrolyze but form insoluble compounds, in particular carbonates, such as ^{90}Sr, ^{140}Ba; and

3) those that hydrolyze in the unsolidified cement with the formation of insoluble hydroxides such as ^{60}Co, ^{54}Mn, ^{114}Ce.

Improved properties are attained in polymer–cement concretes or in concretes impregnated with polymers [10]. In the USSR [11] and in the Federal German Republic [12], studies have been made on the scope for solidifying radioactive wastes using cementing substances derived from metallurgical slags.

Bitumening of LRW is used in virtually all countries along with cementing, and in some cases this has been implemented. The wastes from the CANDU heavy-water reactors are bitumenized in Canada, while extruder bitumenizers have been introduced at nuclear power stations in the Federal German Republic, and at one power station in Sweden a thin-film bitumenizer has been in operation since 1976 for solidifying slimes and ion-exchange materials [13], while in Japan the extruder bitumenizers operating at nuclear power stations such as at Tokai are being supplemented with bitumenizers having horizontal rotor mixers of throughput up to 140 kg/h [14].

Most of the equipments currently used to solidify power-station wastes involve partial or complete preliminary dewatering. Examples are provided by extruders, thin-film rotor equipment, horizontal rotating dryers, fluidized-bed equipment, and spraying dryers. In the use of this equipment, the wastes may be incorporated into thermoplastic materials or into cements, polymers, etc.

Ion-exchange materials are dewatered by vacuum filtration followed by hot-air drying. In that method, the water content of the ion exchanger is reduced to 25 mass %, and in that state the resin becomes a material that can be poured. In Japan, a method has been devised for incorporating dewatered ion-exchange materials, slimes, and concentrates into thermoplastic resins: polyethylene and chlorinated polyethylene [15]. In the USA, a system has

been built for reducing the volume of power station wastes by the use of a fluidized bed, which combines the processes of calcination and combustion, which reduces the volume of the wastes by a factor of 10. A full-scale plant has operated for two years [16].

In all countries, studies are being made on the specific properties of bitumen compounds, which largely determine the conditions for safe storage: Studies are being made on the fire safety and biocorrosion of bitumen compounds, as well as the corrosion of the steel drums holding the solidifed wastes.

In no foreign country with a developed nuclear power industry is there an agreed view on the methods of solidifying medium-level nuclear power station wastes. Virtually all countries have devised and used cementing and bitumening techniques, which have been brought to the stage of industrial use. Studies on waste processing have not only not ceased but have actually acquired larger scales.

Bitumening is being introduced for solidification at Soviet power stations. Conditions have been defined for producing the bitumen compound that ensure that the radioactive wastes are reliably localized. It has been found that for most LRW the optimum salt content in the compound is about 50 mass %, while the content of ion-exchange materials should not exceed 40 mass %, while that of filtered pearlite should not exceed 10 mass % to avoid marked increases in viscosity. Concentrates from heterogeneous LRW (filter pearlites and ion-exchange materials) are solidified periodically.

The optimum bitumening temperature is 160-180°C, at which the water distills off virtually completely and the hazard of the compound igniting is eliminated. The unloading temperature for the compound should be such as to prevent separation: In accordance with the composition of the wastes and the grade of bitumen, it can vary from 80 to 130°C.

A rotor bitumenizer can operate continuously and has high throughput together with certain other advantages, so this appears the most promising for Soviet nuclear power stations. A prototype apparatus with a rotor bitumenizer has been based on a standard rotor dryer and has been operating successfully since 1978 at Moscow Radon production cooperative [17]. Another type of rotor bitumenizer devised specially for processing LRW has passed marker's tests and has been sent for prototype testing on real wastes from power stations containing RMBK reactors [18]. This apparatus is intended to process salt concentrates in continuous mode, while slimes from filter materials are handled in batch mode. The bitumen compound is to be kept in a special store equipped with a monitor system and fire-fighting facilities.

Real wastes from power stations containing VVÉR reactors are being used in testing the BUR bitumenizer, in which the solution is dewatered (to a water content of about 20 mass %) in a concentrator, while the bitumening proper (incorporation of the salts into the bitumen) is performed in a pug mill [19]. The DB-100 semicontinuous bitumening plant with a tubular bitumenizer has been introduced at Leningrad waste-storage station, which has provided completion to the LRW processing cycle giving solidified products and reliable radionuclide localization [20].

Along with the introduction of bitumening systems, studies are continuing designed to resolve the following problems:

1) improving and cheapening the apparatus;

2) improving the properties of the bitumen compounds to provide reliable isolation of the radionuclides for hundreds of years; and

3) reducing the volume of the final materials to be stored.

Much attention is now being given to the properties of solidified wastes in order to ensure safe storage, and in particular estimates have been made of the fire and explosion hazards in the storage of bitumen compounds, along with the biological and radiation stabilities [21, 22]. In parallel with the work on bitumening, searches are being made for alternative materials, including those among the wastes from large-scale chemical processes [23], which can be used instead of bitumen in the same equipment.

An advantage of bitumening is that the water stability of the product is good (leaching rate 10^{-4}-10^{-5} g/cm^2·day), along with the high content of radioactive wastes (up to 50 mass %). The main disadvantage is the fire hazard in the production and storage of the bitumenized wastes. Cementing is free from this deficiency, but the water resistance is poor (the leaching rate is high at about 10^{-2} g/cm^2·day), while the waste contents are low (up to 15

mass %), which firstly requires the creation of a reliable protection barrier having good water-isolating properties and secondly improvement of the solid-product composition [11]. Drying produces the largest reduction in the amount of waste going for storage, but the presence of water-soluble salts in the products complicates the reliable long-term storage.

At present there is no reason to restrict development to one method, since the desirability of any given solidification technology will be dependent on the detailed conditions, and in particular on the storage method. In the USSR and elsewhere, little is known about topics related to the final disposal of solidified wastes; there has been no final decision on the location of the graveyards for bitumen compounds, and at existing power stations and ones under construction it is proposed to locate the stores directly on the station area or at a short distance away. Two forms of storage have been developed for the bitumen compound: in drums or in concrete vessels.

Economic studies are in hand on the best method of disposal in relation to the properties of the various solid materials. Here one has to bear in mind all aspects relating to environmental protection as well as the economy of the method.

Storage on the nuclear power station site in the form of concrete vessels appears preferable because this is more compact and does not require comparatively expensive loading and transportation of the solidified wastes. However, disadvantages are the substantial fire hazard and the complexity of removing the compound from the stores if necessary. Therefore, one cannot rule out the possibility of loading the compound into drums for temporary storage and subsequent shipping to graveyards, which is necessary for example if the hydrogeological conditions in the region of the power station are unfavorable or for combined heat and power stations in cities.

At present, much attention is being given in many countries to underground stores and graveyards for low-level and medium-level solid and solidified wastes [24], since these are considerably cheaper than other stores. The creation of stores is necessary not only to provide reliable containment of the radionuclides but also to provide reliable disposal of the solid radioactive wastes SRW formed at nuclear power stations, which are divided by activity level into low, medium, and high types, and in composition consist of combustible and noncombustible types. The amount of SRW produced at a nuclear power station of power 1 GW(el) is indicated by various sources as ranging from 200 to 400 m^3/yr. The solid wastes include combustible ones (clothing, shoes, paper, rags, polyethylene, and other plastics) and noncombustible wastes (metallic items and broken glass). The processing of SRW includes collection, sorting, batching, combustion, separation, pressing, and solidification.

At all Soviet power stations, the SRW is collected and in the main is stored in special concrete structures. The filling factors for such stores in some cases constitute 50-60%. However, the power stations lack systems for sorting, separating, and pressing the material, which leads to unsound filling of the stores and requires the construction of new costly structures. Pressing can reduce the volume of SRW for storage by factors of 3-5. Much attention is being given in the USSR and elsewhere to the development of reliable equipment for pressing SRW.

When power station wastes are burned, corrosive gases are released (chlorine and so on), which hinders the creation of reliable gas-cleaning systems and ensuring the necessary purification coefficients, while there are also adverse effects on the working life of the purifying plant and pipelines, and there may also be the formation of secondary wastes, etc. There are difficulties in selecting the materials for the furnaces and in automatic control of the combustion control of the combustion equipment.

The equipment devised and operated at power stations for processing liquid and gaseous wastes provide for the discharge of radioactive aerosols and gases and effluents containing radionuclides at levels below the health and safety norms. However, it is necessary to improve the waste-processing systems at power stations to make them more economical and effective, and on this aspect there is no final decision, and much attention should be given to research in this area.

LITERATURE CITED

1. N. S. Babaev et al., in: Nuclear Power, Man, and the Environment [in Russian], Énergoizdat, Moscow (1981), p. 9.

2. H. Christensen, in: Proceedings of the Symposium on Dealing with Nuclear Power Station Wastes within Their Areas, Zurich, 26-30 March (1979), p. 333.
3. D. Roy, et al., "The role of additives in the preparation of dense cements for isolating radioactive wastes," in: Proceedings of the International Symposium on the Scientific Basis for Nuclear Waste Management, Boston, Nov. 28-Dec. 1 (1978).
4. H. Stuenkel, H. Faust, and A. Pusavala, [2, p. 465].
5. M. Lazer, H. Mallek, and W. Jablonski, [2, p. 373].
6. D. Ferret and W. Simons, [2, p. 169].
7. Hideo Matsuzuru and Noboru Moriyama, Nucl. Sci. Eng., 80, 14 (1982).
8. R. Köster and G. Randolph, Waste Management Research Abstract, No. 12, 28 (1978).
9. E. Zange, W. Schlenter, and K. Trumper, ibid., 33.
10. A. Donato, ibid., 37.
11. K. P. Zakharova et al., Inventor's Certificate No. 880149, Byull. Izobret., No. 16, 293 (1982).
12. Federal German Republic Patent No. 2945007.
13. Z. Harfore, [2, p. 449].
14. Teruo Tokubuchi et al., in: Scientific Basis for Nuclear Waste Management, Vol. 3, Boston (1980), p. 219.
15. Seiichi Tozawa et al., Nucl. Sci. Technol., 18, No. 2, 162 (1981).
16. R. Vance et al., in: Decontamination and Decomissioning of Nuclear Facilities, Plenum Press (1980), p. 249.
17. I. A. Sobolev et al., in: Proceedings of the Fifth Comecon Symposium on Researches in the Reprocessing of Irradiated Fuel, Marianske Lazne (1981), p. 246.
18. V. I. Davydov et al., in: Processings of the Fourth Comecon Conf. on Researches in Disposing of Liquid, Solid, and Gaseous Radioactive Wastes and Decontaminating Polluted Surfaces [in Russian], Atomizdat, Moscow (1978), p. 74.
19. A. S. Nikiforov et al., At. Energ., 50, No. 2, 128 (1981).
20. V. I. Davydov et al., [17, p. 240].
21. K. P. Zakharov et al., At. Energ., 44, No. 5, 436 (1978).
22. S. V. Zhukova et al., ibid., 52, No. 5, 326 (1982).
23. K. P. Zakharova et al., ibid., 49, No. 4, 258 (1980).
24. Storage of Radioactive Wastes near the Surface. IAEA Recommendations. Safety Series No. 53, Vienna (1981).

TREATING RADIOACTIVE WATERS WITH A MIXED ION-EXCHANGE BED IN A CONTINUOUS-OPERATION PLANT

B. E. Ryabchikov, E. I. Zakharov, A. P. Darienko,
A. V. Rakhchev, and M. Ch. Murabuldaev

UDC 621.039.73

There are some technological and economic advantages in using continuous ion exchange to purify radioactive waters by comparison with the periodic process operated in ion-exchange filters [1, 2].

When water is purified by demineralization either continuously or periodically, it is necessary to pass the solution in sequence through 1-3 pairs of columns containing cation-exchange and anion-exchange materials. In that case it is preferable to use a mixed bed of cation-exchange and anion-exchange materials, which enables one to perform a high level of purification on passage through a single apparatus, which substantially reduces the equipment size. Installations of this type for preparing feedwater for thermal power stations are operated abroad [3, 4]. The process does not differ essentially from the treatment of liquid radioactive wastes, so the performance of such systems should be high. Difficulties in the design of these systems are associated in the main with organizing the continuous motion of the ion-exchange materials, the dispensing of these, and the separation of the spent mixture into cation-exchange and anion-exchange materials before separate regeneration.

A system of pulsation-type ion-exchange columns has been devised to carry out all the purification operations: sorption, regeneration, and sorbent washing, which enables one to conduct the process effectively at low cost [2, 5]. To separate the ion-exchange materials we have devised an apparatus of novel type, which can separate a mixture of industrial ion-exchange materials.

Here we describe the proposed semiindustrial system for continuous ion exchange with a mixed ion-exchange bed of throughput up to 1 m^3/h and we give test results in the treatment of radioactive waters.

The apparatus (Fig. 1) includes the sorption column 1 containing a hydraulically compressed bed of ion-exchanger [6] of diameter 0.1 m and height 2 m, the column 4 for separating the mixture of saturated resins, and two identical regeneration systems for the cation exchanger and anion exchanger, which each consist of the regeneration columns 3 and 6 and the wash columns 2 and 3 of PSK type (pulsating sorption columns), all of which have fluidized sorbent beds [5, 7]. There are also additional units: the cation and anion exchanger mixer, the separator 7, receiving and supply vessels, and monitoring and automatic systems.

The solution to be treated passes into the bottom of the sorption column containing a mixed layer of ion exchangers, where it is purified from salts and radionuclides. The solution speed during the sorption may be 100-150 m/h. Periodically (every 5-15 min) the mixture of resins in the apparatus moves downward, with fresh resin added at the top, while saturated resin is removed at the bottom. The exchangers are moved by pulsation, which is provided by the pulsation chamber 11, which is slowly filled with air through the valve 10, which is then rapidly discharged through the valve 9, whereupon the liquid in the process zone along with the lower layer of ion exchanger is transferred to the pulsation chamber and the entire layer moves downwards. At the same time, the equivalent amount of the exchanger mixture enters at the top from the buffer tank.

The saturated exchangers entering the lower zone under the pressure of the liquid (0.1-0.2 MPa) pass to the resin-separation column 4, which consists of two zones with distributing plates, with the upper zone having a cross section larger by a factor 1.5-2. The resin mixture is introduced into the middle of the column and water is supplied at the bottom. The separation is produced hydrodynamically because of the density difference between the cation

Translated from Atomnaya Énergiya, Vol. 55, No. 6, pp. 373-376, December, 1983. Original article submitted January 31, 1983.

0038-531X/83/5506-0815$07.50

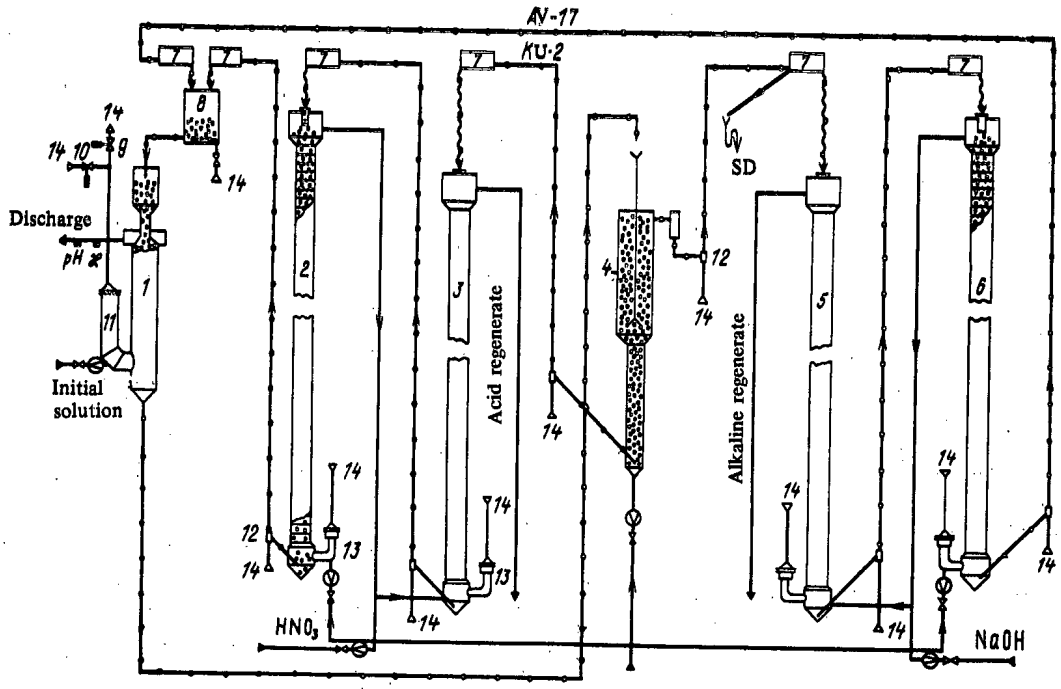

Fig. 1. Apparatus for continuous ion exchange with a mixed bed for demineralizing effluents: 1) sorption column; 3, 6) regeneration columns; 2, 5) wash columns; 4) separation column; 7) separator; 8) mixer tank; 9, 10) valves; 11, 13) pulsation chambers; 12) air lifts; 14) air supply; SD) special drain.

and anion exchangers. The cation exchanger is the denser and collects in the lower zone, from which it is pumped by an air lift system to the regenerator, while the anion exchanger fills the upper zone and is transferred along with the solution into the separator 7, from which it also passes to regeneration.

To facilitate management, the demonstration separation column has been made transparent, while the cation-exchange material has been colored with methylene blue dye. The cation exchanger is partly decolorized on acid treatment, but a color is still readily visible even after 50 sorption-regeneration cycles.

The saturated cation-exchange material passes to the top of the regeneration column 3 containing a fluidized bed of sorbent, and this is of PSK type, where there is motion from the top downwards, with the resin freely falling in a flow of rising regeneration solution. The pulsation and the distributing plates serve to improve the contact between the phases. The regenerated cation exchanger is collected in the lower part of the column, from which it is transferred by an air lift for washing in the column 2 of analogous design. The washed cation exchanger is transferred by air lift into the mixer tank 8.

The bottom of the wash column 2 is supplied with water, which washes the remainder of the regeneration solution out of the resin particles. The resulting solution contains up to 0.5-1.0 g-eq/liter of HNO_3, and this is taken from the top and flows spontaneously because of the cascade arrangement of the columns to the bottom of column 3. HNO_3 is constantly supplied to the transfer line with a concentration of 12 g-eq/liter. The regeneration solution passes through column 3 from the bottom upwards in the opposite direction to the sorbent and regenerates it. The resulting regenerate is taken from the top of the column and sent for processing. The chain of columns 5 and 6 for regenerating the anion exchanger works similarly.

The sorbents are transferred by air lift, and therefore they are separated from the transporting solution by the use of drum-worm separators. The regenerated resins are collected in the mixer tank, where they are mixed by means of air and are transferred automatically to the sorption column as the resin mixture is used up.

TABLE 1. Average Data on the Treatment of Liquid Wastes with a Mixed Exchanger Bed

Parameter	pH	Electrical conductivity, μSm/cm	Concn., mg-eq/liter				βActivity in nCi/liter (1 Ci = 3.700 × 10^{10} Bq)						
			Na	Ca, Mg	Cl	SO_4	Σβ	^{134}Cs	^{137}Cs	^{60}Co	^{131}I	^{124}Sb	^{90}Sr
Experiment													
Initial solution	6,7	350	2,3	3,4	1,2	3,4	200	68	110	4,7	1,5	24	8,7
Effluent	6,1	8,8	0,08	0,13	0,1	0,05	3	0,33	0,58	0,41	0,003	1,6	0,005
Purification coefficient		—	29	26	12	68	66	206	190	11,4	470	15	1720
Experiment 2†													
Initial solution	6,7	230	2,5	3,5	1,2	3,4	200	68	120	17	1,5	17	8,7
Effluent	6,1	4,8	0,08	0,05	0,1	0,05	1	0,18	0,18	0,35	0,003	0,31	0,005
Purification coefficient			31	70	12	68	200	380	665	485	470	55	1720
PC_B‡			—	—	—	—	—	8,6	15	35	1	22	0,4

* $V_{cat} : V_{an} = 1 : 1$; $Q_S = 0,6$ m^3/h
† $V_{cat} : V_{an} = 1 : 2$; $Q_S = 0,8$ m^3/h
‡ PC_B is the permissible radionuclide concentration in water (see NRB-76, OSP-12/80, Energoizdat (1981), p. 35).

TABLE 2. Parameters of Equipment Using Pulsation Columns and Ion-Exchange Filters of Throughput 1 m^3/h with Identical Degrees of Purification

Apparatus type	Number		Volume, liter			Concn. coeff.	Water flow for internal use, %
	equip.	vessels	equip.	vessels	ion exchangers		
Filters	6	6	900	1200	600	50	5—8
Columns	6	2	250	80	30	70	1,5—2

The treatment is applied to a solution (Table 1) that has previously been averaged, coagulated, and mechanically filtered. Preliminary experiments on purifying this solution with laboratory filters led to the selection of the strongly acid cation exchanger KU-2-8 and the strongly basic anion exchanger AV-17-8. The exchange materials are regenerated in solutions of HNO_3 and NaOH of concentration 2 g-eq/liter. Tap water is used to separate the resins and wash them.

The purpose of the tests was to determine the performance in purifying the solution from radionuclides using a mixed ion-exchange bed, together with the scope for subsequent separation of this into its components, and also the scope for producing a uniform mixture of the regenerated exchangers. Most of the radionuclides in the solution that make the main contribution to the overall β activity are usually in cationic form ($^{134,137}Cs$, ^{90}Sr), so we initially checked the state in which the cation-exchange material is regenerated with a large excess (200%), while the anion exchanger, which in the main only corrects the pH, was regenerated with a small excess (50%). The volume ratio of the exchangers in the mixture was 1:1, and the flow rate was 5-6 liter/h. The experiments were performed continuously for 100 h, and the results are given in Table 1.

As would be expected, there was complete extraction of the salt cations and of the radionuclides in cation form. The purification factor for the salts was about 30. The concentrations of all the radionuclides were substantially less than PC_B. However, the extraction of ^{124}Sb and ^{60}Co in anion or complex form was incomplete. The relatively high electrical conductivity was due to considerable amounts of unextracted carbonic acid (up to 50% of the sum of the anions in the initial solution).

More extensive purification from radionuclides in anion form requires an increase in the degree of purification from salt anions. For this purpose, a second series of experiments was performed in which the regeneration of the anion exchanger was greater (excess alkali

180%) and the amount of anion exchanger in the mixture was increased to make the ratio of cation and anion exchanger volumes 1:2. The consumption of acid in regenerating the cation exchanger was reduced to 50-80% excess (the flows of cation exchanger and anion exchanger were then 3.3-4.0 and 6.6-8.0 liter/h correspondingly).

In the second series, the fuller regeneration of the anion exchanger led to better extraction of the weak-acid anions and radionuclides in anion form, and there was also improved performance in the cation exchanger, which is characteristic of a mixed bed. The contents of all the radionuclides were at the limit of detection of the radiometers, while the salt content was reduced to an extent such that the conductivity was $2\text{-}5 \times 10^{-6}$ Sm/cm. Water of such quality can not only be discharged to any body of water but can also be used to supply steam boilers.

The separation of the saturated resins (flows of 10-12 liter/h) was performed with tap water with a flow rate of 20-22 liter/h. The resulting partially demineralized solution can be used to wash the regeneration solutions out of the resins. The separation boundary between the cation and anion exchangers was very sharp. The position was controlled by the output of the air lift handling the cation exchanger. In a check on the resin separation performance it was found that the content of cation exchanger in the anion exchanger was not more than 3-4%, while that of the anion one in the cation one was 2%. This degree of separation is more than sufficient to provide demineralization to a conductivity of 1×10^{-6} Sm/cm.

The resins were washed free of the regeneration solutions with a flow ratio of 1:1 or 1:2, and all the washed solution was then treated with acid or alkali and used in the regeneration. The overall flow rate of the wash water was about 15 liter/h. Despite this low flow rate, the washing performance was high, as is evident from the low conductivity of the purified solution.

It was not the purpose of this study to minimize the flow rates of the regeneration solutions, since it had previously been shown [2] that it is possible to reduce the volumes by factors of 1.5-3 relative to the traditional levels in the continuous process. However, in that case also we obtained good results in regenerating both resins.

The flow rates of the regeneration solutions were less than 2.5% of that of the initial solution. The mean content of sodium salts in the acid regeneration solution was 260 eq/m^3, hardness 330 eq/m^3. The concentration coefficients for salts and radionuclides is about 100, which is better by a factor of 1.5 than in the traditional equipment (two-stage ion exchange in filters). Analysis of the saturated and regenerated resins showed that the degrees of regeneration for the various radionuclides and ions vary from 50 to 90%, which was sufficient to provide complete purification by the mixed exchanger bed.

Therefore, this continuous-operation plant with a mixed exchanger bed can provide a high degree of purification for liquid radioactive wastes with initial salt contents up to 0.5 g/liter at high solution speeds (70-100 m/h) and small flows of regeneration solutions (up to 2.5% of the volumes of the input solutions) with the absence of wash water returning to the start. The equipment dimensions and the load of exchangers are also much less than in the traditional apparatus (Table 2).

LITERATURE CITED

1. F. V. Rauzen et al., At. Energ., 36, No. 1, 27 (1974).
2. B. E. Ryabchikov et al., At. Energ., 38, No. 4, 222 (1975).
3. C. Thorborg, Power, 113, 76 (1969).
4. C. Dallmann, in: Proc. 32nd Int. Water Conf., Pittsburgh (1971), p. 113.
5. S. M. Karpacheva and E. I. Zakharov, Principles of the Theory and Calculation of Pulsation-Type Column Reactors [in Russian], Atomizdat, Moscow (1980).
6. B. E. Ryabchikov, E. I. Zakharov, and V. S. D'yachkov, Inventor's Certificate No. 712118, Byull. Izobret., No. 4, 16 (1980).
7. Pulsation Columns: Catalog, Part 2 [in Russian], Atomizdat, Moscow (1981).

EXPERIMENTAL INVESTIGATIONS OF μ-ATOMIC AND μ-MOLECULAR PROCESSES IN HYDROGEN ON THE JINR SYNCHROCYCLOTRON

V. P. Dzhelepov and V. V. Fil'chenkov

UDC 539.1.18:539.1.19:621.039.633

Two main stages can be identified in the development of experimental investigations on μ-atomic and μ-molecular processes in hydrogen. The first stage began in 1957 when the Alvarez group first recorded [1] the μ-catalysis of fusion reactions in p + d and d + d nuclei, which had been predicted theoretically earlier [2, 3]. By 1960 the foundations had been laid for the theory of μ-atom proceses, the main results of which were expounded in a review by Zel'dovich and Gershtein [4].

In 1957-1965 processes involving μ atoms were investigated intensively in a number of scientific centers such as Columbia University, CERN, the Joint Institute for Nuclear Research (JINR), etc. These processes were studied most extensively in the Laboratory of Nuclear Problems at JINR on a 680-MeV synchrocyclotron using a high-pressure diffusion chamber placed in a magnetic field [5]. The use of a track detector during a stage of the investigations when many of the experiments were in the nature of a search ensured the success of this work. The main results were published in [6]. As for other experiments carried out during this period, we should point out the work done by the group of Lederman [6]. The results they obtained for the rate of formation of ppμ mesic molecules and the rate of stripping of a muon from a proton by a deuteron are consistent with our data [5].

By 1965 many laboratories had experimentally investigated the characteristics of many processes initiated by negative muons in hydrogen (H_2, D_2, and $H_2 + D_2$ mixture) and in most cases the results were in good agreement with the predictions of the theory [8]. To a considerable degree these investigations also fulfilled the "applied" objective, viz., experimentally obtaining information about μ-atomic processes so as to permit correct interpretation of the results of measurements of the rate of the fundamental reaction of weak interaction, i.e., nuclear absorption of a muon by a proton.

A special place in the physics of μ-molecular processes is occupied by μ-catalysis of nuclear fusion reactions synthesizing hydrogen isotopes. The essence of μ-catalysis is well known. Since in muonic hydrogen molecules the distance between nuclei is small ($5 \cdot 10^{-11}$ cm), the probability of nuclei penetrating the Coulomb repulsion barrier becomes high enough so that the nuclear fusion reaction would occur with a probability of nearly one during the muon lifetime ($\tau_\mu = 2.2 \cdot 10^{-6}$ sec). Under conditions when the rate of formation of a muonic molecule and the rate of the nuclear reaction in it are much higher than the muon decay rate ($\lambda_0 = 1/\tau_\mu = 4.55 \cdot 10^5$ sec^{-1}), one muon can successively initiate many fusion reactions, with a release of energy in each of them. It is of the utmost interest to determine the maximum possible number of successive muonic-catalysis events. According to the concepts of the theory which existed in the early 1960s, an efficient (multiple) muonic catalysis process was impossible for two reasons [4]: first, because of insufficiently high expected values of the rate of formation of muonic molecules and, second, because of the finite probability of a muon "sticking" to one of the fusion reaction products, the helium nucleus, which breaks the chain of successive catalysis.

The results of the first experiments on muonic catalysis of p + d and d + d reactions, it seemed, supported this pessimistic conclusion of the theory. The process of formation of dtμ molecules with a subsequent reaction d + t → ^{4}He + n + 17.6 MeV, it is true, had not been investigated at all experimentally. In this case, however, the theory predicted a small value (~10^4-10^5 sec^{-1}) of the dtμ formation rate. All of this considerably dampened interest in further experimental investigation of μ-catalysis. It is significant that from 1963 to 1977 foreign laboratories did not carry out a single experiment in this area.

Translated from Atomnaya Énergiya, Vol. 55, No. 6, pp. 376-391, December, 1983. Original article submitted April 11, 1983.

0038-531X/83/5506-0819$07.50

Meanwhile, precisely the study of the process of muonic catalysis revealed an interesting new effect which did not fit within the framework of the theoretical concepts at the time. The essence of this effect was that the value of the rate of formation of ddμ molecules ($\lambda_{dd\mu}$), which we measured [5] in gaseous deuterium at 240°K, was roughly an order of magnitude higher than that obtained in liquid deuterium [9] at 30°K. In order to explain this anomaly, we hypothesized [5] the existence of a previously unknown mechanism of ddμ molecule formation, a mechanism that would be resonant in the energy of the dμ atom (in the deuterium temperature). It must be pointed out that back in 1954 Zel'dovich [3] pointed out that the existence of a weakly bound state in a muonic molecule could result in a resonant enhancement of the μ-catalysis yield.

Later, in 1967 É. A. Vesman considered a concrete mechanism [10] of formation of ddμ molecules such that the hypothesized resonance dependence $\lambda_{dd\mu}(T)$ could be realized. At the same time, however, the hypothesis that a resonance existed in the cross section for ddμ formation remained insufficiently substantiated, both theoretically and experimentally. On the one hand, it had not been established reliably that ddμ had a weakly bound state leading to resonance while, on the other hand, the body of experimental data (in actual fact, only two points) was not sufficient to establish the character of $\lambda_{dd\mu}(T)$.

Another important problem, which was not solved in the initial stage of the research, became particularly clear upon completion of measurements [11] of the rate of muon trapping by a deuteron in gaseous hydrogen (H_2 + 5% D_2, 0.69 MPa) and was associated with the determination of the spin states of dμ atoms. Such atoms, formed initially in a random mixture of states with a total spin $F_{d\mu} = 3/2$ and $F_{d\mu} = 1/2$, can then fall to the lower state with $F_{d\mu} = 1/2$. Until recently it was assumed [4, 8] that these transitions take place only in dμ + d spin-exchange collisions. The initial estimate [12] of the rates λ_d of these transitions, it seemed, was confirmed in the experiment in [7]. To reconcile the results of the experiment in [11] with those expected from the weak-interaction theory it was necessary to assume for λ_d a value several orders of magnitude higher than the result of [12] and the data of later calculations [13, 14] or to assume the existence of some other (not spin-exchange) mechanism [14] leading a high rate of 3/2 → 1/2 transitions in a gaseous hydrogen–deuterium mixture.

Mainly in view of these two problems, viz., the question of the existence and the nature of the resonance dependence $\lambda_{dd\mu}(T)$ and the problem of determining the spin states of dμ atoms, the Laboratory of Nuclear Problems at JINR decided to carry out a new cycle of investigations of μ-atomic and μ-molecular processes; this cycle began in 1974-1975.

It must be pointed out that while in the early 1970s such investigations were conducted practically nowhere (the sole exception was the CERN group), at the present time experiments along these lines are being carried out on many accelerators (B. P. Konstantinov Institute of Nuclear Physics of the Academy of Sciences of the USSR, Leningrad; Swiss Nuclear Research Institute; meson factory in Los Alamos). Thus, one can speak of a new stage of intensive research on μ-atomic and μ-molecular processes in hydrogen. This stage is characterized primarily by the fact that in recent years significant progress has been made in attaining a more profound understanding of μ-atomic effects and in determining their quantitative characteristics at a new level of accuracy.

We point out only two of the most important achievements of the theory: weakly bound states with an energy of approximately 2 eV and 1 eV, respectively, have been shown to exist in ddμ and dtμ systems; higher resonance values of the formation rates for these systems have been predicted.

Experiments have obtained substantially improved capabilities: Work has started with meson factories at Los Alamos (USA) and Villingen (Switzerland) making it possible to obtain high-intensity meson beams. All of our measurements pertaining to the new stage of investigations have been carried out on the same 680-MeV synchrocyclotron, but with improved characteristics of the muon beam.

Investigation of the Processes of Formation of Muonic ppμ and pdμ Molecules in Gaseous Hydrogen. Measurement of the rate of formation of muonic ppμ and pdμ molecules ($\lambda_{pp\mu}$ and

TABLE 1. Formation Rate of ppμ and pdμ Molecules, 10^6 sec^{-1}*

Source of data	$\lambda^0_{pp\mu}$	$\lambda^0_{pd\mu}$
Experiment		
Columbia Univ., liquid H_2 [7]	1,89±0,2	5,8±3
CERN, liquid H_2 [15]	2,55±0,18	6,82±0,25
JINR, gaseous H_2 [16]	2,74±0,25	—
JINR, liquid H_2 [17]	2,34±0,17	5,53±0,16
Calculation		
Ref. [14]	2,2	5,9

*The values of $\lambda^0_{pp\mu}$ and $\lambda^0_{pd\mu}$ are given for a liquid-hydrogen density $\rho_0 = 4.25 \cdot 10^{22}$ nuclei/cm^3 and can be converted for gaseous hydrogen with a density ρ: $\lambda_{pp\mu} = \lambda^0_{pp\mu}\varphi$ and $\lambda_{pd\mu} = \lambda^0_{pd\mu}\varphi$, where $\varphi = \rho/\rho_0$ is the relative density.

$\lambda_{pd\mu}$) not only is important from the point of view of comparing experimental results and explaining their agreement with present-day calculations but also is entirely necessary in order to choose the optimal conditions for the formulation of experiments on muon capture by a proton and a deuteron and for the correct interpretation of the data obtained in such experiments. It was also important for us to know $\lambda_{pd\mu}$ for gaseous hydrogen since this enabled us to obtain information about the spin states of dμ atoms on the basis of measurements of the yield of the nuclear fusion reaction in a pdμ molecule.

The data from previous measurements of $\lambda_{pp\mu}$ and $\lambda_{pd\mu}$ are given in Table 1. As can be seen, $\lambda_{pd\mu}$ had been measured earlier only in liquid hydrogen. The value of $\lambda_{pp\mu}$ for gaseous hydrogen was measured only in [18]; the data processing method employed there did not exclude a certain systematic error in the result.

In order to determine $\lambda_{pp\mu}$ and $\lambda_{pd\mu}$ we employed the method of [15, 18], in which the target consisted of hydrogen with a small impurity of gas with $Z \gg 1$ (in our case we used xenon with an atomic concentration of 10^{-5}). The sequence of processes occurring in an $H_2 + D_2 + Xe$ mixture after a negative muon has halted in it is shown schematically in Fig. 1. In the experiments conducted by our group [17] $H_2 + Xe$ and $H_2 + D_2 + Xe$ mixtures were used; we detected electrons from muon decay and γ rays from mesic x radiation, arising as a result of the process of stripping of a muon from a pμ or dμ atom to the excited state of an Xe μ atom. The time distributions of electrons and γ rays can be written in one way for $H_2 + Xe$ and $H_2 + D_2 + Xe$:

$$dn_\gamma/dt = \lambda_{Xe} \exp(-\lambda_s t); \tag{1}$$

$$\frac{dn_e}{dt} = \left(\lambda_0 - \frac{\lambda_0 \lambda_{Xe}}{\lambda_s - \lambda_0' - \lambda^c_{Xe}}\right) \exp(-\lambda_s t) + \frac{\lambda_0 \lambda_x}{\lambda_s - \lambda_0} \exp(-\lambda_0 t). \tag{2}$$

In these expressions for the $H_2 + Xe$ mixture $\lambda_s = \lambda_{p\mu}$ is the rate of decay of a pμ atom, $\lambda_x = \lambda_{pp\mu}$, and $\lambda_{Xe} = \lambda_{pXe}$ is the rate of stripping of a muon from a proton by xenon; for the $H_2 + D_2 + Xe$ mixture $\lambda_s = \lambda_{d\mu}$ is the decay rate of a dμ atom, $\lambda_x = \lambda_{pd\mu}$, and $\lambda_{Xe} = \lambda_{dXe}$ is the rate of stripping of a muon from a deuteron by xenon. The remainder of the notation is: $\lambda_0 = 4.55 \cdot 10^5$ sec^{-1} is the rate of decay of a free muon, λ_0' is the rate of μ-decay in an Xe

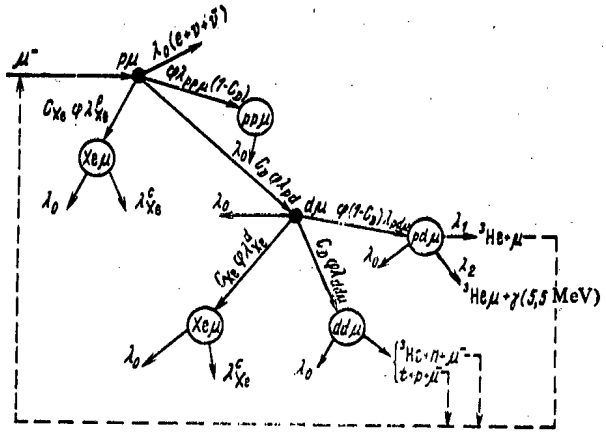

Fig. 1. Scheme of μ-atomic and μ-molecular processes in a hydrogen–deuterium mixture.

μ-atom, and λ_{Xe}^{c} is the rate of nuclear capture of a muon in an Xe μ-atom.

The decay rate of μ atoms is $\lambda_{p\mu} = \lambda_0 + \varphi\lambda_{pp\mu}^{0}(1 - C_D) + \varphi C_{Xe}\lambda_{pXe}^{0} + \varphi C_D\lambda_{pd}^{0}$; $\lambda_{d\mu} = \lambda_0 + \varphi\lambda_{pd\mu}^{0}(1 - C_D) + \varphi C_D\lambda_{d,d\mu}^{0} + \varphi C_{Xe}\lambda_{dXe}$. Here λ_{pd}^{0} is the rate of stripping of a muon from a proton by a deuteron, $\lambda_{dd\mu}$ is the rate of formation of dd_{μ} molecules, C_{Xe} and C_D are the atomic concentrations of xenon and deuterium, φ is the ratio of the gas density ρ_0 to the density of liquid hydrogen ($\rho_0 = 4.25 \cdot 10^{22}$ nuclei/cm^3), $\lambda_{pp\mu}^{0}$, $\lambda_{pd\mu}^{0}$, and $\lambda_{dd\mu}^{0}$ are the rates of formation of muonic molecules for the density of liquid hydrogen, and λ_{pXe}^{0} and λ_{dXe} are the rates of stripping of a muon by xenon for the density of liquid hydrogen.

From Eqs. (1) and (2) we can see that the time distribution of the electrons is the sum of two exponents, the contribution of the exponent with the index $-\lambda_0 t$ being proportional to the sought $\lambda_{pp\mu}$ or $\lambda_{pd\mu}$. Upon analyzing the experimental time distributions of electrons and γ rays, using Eqs. (1) and (2), we can determine $\lambda_{pd\mu}$ and $\lambda_{pp\mu}$.

In the experiment we used a muon beam with a momentum of 130 MeV/sec and an intensity of $2 \cdot 10^4$ μ/sec. The entire cycle of investigations of μ-atomic processes is characterized by the following distinctive features of the technique of the experiments:

a) In order to reduce the background the experiments were carried out in a low-background laboratory, separated from the main experimental hall of the synchrocyclotron by a 2-m concrete wall.

b) In order to reduce the background due to the stopping of muons in the walls of the target casing, which is especially important in work with gaseous hydrogen, in the experiments we used a target with scintillators installed inside it to record the stopping of muons in the gas.

c) In order to suppress the background caused by the stripping of muons from the hydrogen by nuclei of possible impurities, in the experiments we used ultrapure hydrogen obtained using apparatus with a palladium filter.

d) A multiparameter analysis was made of events recorded by the electron and γ-ray detectors. The data were processed on-line during the measurements with the aid of a small computer.

The layout of the apparatus in the muon beam is shown in Fig. 2. Upon passing through the monitoring counters 2 and 3 and the wide-aperture counter 1 used to block "doubled" muons, the muons were slowed down in the moderator 4 and entered the volume of the gas target. Stoppings of muons in the gas were recorded with CsI(Tl) scintillators. One of them (counter 6) was made in the form of a disk 110 mm in diameter and 0.3 mm thick while the other (counter 7) was made in the form of a cup 200 mm high, 120 mm in diameter, and with a wall thickness of 5 mm.

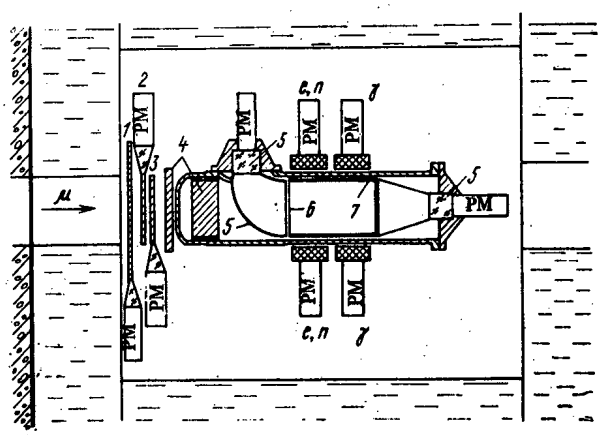

Fig. 2. Experimental layout used to investigate processes of the formation of ppμ and pdμ molecules [17] and μ-catalysis of the p + d reaction [19] and d + d reaction [20, 21]: 1-3) muon detectors (plastic scintillator); 4) muon moderator; 5) light guides; 6) CsI(Tl) detector of slow muons; 7) CsI(Tl) muon and electron detector; n and e are neutron and electron detectors; γ are γ-ray detectors.

The choice of the scintillator material for counters 6 and 7 was dictated by two circumstances: First, the lifetime of CsI(Tl) muons is only 0.08 μsec, which makes it easy to discriminate the background caused by muons stopping in the scintillator itself; second, the presence of cesium iodide inside the gas target did not (unlike the experiments of [18] with plastic scintillators) lead to additional difficulties involved in ensuring the necessary purity of the hydrogen in the target.

Electrons and γ-rays were recorded by two detectors (γ1, γ2) with NaI(Tl) crystals 150 mm in diameter by 100 mm and four counters (e1-e4) with 70 × 30-mm stilbene crystals. The logic of the selection of events came down to the following. It was required that there be pulses from the γ-ray and electron detectors for 10 μsec after a muon was stopped in the gas. Moreover, during that time pulses were recorded from detector 7. Using the criterion of coincidence or anticoincidence of pulses from γ-ray or electron detectors with pulses from detector 7, we can vary the contribution of the electron or γ-components to the total spectrum of events, making possible a more accurate determination of the parameters of each component.

The main measurements were carried out with the mixtures $H_2 + 3\cdot10^{-5}$ Xe and $H_2 + 3\cdot10^{-5}$ Xe + 7% D_2 at a pressure of 3.92 MPa. Moreover, we also carried out measurements with H_2 for normalization and with an evacuated target for an independent determination of the background of random events. The time distributions of events recorded by γ-ray and electron detectors were analyzed with the aid of expressions of the form (1) and (2).

The values of $\lambda^{o}_{pp\mu}$ and $\lambda^{o}_{pd\mu}$ found by analyzing the experimental data are $(2.34 \pm 0.17)\cdot 10^6$ sec^{-1} and $(5.53 \pm 0.16)\cdot 10^6$ sec^{-1}, respectively (see Table 1). As seen from the data of Table 1 the measured values of $\lambda_{pp\mu}$ and $\lambda_{pd\mu}$ are in good agreement with the calculations of [22]. Table 1 also shows that the values of $\lambda^{o}_{pp\mu}$ and $\lambda^{o}_{pd\mu}$ found from the experiments with gaseous hydrogen do not differ from those obtained using liquid hydrogen.

Investigation of the μ-Catalysis of the Nuclear Reaction p + d ^{3}He + γ. The process of muonic catalysis of the p + d fusion reaction in an $H_2 + D_2$ mixture

$$d\mu + p \xrightarrow{\lambda_{pd\mu}} pd\mu \xrightarrow{\lambda_F^{pd}} \begin{cases} {}^3\mathrm{He}\,\mu + \gamma + 5.5\ \mathrm{MeV} & (3a) \\ {}^3\mathrm{He} + \mu + 5.5\ \mathrm{MeV} & (3b) \end{cases}$$

has interesting features.

TABLE 2. Weights of States of pdμ Molecules with Different Values of the Moment J and the Relative Values of the p + d Fusion Reaction Rate for Those States

J	Spin states of a dμ atom forming a pdμ molecule			Relative values of the fusion reaction $pd\mu \to {}^3He\mu + \gamma$
	$F_{d\mu} = 3/2$	$F_{d\mu} = 1/2$	statistical mixture of states with $F_{d\mu} = 1/2$ and $F_{d\mu} = 3/2$	
0	$a_1 = 0$	$b_1 = 0,25$	$C_1 = 0,083$	$d_1 = 1$
1	$a_2 = 0,195$	$b_2 = 0,36$	$C_2 = 0,25$	$d_2 = 0,86$
1	$a_3 = 0,180$	$b_3 = 0,39$	$C_3 = 0,25$	$d_3 = 0,14$
2	$a_4 = 0,625$	$b_4 = 0$	$C_4 = 0,417$	$d_4 = 0$

First, the rate λ_F^{pd} of the p + d reaction in a pdμ molecule, upon comparison with all other known values of the nuclear fusion reaction rate in muonic molecules, does not differ markedly (as to order of magnitude) from the muon decay rate λ_0 [4, 7, 8, 14]. This makes it possible to determine λ_F^{pd} directly from the shape of the time distribution of the products of the process (3).

Second, the yield W of the reaction (3) depends on the population of the states of the hyperfine structure (HFS) of the pdμ molecules. According to the theory of [8], the probability of the reaction (3) from an initial state corresponding to the parallel orientation of the proton and deuteron spins (total spin $S_{pd} = 3/2$) should be strongly suppressed. A pdμ molecule in a state with the orbital moment L = 0 has four HFS states with a total moment J = 2, 1, 1, 0. Different probabilities for $S_{pd} = 3/2$ and $S_{pd} = 1/2$, i.e., different p + d reaction rates, correspond to each state. Table 2 gives the weights of the HFS states of pdμ and the relative values of the fusion reaction rate for these states [8]. In accordance with Table 2 we shall henceforth denote the rates of the reactions (3a) and (3b) in the pdμ state with J = 0 as $\lambda_\gamma \equiv \lambda_1$ and $\lambda_\mu \equiv \lambda_2$ and their sum as $\lambda_F^{pd} = \lambda_1 + \lambda_2$.

As is seen from the data of Table 2 the population of the HFS states of pdμ depended strongly on the spin states of the dμ atoms. The transitions between the HFS levels of dμ atoms, therefore, should lead to a change in the yield of process (3) (the Gershtein–Vol'kenshtein effect). The transition from the upper spin state of a dμ atom with spin F = 3/2 to the lower state with F = 1/2 corresponds to an expected change in the yield W of process (3) by a factor of roughly 2.

The time distribution of γ rays from process (3) can be represented as

$$dn_\gamma/dt = \lambda_{pd\mu} \exp(-\lambda_0 t)\,[P_{3/2}(\lambda_{pd\mu},\ \lambda_F^{pd},\ \lambda_d;\ t) + P_{1/2}(\lambda_{pd\mu},\ \lambda_F^{pd},\ \lambda_d;\ t],$$

where the functions $P_{3/2}$ and $P_{1/2}$ correspond to fusion in pdμ molecules formed by dμ atoms with spins F = 1/2 and 3/2. These functions have the following form:

$$P_{3/2} = \frac{2}{3}\sum_{i=3} a_i d_i \lambda_1 \frac{\exp(-\lambda_{pd\mu}t) - \exp(-d_i\lambda_F^{pd}t)}{d_i\lambda_F^{pd} - \lambda_{pd\mu} - \lambda_d}; \qquad (4)$$

TABLE 3. Rate of the Nuclear Fusion Reaction in a pdμ Molecule and the Rate of Transition of a dμ Atom from the Upper Spin State to the Lower State (10^6 sec^{-1})

Source of data	λ_F^{pd}	$\lambda(3/2-1/2)$
Experiment		
Columbia Univ. [7]	0,305±0,010	7
Univ. of Vienna [23]	—	43±1
JINR 19	0,287±0,022	< 15 *
JINR [24]	—	40
Calculation		
Ref. [14, 25]	0,263	47

*This estimate was obtained with the assumption that under the conditions of the experiments of [19] (H_2 + 7%D_2, 4.12 MPa) the 3/2 → 1/2 transitions in dμ + d collisions are irreversible. It can be reduced if the possible incomplete thermalization of dμ atoms is taken into account.

$$P_{1/2}=\sum_{i=1} b_i d_i \lambda_1 \left\{ \frac{2}{3} \frac{[\exp-(\lambda_d+\lambda_{pd\mu})t]}{\lambda_d+\lambda_{pd\mu}-d_i\lambda_F^{dp}} + \frac{\exp(-\lambda_{pd\mu}t)}{d_i\lambda_F^{pd}-\lambda_{pd\mu}} - \right.$$
$$\left. - \frac{\left[\lambda_d-\frac{1}{3}(d_i\lambda_F^{pd}-\lambda_{pd\mu})\right]\exp(-d_i\lambda_F^{pd}t)}{(\lambda_d+\lambda_{pd\mu}-d_i\lambda_F^{pd})(d_i\lambda_F^{pd}-\lambda_{pd\mu})} \right\}. \quad (4)$$

In deriving Eq. (4) in accordance with the theories of [8, 14], we assumed that the 3/2 → 1/2 transitions can occur only in dμ + d collisions and we introduced the notation $\lambda_d = \lambda_d^0 \varphi C_D$ for the rates of such transitions; the values of a_i, b_i, and d_i are given in Table 2. The calculated values of λ_d^0 [12-14] are given in Table 3.

Since λ_d is proportional to C_D, by varying the deuterium concentration in the H_2 + D_2 mixture we can change the population of the HFS levels of pdμ and, therefore, the yield of the process (3). Such an effect was observed experimentally in [7] in which the value obtained for the ratio of yields $W(C_D = 0.25)/W(C_D = 0.007) = 1.17 \pm 0.01$ is in good agreement with early calculations of λ_d in [12].

The first (and thus far the only) measurements of the reaction rate for capture by a deuteron $\mu^- d \to nn\nu_\mu$ in gaseous hydrogen (H_2 + 5% D_2, 0.69 MPa) were completed in 1973 [11]. It must be said that it is very important to investigate this process both in order to measure the constants of μ capture in the simplest Gamow–Teller transition and in order to determine the parameters of the nn interaction. As we have already pointed out, however, the result obtained in [11] proved very difficult to explain within the framework of the existing theory since it was necessary to assume the existence of fast irreversible 3/2 → 1/2 transitions under the conditions of the experiment of [11].

The aim of the experiments conducted by our group [19] was to measure the absolute yield of process (3a) and the time distribution of γ rays from the reaction $pd\mu \to {}^3He\mu + \gamma$ in order to determine the rate of this reaction information about the spin states of dμ atoms in gaseous hydrogen. The measurements were carried out with a H_2 + 7% D_2 mixture at a pressure of 4.12 MPa, i.e., under conditions similar to those of the experiments of [11]. In order to investigate process (3a) we used the same apparatus that had been used to measure $\lambda_{pp\mu}$ and $\lambda_{pd\mu}$ (see Fig. 2). In the experiment we carried out two main exposures: with an H_2 + D_2 mixtures and an experiment with helium (background). The logic of the experiment consisted in selecting events recorded by the γ- and e-detectors in 10 μsec after stopping of a muon in the target.

The measured time distributions of γ rays from reaction (3a) were analyzed using Eq. (4), the values found in these experiments for the electron yield from the decay, and the experimentally measured γ-ray counting efficiency (see Table 3). As can be seen, the value obtained for λ_F^{pd} is in good agreement with the measurement of [7]. It would be interesting to compare the cross section for the reaction $pd\mu \to {}^3He\mu + \gamma$ with the cross section for the reverse process $\gamma + {}^3He \to p + d$ as well as with the cross section for the reaction $n + d \to t + \gamma$ at zero energy, but in order to do this it is necessary first to calculate the Coulomb barrier factor in pdμ.

The data we obtained on the yield and time distribution of γ rays from process (3a) are in agreement with the theoretically expected values for the statistical population of the HFS states of the molecule. It thus follows that contrary to the conclusion of Bertin et al. [11] the character of the population of the spin states of dμ atoms in gaseous hydrogen is nearly statistical.

Analysis of the time distributions of the γ rays with the aid of Eq. (4) made it possible to obtain data on the rate of the 3/2 → 1/2 transitions in collisions of dμ atoms with deuterons (at a confidence limit of 90%):

$$\lambda_d^0 < 15 \cdot 10^6 \text{ sec}^{-1}. \qquad (5)$$

The estimated value of λ_d^0 [Eq. (5)] is consistent with the data of the experiment of [7] and the calculations of [12] but is smaller than the result of present-day calculations [13, 14] ($\lambda_d^0 = 4.6 \cdot 10^7$ sec^{-1}).

When comparing the data of Eq. (5) with the theory we must bear in mind the following circumstance. Analysis of the experimental data using Eq. (4) implies that the 3/2 → 1/2 transitions in collisions of dμ atoms with deuterons are irreversible, and this may be the case only when their energy is lower than the energy of the hyperfine splitting by dμ atoms: Δε = 0.05 eV. However, under the conditions of our experiment, which were chosen with allowance for the possibility of a critical verification of the conclusions of Bertin et al. [11] as to the character of the population of the spin states of dμ atoms in gaseous hydrogen, the energy spectrum of dμ atoms could extend up to $\varepsilon_{d\mu} > \Delta\varepsilon$. At 300°K the mean energy of thermalized μ atoms is $\bar{\varepsilon}_{d\mu} \approx 0.04$ eV, i.e., is close to Δε. Moreover, because of the small cross section for thermalization in dμ + p collisions and the low density of the deuterium the thermalization of dμ atoms under the conditions of our experiments was most likely incomplete (according to estimates the average thermalization time is ~1 μsec, i.e., is comparable with the average lifetime $\tau_{d\mu} = [\lambda_0 + \lambda_{pd\mu}^0 \varphi (1 - C_D)]^{-1} \approx 1.3$ μsec). This means that besides 3/2 → 1/2 transitions the reverse 1/2 → 3/2 transitions could also occur. When these circumstances are taken into account the estimate given by Eq. (5) may be underestimated.

Conclusions as to the state of the problem of spin states of dμ atoms will be given at the end of the next section.

Measurement of the Residual Polarization of Negative Muons in Hydrogen. Investigation of the process of depolarization of negative muons in hydrogen is of interest from at least two points of view. One the one hand, the residual polarization P_μ is determined in great measure by the features of the cascade de-excitation of the muonic atom [26, 27] and, hence, measurement of P_μ makes it possible to obtain information about the relatively little-investigated initial stage in the life of the muonic atom. Moreover, the process of muon depolarization* in hydrogen is affected appreciably by various μ-atomic processes, the principal processes being spin-exchange collisions [4, 8, 14] of pμ atoms with protons and of dμ atoms with deuterons in the ground state. Thus, a new approach becomes possible to the study of these processes, including transitions between the HFS states of muonic hydrogen atoms. At the same time, unlike the yields of the μ-capture or μ-catalysis reactions, a decrease in the polarization of muons in spin-exchange collisions is observed regardless of whether or not these transitions are irreversible.

*Here and henceforth in speaking of negative muons we omit the word "negative."

Cascade depolarization occurs because of the spin–orbit $s-l$ interaction (s is the muon spin, l is the orbital moment) at those levels whose width Γ is much smaller than the fine splitting Δ, i.e., wherever the muon spin manages to complete many rotations around the total moment $j = s + l$. The radiation width is always smaller than the fine splitting (by a factor $\alpha^{-1} \approx 100$). Another mechanism of de-excitation, Auger ionization, dominates at the upper levels, where the corresponding width is $\Gamma_{Aug} \gg \Delta$, but its rate falls with a decrease in the principal quantum number n. Depolarization, obviously, occurs when $\Gamma_{Aug} \sim \Delta$. Since $\Delta \sim Z^4$ (Z is the atomic number) and Γ_{Aug} depends weakly on Z, this condition is satisfied at different values of the principal number $n = n_0$ for light and heavy atoms. As follows from [27], for the lightest mesic atoms $n_0 = 3$–4.

The residual polarization P_{s-l}, calculated with allowance for only the spin–orbit interaction, can be represented as a function of n_0 [27];

$$P_{s-l} \approx \frac{3}{20n_0^2}(n_0+6)(n_0-1). \tag{6}$$

From Eq. (4) we can see that for $n_0 = 3$–4 we have

$$P_{s-l} \approx 0.30. \tag{7}$$

An additional loss of polarization occurs because of the hyperfine s-I interaction (I is the nuclear spin). The residual polarization due to the hyperfine interaction for pμ and dμ atoms in a statistical mixture of HFS states is [28]

$$P_{s-I}^{stat}(p\mu) = 1/2; \quad P_{s-I}^{stat}(d\mu) = 11/27. \tag{8}$$

Thus, when a muon passes through an atomic cascade its polarization is expected to be

$$P_\mu^0 = \beta P_{s-l} P_{s-I} = (0.10 - 0.12), \tag{9}$$

where the values of P_{s-l} and P_{s-I} are found from Eqs. (7) and (8) and $\beta = 0.85$ [29] is the initial polarization of the muon beam.

Being in the ground state, the hydrogen atoms undergo exchange collisions [4, 8, 12, 30] (this refers to the exchange of a muon between two nuclei) with protons or deuterons, and this results in a further loss of polarization. An effective mechanism of depolarization is that of exchange collisions with a change in the total spin of the atom. When the energy of the atoms is lower than the energy of hyperfine splitting the only possible transitions are

$$p\mu\,(F=1) + p' \to p'\mu\,(F=0) + p; \tag{10a}$$

$$d\mu\,(F=3/2) + d' \to d'\mu\,(F=1/2) + d. \tag{10b}$$

In each collision (10a) the polarization is lost completely while in the collision (10b) the polarization decreases by roughly an order of magnitude.

Muon polarization is also lost in exchange collisions without a change in the total spin of the atom but with a reorientation of the spin, i.e., with a change in the projection on the direction of the initial polarization of the muon. In this case the polarization decreases on average by roughly a factor of two in each collision. As follows from [12, 30], the cross sections for exchange collisions with and without a change in the spin are of the same order of magnitude. Thus, as estimates of the expected values of the depolarization rate γ_d in exchange collisions we can take $\gamma_d(H_2) \sim \lambda_{1\to 0}$ and $\gamma_d(D_2) \sim \lambda_{3/2 \to 1/2}$; then, in accordance with the results of the calculations in [13, 14] we have

$$\gamma_d^0(H_2) \sim \lambda_{1\to 0}^0 = 1.3 \cdot 10^{10}\ \text{sec}^{-1}; \tag{11}$$

$$\gamma_d^0(D_2) \sim \lambda_{3/2\to 1/2}^0 = 4.7 \cdot 10^{7}\ \text{sec}^{-1}. \tag{12}$$

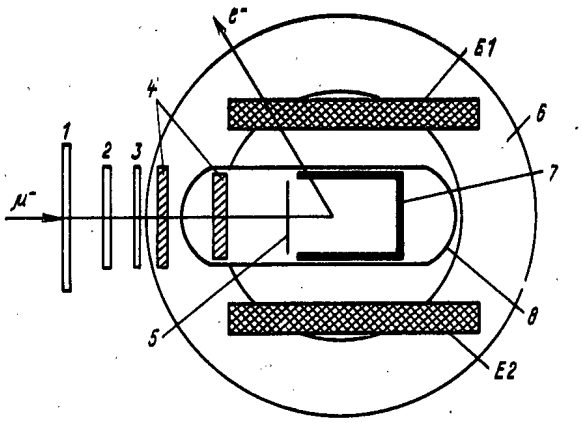

Fig. 3. Experimental setup for measuring [24] the residual polarization of negative muons in gaseous hydrogen: 1-3) muon detectors (plastic scintillator); 4) moderator; 5) CsI(Tl) detector of slow muons; 6) magnet; 7) CsI(Tl) detectors of muons and electrons; 8) target; E1 and E2 are electron detectors (plastic scintillator).

From Eqs. (11) and (12) it follows that rapid total depolarization (in roughly 10^{-9} sec at 3.92 MPa) is expected in protium. In deuterium the depolarization rate is substantially lower and should have a value $\gamma_d \approx 2.5 \cdot 10^6$ sec^{-1} at a pressure of 3.92 MPa. Before the experiments of our group [24] the residual polarization of muons had been measured [31, 32] only in liquid protium.

The experimental [31, 32] values of the residual polarization P_μ of negative muons in hydrogen and deuterium are presented below (in %):

Liquid H_2 [32]	3 ± 3
Liquid H_2 [31]	7 ± 4
H_2 at 3.92 MPa [24]	0.3 ± 0.9
D_2 at 3.92 MPa [24]	1.0 ± 0.9

We see that the accuracy of the earlier measurements of P_μ had been 3-4% and, therefore, definite conclusions about the depolarization cross section were difficult to make from a comparison of the experimental results of those investigations with the expected theoretical "initial" values (i.e., until the formation of a μ atom in the ground state) $P_\mu^0 \approx 10\%$.

Our goal was to measure P_μ not only in protium but also in deuterium with an accuracy several times better than in [31, 32] and, most important, under the conditions of gaseous hydrogen, making possible a sharp increase in the sensitivity of the data to the depolarization cross section.

In order to determine the residual polarization we employed the well-known μSR method (precession of the muon spin), which records and analyzes the time distribution of electrons from the decays of muons that have stopped in a certain volume placed in a magnetic field. The time distribution of electrons recorded in the plane of precession has the form

$$N_e(t) = B \exp(-\lambda t)[1 + A \exp(-\gamma t) \cos(\omega t + \psi)], \quad (13)$$

where λ is the rate of muon decay in the material (for hydrogen $\lambda = \lambda_0 = 4.55 \cdot 10^5$ sec^{-1}), γ_d is the rate of depolarization, $A = P_\mu/3$ and ω, respectively, are the amplitude and angular frequency of precession, ψ is the initial phase, and B is the normalization constant.

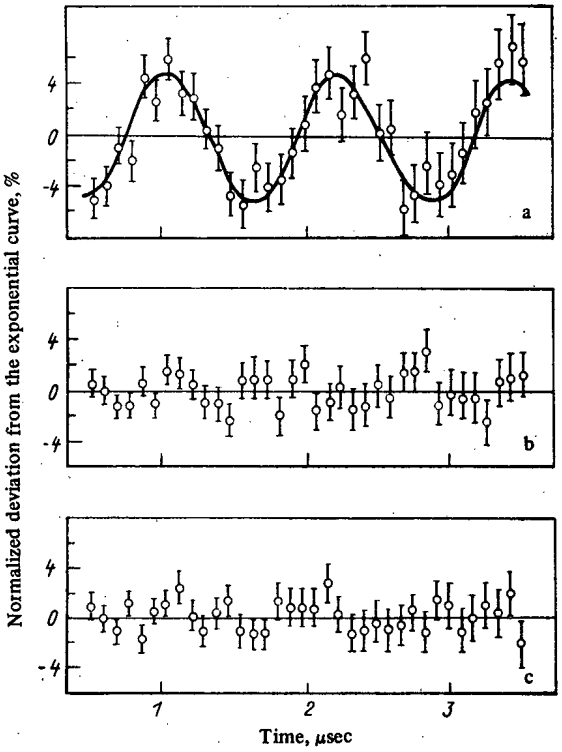

Fig. 4. Time distributions of electrons, measured in experiments with graphite for H = 70 Oe (*a*); with protium (b) and deuterium (c) for H = 140 Oe. Each distribution has been normalized to exp $(-t/\tau)$, where τ is the muon lifetime in carbon or hydrogen. The curve in Fig. 4a is a function of the form $y = A \cos \times (\omega t + \psi)$ with optimal values of the parameters A, ω, and ψ, found by computer.

For the chosen value H = 140 Oe (1 Oe = 79.57 A/m) the expected values of the precession frequency in protium and deuterium were

$$\omega\,(F_{p\mu}=1)=0.34\omega\mu=4.1\ \text{rad/}\mu\text{sec}; \tag{14}$$

$$\omega\,(F_{d\mu}=3/2)=0.30\omega_{\mu}=3.6\ \text{rad/}\mu\text{sec}, \tag{15}$$

where $\omega_{\mu} = 8.53 \cdot 10^4$ H (Oe) is the precession frequency for a free muon (rad/sec). The values of Eqs. (14) and (15) were obtained using the expressions found in [28] for the gryomagnetic ratios in the upper and lower spin states of the μ atom.

The experimental setup for measuring the residual polarization of muons in hydrogen is given in Fig. 3. As in our previous work, in the measurements we employed a gas target with internal CsI(Tl) scintillators. In the experiments we used ultrapure hydrogen (containing no more than 10^{-7} of impurities with Z > 1). The magnetic field was produced by Helmholtz coils with R = 42 cm. The spatial inhomogeneity and the time instability of the field strength did not exceed 1%. Electrons from decay were recorded by detector 7 [a CsI(Tl) cup] and two scintillation detectors E1 and E2 (350 × 250 × 60 mm).

During the measurements we carried out several experiments. The main experiments involved exposure with protium and deuterium (pressure 3.92 MPa) in a field H = 140 Oe. In order to check possible sources of systematic errors, we also carried out control measurements with graphite for which the amplitude and frequency of precession (Fig. 4) had been known earlier [29].

Upon analyzing the experimental data we established that the time distributions of electrons, obtained in experiments with protium and deuterium, are described well by a simple

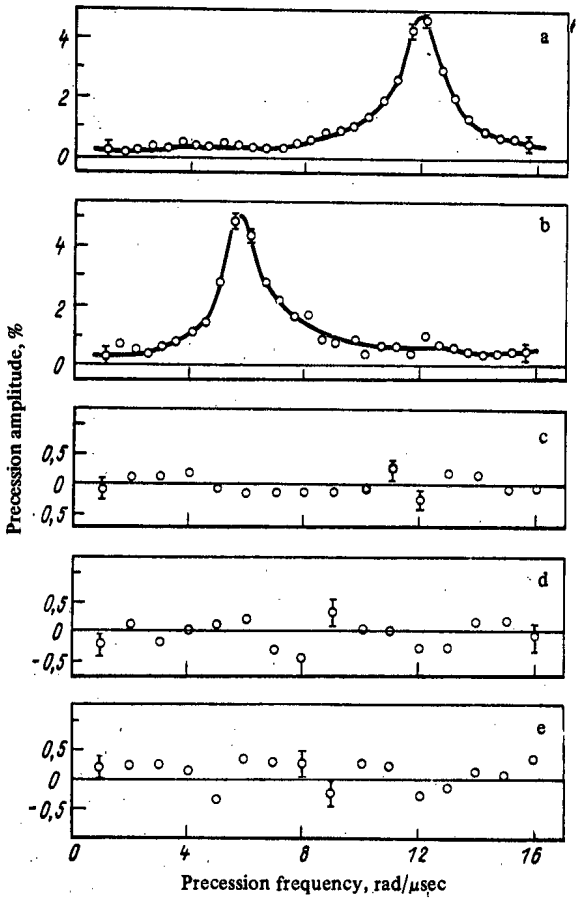

Fig. 5. Time distributions of electrons obtained in exposures with graphite with H = 140 Oe (a), H = 70 Oe (b), H = 0 (c); and with protium (d) and deuterium (e) for H = 140 Oe.

expression of the form $y = B \exp(-\lambda t) + C$. Thus, these data are not at variance with the assumption of zero residual polarization of muons in hydrogen. In the next stage of the analysis we compared the experimental distributions with the function

$$y = B \exp(-\lambda t)[1 + A \cos(\omega t + \psi)] + C, \tag{16}$$

i.e., with an expression of the form (13) for $\gamma_d = 0$. During the analysis we either independently varied all the parameters of Eq. (16) or we varied the parameters A, B, λ, and ψ for a number of successive fixed values of ω — so-called frequency analysis (Table 4 and Fig. 5). These data indicate that the values of the muon lifetime ($\tau_\mu = \lambda^{-1}$) in carbon and hydrogen are in agreement with the data of measurements in [33] while the values of the frequency of precession in graphite are in agreement with the expected values $\omega = \omega_\mu$ for H = 70 and 140 Oe. The accuracy of the determination of A, λ, and ω is also in agreement with the expected accuracy. This indicates the absence of appreciable systematic errors in the measurements.

From the data of Table 4 and Fig. 5 we can see that within the limits of experimental errors we do not observe the amplitude of precession in hydrogen and deuterium to exceed the average value $A \approx 0$. The values of the residual polarization P_μ of muons in hydrogen for the frequencies (14) and (15) are given above.

Further analysis gave estimates of the depolarization rate of muons in hydrogen, $\gamma_d(H_2)$, $\gamma_d(D_2) > 2 \cdot 10^6$ sec^{-1} (at a 90% confidence level), or for the density of liquid nitrogen

TABLE 4. Analysis of the Time Distributions of Electrons Using the Expression $y(t) = B \exp(-\lambda t)\,[1 + A\cos(\omega t + \psi)]$

Conditions of measurement	λ, 10^6 sec^{-1}	ω, rad/μ sec	A, %
Graphite, H = 140 Oe	0,492±0,002	11,8±0,2	4,9±0,2
Graphite, H = 70 Oe	0,494±0,002	5,8±0,3	5,1±0,2
H_2, $H = 140$ Oe	0,454±0,002	4,1	0,08±0,25
D_2, $H = 140$ Oe	0,455±0,002	4,8	0,28±0,25

$$\gamma_d^0(H_2) > 4\cdot 10^7 \text{ sec}^{-1}; \tag{17a}$$

$$\gamma_d^0(D_2) > 4\cdot 10^7 \text{ sec}^{-1}. \tag{17b}$$

If, in accordance with the theory of [26, 27], we assume that after an atomic cascade polarization is conserved at a 10-15% level, then the estimates (17a) and (17b) should be assumed to apply to the depolarization rate in the ground state of the μ atom, i.e., in spin-exchange collisions and, possibly, in collisions with hydrogen molecules with a change in their rotational state [14].

In order to compare the estimates (17) with the theoretical predictions we must use Eqs. (11) and (12). The results of comparison show that the value given by Eq. (17a) is consistent with the large calculated value (11) for the rate of spin-exchange collisions of p_μ atoms with protons. Data on the depolarization of muons in deuterium (17b) are consistent with the calculations of [13, 14] and the experiment of [23], which yielded the value

$$\lambda^0_{3/2\to 1/2} = (4.3 \pm 0.1)\cdot 10^7 \text{ sec}^{-1} \tag{18}$$

and are in poor agreement with earlier estimates [12].

Analyzing the whole body of data on the spin states of $d\mu$ atoms, we can make the following conclusions.

1. The conclusion of Bertin et al. [11] that fast irreversible $3/2 \to 1/2$ transitions exist under the conditions of their experiments (H_2 + 5% D_2, 0.69 MPa) does not find explanation in the theory [8, 14] and is not supported experimentally [19]. Accordingly, as before, major difficulties are encountered in interpreting the result of measurements of the rate of capture by a deuteron in [11].

2. The results of our measurements [24] of P_μ and of the experiment in [23] are in good agreement with the $\lambda_{3/2 \to 1/2}$ calculations in [13, 14], and our data [19] perhaps are not at variance with them.

3. New investigations, both theoretical and experimental, are necessary. Apparently, it makes sense once again to consider the reaction $p + d \to {}^3He + \gamma$ in $pd\mu$ and the process of the $3/2 \to 1/2$ transition. Of great interest is the mechanism, proposed in [14], of the $3/2 \to 1/2$ transition as a result of the interaction of the spin of a $d\mu$ atom with the orbital moment of H_2, D_2, or HD molecules, since this mechanism may turn out to be resonant in the energy of the $d\mu$ atom. It is of interest experimentally to measure the yield of the reaction $pd\mu \to {}^3He\mu + \gamma$ and the rate of the $\mu^- d \to nn\nu_\mu$ process in an $H_2 + D_2$ mixture as a function of the deuterium density.

Taking account of the concepts of the theory of muon depolarization in hydrogen, we can hope to measure the nonzero residual polarization and its time dependence in gaseous deuterium at a pressure $\lesssim$0.98 MPa. The statistical difficulties involved in obtaining a result of the necessary accuracy in experiments with a low-density gas can be overcome completely in meson factories [34]. Such measurements are important not only for ascertaining the mechanisms of inelastic interactions of atoms with nuclei and molecules but also from the point of view of the possible application of the μSR method in the investigation of various μ-atomic and μ-molecular processes.

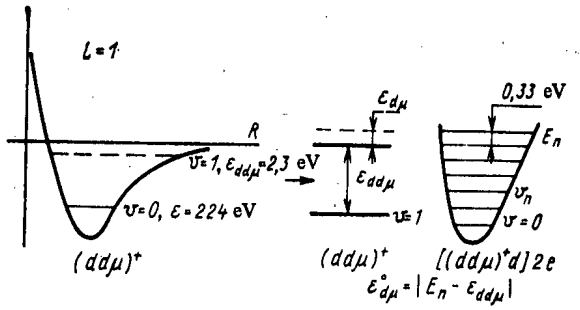

Fig. 6. Scheme of resonant formation of ddμ muonic molecules.

Investigation of the Resonant Mechanism of the Formation of Muonic Molecules of Deuterium. The history of the investigations (up to 1977) of resonant formation of ddμ molecules has been outlined at the beginning of this paper. By 1977 the hypothesis of the existence of a resonant mechanism of the formation of ddμ molecules [3, 5] had received serious theoretical substantiation. First, Vesman [10] presented a mechanism of ddμ formation, in which the dependence of the rate $\lambda_{dd\mu}$ of ddμ formation on the energy $\varepsilon_{d\mu}$ of the dμ atoms received a reasonable explanation. Second, it was established [14, 16, 35, 36] that a weakly bound state with the quantum numbers L = v = 1 and binding energy $\varepsilon^{1,1}_{dd\mu} = -1.91$ [16] exists in the ddμ system; this is a necessary condition for the realization of this mechanism.

The scheme of resonant formation of ddμ molecules

$$d\mu + D_2 \to [dd\mu,\ d,\ 2e]^{**}_{v} \tag{19}$$

is illustrated well in Fig. 6, which is cited from [14].

The kinetic energy $\varepsilon_{d\mu}$ of the dμ atom, along with the energy $\varepsilon^{1,1}_{dd\mu}$ liberated during the formation of ddμ, is transferred to the excitation of vibrations of a peculiar deuterium molecule in which one of the deuterons is replaced by a $(dd\mu)^+$ ion. Since the excitation energy of vibrations in the [ddμ, d, 2e] complex (for a given ν) and the binding energy of the ddμ molecule have specific values, the energy of the dμ atom at which process (19) is possible is also determined:

$$\varepsilon^0_{d\mu} = E_v - E_0 - |\varepsilon^{1,1}_{dd\mu}|. \tag{20}$$

Thus, process (19) is resonant in the energy of the dμ atom.† When the Maxwellian energy distribution of dμ atoms is taken into account we get the following dependence of the formation rate of ddμ molecules on the deuterium temperature (or on the energy $\varepsilon_{d\mu}$ = 3/2 kT of thermalized dμ atoms) [10, 36]:

$$\lambda^{res}_{dd\mu}(T) = aT^{-3/2}\exp(-\varepsilon^0_{d\mu}/kT), \tag{21}$$

where $\varepsilon^{\circ}_{d\mu}$ = 32 kT_0 is the position of the resonance and a is a normalization factor whose value depends on the level to which the transition (19) occurs.

In addition to the resonant mechanism, we must also take account of "ordinary" mechanisms of ddμ formation by means of E1 and E0 transitions with electron conversion of the D_2 molecule. According to [22], the rate of such transitions should be 10^4-10^5 sec^{-1} while the value of $\lambda^{res}_{dd\mu}$ may reach 10^6 sec^{-1} [36].

†Obviously, there exists a set of resonance energies $\varepsilon^{o,i}_{d\mu}$ corresponding to different excitation levels of the [ddμ, d; 2e] system, the distance between which, however, is large (ΔE ≈ 0.3 eV) and corresponds to the temperature range T ≈ 3000°K. Moreover, Eq. (20) has not taken account of the effect of hyperfine splitting [37] in the dμ atom and the ddμ molecule.

The position of the resonance ($\varepsilon^{\circ}_{d\mu}$ or T_0) can be predicted with an error ~0.05 eV (which is determined by the error of the calculation of $\varepsilon^{1,1}_{dd\mu}$), which corresponds to the indeterminacy of T_0 (~500°). Taking the form of the expected function $\lambda_{dd\mu}(T)$ into account, we could expect to find T_0 experimentally with an error of ~10°K, which corresponds to an energy of ~1 meV.

Thus, experimental verification of theoretically predicted resonant nature of ddμ formation was of interest not only in order to ascertain the mechanism of μ-molecular processes but also to make a precise determination of the energy of the levels of μ-molecular systems. We recall that the scale of the energy of levels of μ-atomic systems is determined by the value $1/2\ m_\mu\alpha^2$, i.e., $6\cdot10^3$ eV, while the binding energy of "ordinary" levels of μ molecules is ~10^2 eV.

The purpose of our measurements [20] was to determine $\lambda_{dd\mu}$ in the deuterium temperature range 120–400°K, which corresponds to an energy $\varepsilon_{d\mu}$ = 0.015–0.050 eV of thermalized dμ atoms.

On the basis of the data from previous measurements of $\lambda_{dd\mu}$ in liquid [9] and in gaseous deuterium at T = 240 and 300°K [5] we could expect $\lambda_{dd\mu}(T)$ to have a maximum in, or close to, the temperature range investigated.

The method used to determine $\lambda_{dd\mu}$ was that of measuring the yield and the time distribution of neutrons (with an energy E = 2.5 MeV):

$$dd\mu \xrightarrow{\lambda_F^{dd}} \begin{cases} {}^3\mathrm{He} + n + \mu + 3{,}3\ \mathrm{MeV}; & (22a) \\ t + p + \mu + 4{,}0\ \mathrm{MeV}. & (22b) \end{cases}$$

Once again we used a gas target with scintillators placed inside it (see Fig. 2, counters 6 and 7) to record muon stoppings. Neutrons from reaction (22a) and electrons from μ decay were recorded by scintillation detectors with stilbene crystals measuring 70 mm in diameter ×30 mm.

It should be pointed out that the arrangement with the gas target was used by us earlier [21] to measure $\lambda_{dd\mu}$ at T = 300°K back in 1974. Those were the first measurements of the rate of process (19) by an electronic technique; in those experiments for the first time we managed to obtain an experimental estimate for the rate λ_F^{dd} of the d + d reaction in the ddμ molecule: $\lambda_F^{dd} > 10^6\ \mathrm{sec}^{-1}$. The value of $\lambda_{dd\mu}$ was found on the basis of measurements of the neutron yield from reaction (22a) using the calculated value of the neutron detection efficiency and turned out to be consistent with those measured earlier [5] in a diffusion chamber.

A distinctive feature of the measurements in [20] was the use of a gas target with internal scintillators for investigations over a wide range of temperatures. The main difficulties which had to be overcome involved ensuring the necessary parameters of the detectors with internal scintillators as well as with maintaining the hermeticity of the target and the necessary purity of the deuterium filling it.

In order to separate the neutrons and γ rays we made use of the difference in the shape of the light pulse in stilbene for electrons and protons. For each neutron detector we measured the amplitude of two signals, which were proportional to the total area A_Σ of the light pulse and its "fast" part A_f, respectively. In the two-dimensional distribution (A_Σ, A_f) the neutron and electron events are located in two overlapping regions. The events due to the detection of neutrons from reaction (22a) should be projected onto the A_Σ axis in the form of a characteristic stepped spectrum with a limit corresponding to the energy E_n = 2.5 MeV. Figure 7 shows the distribution (A_Σ, A_f) obtained in an exposure with deuterium at T = 250°K.

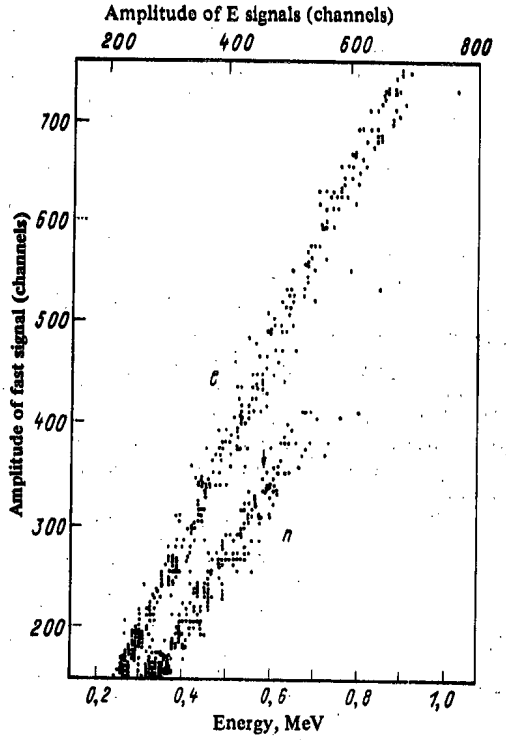

Fig. 7. Two-dimensional distribution (A_f, A_Σ) for one neutron detector. The arrow indicates the position corresponding to the limit of the spectrum for a neutron energy E_n = 2.5 MeV from reaction (22a).

The temperature range investigated wa divided into two overlapping subranges: in the subrange from −160 to −20°C we used a plastic scintillator in counters 6 and 7 (see Fig. 2; experiment 2); in the subrange from −60 to +110°C we used a CsI(Tl) scintillator (experiment 2). In each experiment we carried out five main exposures with deuterium, differing as to the target temperature. The temperature was changed in steps of 30-40°.

The neutron background was determined in exposures with a target filled with helium to a pressure equivalent to the deuterium pressure in the main exposures as far as the number of muon stoppings was concerned. The background measurements were carried out at a different temperature. The contribution of the neutron background was a maximum (20%) at the lowest temperature.

For each exposure with deuterium the time distributions of neutrons was analyzed with the aid of the expression

$$\frac{dN_n}{dt} = \frac{N_\mu \eta_n \lambda^0_{dd\mu}\varphi\lambda^{dd}_F}{2(\lambda^0_{dd\mu}\varphi+\lambda^{dd}_F)}\{\exp(-\lambda_0 t)-\exp[-(\lambda_0+\lambda^0_{dd\mu}\varphi+\lambda^{dd}_F)t]\}, \quad (23)$$

which was derived with allowance for the regeneration of muons in reaction (22).* Here, N_μ

*In the derivation of Eq. (23) we assumed that the coefficient of "sticking" of a muon to helium in reaction (22) $\omega_{dd} = \frac{dd\mu \to {}^3\mathrm{He}\,\mu + n}{dd\mu \to {}^3\mathrm{He} + n + \mu}$ is zero. In the general case the expression for dN_n/dt has the form $A[\exp(-\gamma_1 t) - \exp(-\gamma_2 t)]$, where

$$\gamma_{1,2} = \frac{1}{2}[(2\lambda_0 + \lambda^0_{dd\mu}\varphi + \lambda^{dd}_F) \pm \sqrt{(\lambda^{dd}_F + \lambda^0_{dd\mu}\varphi)^2 - 2\lambda^0_{dd\mu}\varphi\lambda^{dd}_F\omega_{dd}}].$$

If the value ω_{dd} = 0.14 ± 0.01 obtained in recent measurements [38] is used and if it is noted that $\lambda^0_{dd\mu\varphi} \leq 0.1\lambda_0$ under the conditions of our experiments, then it is easy to see that γ_1 and γ_2 differ from the corresponding exponents in Eq. (23) by no more than 1%.

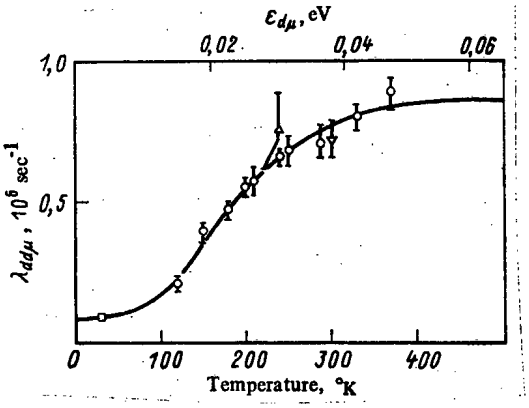

Fig. 8. Experimental function $\lambda_{dd\mu}(T)$: □) measurements of [9]; Δ, ▽) experiment of [5] and [21]; ○) measurements of [20]; —) function of the form of Eq. (24) with optimal values of the parameters found by computer.

is the number of muon stoppings in deuterium, η_n is the detection efficiency for neutrons from reaction (22a), and φ is the relative deuterium density. From an analysis of the time distributions we obtained the lower limit of the reaction rate $\lambda_F^{dd} > 9\lambda_0$, which is consistent with the theory [39].

The expression for the neutron yield in the interval of measurements (t_1, t_2) is obtained by integrating Eq. (23),

$$N_n = N_\mu \eta_n \frac{\lambda^0 d\, d\mu \varphi}{2\lambda_0} [\exp(-\lambda_0 t_1) - \exp(-\lambda_0 t_2)]$$

(we have taken account of the fact that $\lambda_F^{dd} >> \lambda_0$), and the analogous expression for decay electrons has the form $N_e = N_\mu \eta_e [\exp(-\lambda_0 t_1) - \exp(-\lambda_0 t_2)]$, where η_e is the detection efficiency for electrons, whereupon

$$\lambda^0_{dd\mu} = \frac{2\lambda_0}{\varphi} \frac{N_n}{N_e} \frac{\eta_e}{\eta_n} = \text{const} \frac{N_n}{N_e}.$$

The values of N_n/N_e found experimentally for different values of the temperature were approximated by $(N_n/N_e)_m = \text{const} > \lambda_{dd\mu}(T_m)$, where in accordance with [36]

$$\lambda_{dd\mu}(T) = \lambda_1 + \lambda_2 T + aT^{-3/2} \exp(-\varepsilon^0_{d\mu}/kT). \tag{24}$$

In this expression the terms λ_1 and λ_2 make allowance for the contribution of nonresonant mechanisms to the formation of ddμ molecules. For absolute normalization, the values of $\lambda_{dd\mu}$ measured in [5, 9, 21] were incorporated into the analysis.

The results of analysis of the experimental data are presented in Fig. 8. It can be seen that our results are in good agreement with predictions based on a consideration of the resonant mechanism of the formation of ddμ molecules and they confirm the existence of this mechanism. For the position of the resonance we found the value

$$\varepsilon^0_{d\mu} = (0.050 \pm 0.003) \text{ eV}, \tag{25}$$

while for the extreme value of the rate of formation

$$\lambda_{dd\mu}(\varepsilon^0_{d\mu}) = (0.85 \pm 0.11) \cdot 10^6 \text{ sec}^{-1}. \tag{26}$$

As we see from Eq. (25) the experimental accuracy of the determination of $\varepsilon^{0}_{d\mu}$ was 3 MeV. The other terms (E_ν and E_0) of Eq. (20) can be calculated with roughly the same or better accuracy. It thus follows that the investigation of the characteristics of the resonant formation of ddμ molecules makes it possible for the energy of the level with L = v = 1 to be determined precisely. It is important to calculate $\varepsilon^{1,1}_{dd\mu}$ with an error ~1 MeV, which would make it possible, by comparing the calculations with experiment, to find the contributions to that energy from interactions, in particular vacuum polarization, which are in addition to the Coulomb interaction. According to [40], the expected value of this contribution is 10 MeV.

The results of measurements of $\lambda_{dd\mu}$ [5, 9, 20, 21] were analyzed by us in [20] taking into account the existence of one resonance whose position was determined from Eq. (25). As can be seen from Fig. 8, in this case it was possible to get a fair description of all the available experimental data for $\lambda_{dd\mu}$. In actual fact, however, because of the presence of hyperfine splitting [37] of the ground state of the dμ atom and of the ddμ state with L = v = 1 instead of one resonance condition (20) it is necessary to account of several such relations which correspond to transitions from states with $F_{d\mu}$ = 3/2, 1/2 to states of the ddμ molecule with a total spin $S_{dd\mu}$ = 3/2, 1/2. In accordance with this, instead of one resonant dependence $\lambda^{res}_{dd\mu}(T)$ it is necessary to consider several functions $\lambda^{res,i}_{dd\mu}(T)$, each of which has the form of Eq. (21) and differs from others by the position of the resonance (T^{i}_{0}). The contribution of each of these components to the total value of $\lambda_{dd\mu}$ is determined by the population of the spin states of the dμ atoms at the time of the formation of the ddμ molecules and, hence, $\lambda_{dd\mu}$ should depend not only on the temperature but also on the deuterium density. This effect was observed in the experiment of [23] which was carried out at T = 34°K and a deuterium pressure of 1.57, 3.14, and 6.28 MPa. Taking the time dependence of the neutron yield from reaction (22a), Breunlich et al. [23] obtained the value (18) for the rate of the transition $F_{d\mu}$ = 3/2 → $F_{d\mu}$ = 1/2. The experiment of [23] has not yet been completed and Breunlich et al. propose also to measure the temperature dependence $\lambda_{dd\mu}(T)$.

As for other work done recently, we should mention the experiment of [38]. The use of an original procedure (pulsed ionization chamber) enabled Balin et al. to determine the coefficient for sticking of a muon to helium in the reaction (22a) with good accuracy and to obtain the relation

$$\omega_{dd}=\frac{dd\mu\to{}^{3}\mathrm{He}\mu+n}{dd\mu\to{}^{3}\mathrm{He}+n+\mu}=0.14\pm0.01.$$

Analysis of all results now available from investigations [5, 9, 20, 21, 23] of the process by which the system is formed permits the conclusion that these data support the theory of resonant formation of ddμ molecules. For reliable determination of all the parameters that specify the resonant formation of ddμ molecules it is important to measure the temperature dependence of $\lambda_{dd\mu}$ for different values of the deuterium density.

Investigation of μ Catalysis of the Fusion of Deuterium and Tritium Nuclei. Experimental confirmation [20] of the conclusions of the theory [14, 35, 36] concerning the resonant formation of ddμ molecules was a serious argument in favor of the predictions [35, 36] that an analogous, but much more intense (by 2-3 orders of magnitude) resonance exists in the cross section for the formation of dtμ molecules. The scheme of the processes initiated by negative muons in a D_2 + T_2 mixture is given in Fig. 9. Once the dtμ system is formed the fusion reaction

$$dt\mu \xrightarrow{\lambda_F^{dt}} \begin{cases} {}^{4}\mathrm{He}+n+\mu+17.6\ \mathrm{MeV}\ ; & (27a)\\ {}^{4}\mathrm{He}\,\mu+n+17.6\ \mathrm{MeV} & (27b)\end{cases}$$

occurs in it rapidly (10^{12} sec^{-1} [41]); in one channel of this reaction the muon is liberated while in the other it is "stuck" to helium.

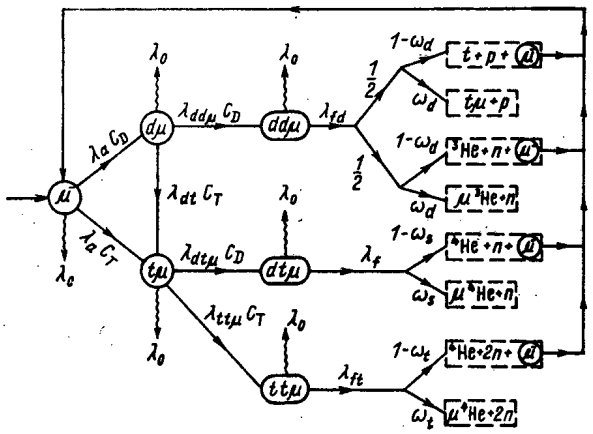

Fig. 9. Scheme of processes initiated by negative muons in $D_2 + T_2$.

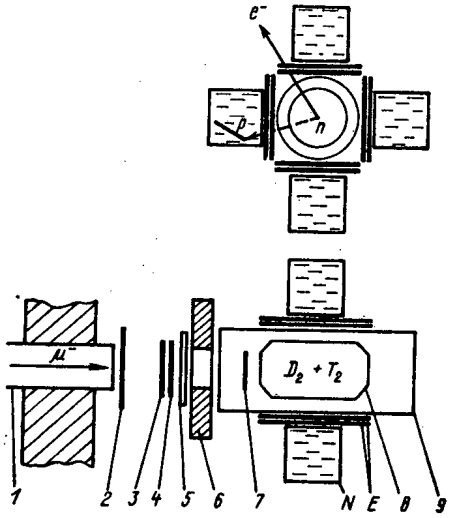

Fig. 10. Experiment [48] to detect and investigate μ catalysis of the d + t reaction: 1) muon channel; 2, 3, 4, 7) scintillation muon detectors; 8) gas target; 9) vacuum jacket; 1N-4N) neutron detectors (NE-213, volume 10^3 cm^3); E1-E8) scintillation electron counters.

Muonic catalysis of the reaction (27) and its possible use for practical purposes [42] have been discussed in detail in a number of reviews [43-46]. According to the theory it is expected that one muon in a deuterium-tritium mixture can initiate ~100 cycles of the reaction (27) and thus release an energy of ~2 GeV. In order to ascertain whether effective (multiple) μ catalysis of the d + t reaction is possible it is necessary experimentally to determine the parameters of many μ-atomic and μ-molecular processes [45]. In this problem, however, it is possible to isolate three main conditions: The formation rate of dtμ molecules ($\lambda_{dt\mu}$) and the rate of muon capture from deuterium by tritium (λ_{dt}) should be sufficiently high ($\lambda^{0}_{dt\mu}$, $\lambda^{0}_{dt} > 10^{8}$ sec^{-1}) while the probability of a muon "sticking" to helium, on the other hand, should be low ($\omega_s \lesssim 0.01$). Theoretically, all of these conditions should be satisfied [14, 35, 47].

Experimentally, μ-atomic and μ-molecular effects in a deuterium-tritium mixture (as well as in pure tirtium) had not been studied at all until 1978 (the beginning of the experiments of our group [48]). The aim of the measurements [48] was to determine $\lambda_{dt\mu}$ and λ_{dt} and to try to find the parameters of $\lambda_{dt\mu}(T)$. To this end we decided to use a high-pressure gas target (relative gas density $\varphi \approx 0.1$), filled with a $D_2 + T_2$ mixture at different relative deuterium and tritium contents.

The experimental arrangement for the investigation of catalysis of the d + t reaction is shown in Fig. 10. Its main part consisted of a gas target and neutron detectors (1N-4N). The process (27) was identified by detecting neutrons with an energy E_n = 14 MeV, correlated with stoppings of muons in the target.

Two major problems had to be solved because a large quantity of radioactive tritium (5000 Ci; 1 Ci = $3.700 \cdot 10^{10}$ Bq) was used in the experiments. One of them involved the observance of special, more stringent safety measures to ensure that the target remained leakproof. The second problem was that of suppressing the intense background (neutrons from capture in iron and random coincidences) owing to the large number of muon stoppings in the target walls, this number being 2-3 orders of magnitude larger than the number of stoppings in the gas. Since they can be "irradiated" by β rays from the tritium, scintillators inside the target to record stoppings in the gas cannot be used in order to suppress that background. The following measures were undertaken to discriminate the background:

a) A logic of ternary delayed μ–n–e coincidences was used, i.e., it was required that in the 10 μsec following a muon stopping there at first be a signal of detection of a neutron from the reaction (27), followed by detection of an electron from a μ decay;

b) only those events associated with the detection of neutrons 1 μsec after a muon stopping [muon lifetime in iron τ_μ(Fe) = 0.2 μsec] were selected;

c) neutrons and γ rays (electrons) were separated according to the shape of the light pulse in the scintillator of the neutron detector.

For the neutron detection we employed detectors with an original design with an NE-213 scintillator (volume 1 liter). For each detector we measured the recording time of an event and the amplitude of two pulses, one of which (A_f) was proportional to the intensity of the "fast" part of the light pulse while the other (A_s) was proportional to the intensity of its "slow" component. Joint analysis of the amplitudes A_f and A_s permitted separation of the neutrons from the γ rays and electrons. Figure 11 shows a two-dimensional distribution (A_f, A_s) measured in an exposure with a $D_2 + T_2$ mixture. An idea of the clearcut identification of the process (27) under investigation can be had from Fig. 11.

The electron detectors E1-E8 (see Fig. 10) consisted of four telescopes, used in "fast" $\overline{NE}$ anticoincidences during detection of neutron events and in delayed μ–n–e coincidences during detection of an electron from a μ decay, following a neutron from reaction (27).

During the experiment we carried out 14 exposures, which differed as to the temperature of the $D_2 + T_2$ gas mixture or the deuterium (C_D) contents in them. The relative tritium content varied from 0.8 to 3%. The temperature range investigated was 93-613°K. For control and normalization we also carried out measurements with pure deuterium and with an evacuated target.

The experimental data were analyzed using expressions for the yield and time distribution of neutrons from the d + t reaction obtained in [49], according to which at a mixture pressure of 0.49-9.81 MPa and a tritium concentration $C_T \leq 0.5$ the yield of reaction (27) is

$$Y_n = \frac{\lambda_{dt\mu} C_D C_T (\lambda_0 + \lambda_{dt})}{\lambda_0 (\lambda_0 + \lambda_{dt} C_T + \lambda_{dt\mu} C_D^2)}, \quad (28)$$

while the time distributions are

$$\frac{dY_n}{dt} = \frac{\lambda_{dt\mu} C_D C_T}{\lambda_{dt} C_T + \lambda_{dt\mu} C_D^2} [\lambda_{dt} \exp(-\lambda_1 t) + C_D (\lambda_{dt\mu} C_D - \lambda_{dt}) \exp(-\lambda_2 t)], \quad (29)$$

where

$$\lambda_1 \approx \lambda_0, \lambda_2 = \lambda_0 + \lambda_{dt} C_T + \lambda_{dt\mu} C_D^2, \quad \lambda_{dt\mu} = \lambda_{dt\mu}^0 \varphi, \lambda_{dt} = \lambda_{dt}^0 \varphi.$$

During the preliminary analysis we compared the values $Y_n^{exp} = N_n/N_e$, where N_n and N_e are the numbers of neutrons and electrons, respectively, which had been obtained for the experimental yield of the reaction (27) with different exposures.

In this case we establish that:

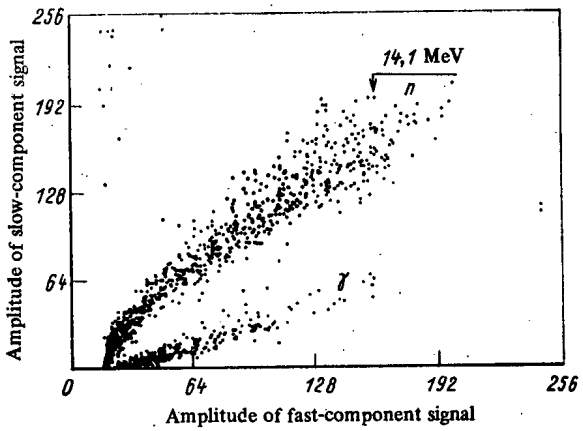

Fig. 11. Two-dimensional distribution (A_f, A_s) for a neutron detector measured in an exposure with $D_2 + T_2$.

a) The values of Y_n^{exp} remain practically constant in the temperature range 93-613°K;

b) the relative neutron yield does not change when only the deuterium content in the $D_2 + T_2$ mixture is varied and, on the other hand, varies roughly in proportion to the tritium content (C_T) in the mixture. As follows from Eq. (28), such laws in the variation of the neutron yield could be explained by the fact that under our experimental conditions $\lambda^0_{dt\mu\varphi} C_D >> \lambda_0$. The nature of the time distributions of neutrons is also consistent with that expected [49] for a high value of $\lambda_{dt\mu}$. For each exposure such a distribution, in accordance with Eq. (29), can be represented as the sum of two exponential functions with exponents $(-\lambda_1 t)$ and $-\lambda_2 t$, where $\lambda_1 \approx \lambda_0$ and $\lambda_2 >> \lambda_0$.

The complete analysis consisted of comparing the experimental time distributions of neutrons with an expression of the form (29), using the method of least squares. For absolute normalization we used the calculated value of the detection efficiency for 14-MeV neutrons. As a result of the analysis we found (at a 90% confidence level) the values of the rate of stripping of a muon from deuterium by tritium

$$\lambda^0_{dt} = (2{,}9 \pm 0{,}4) \cdot 10^8 \text{ sec}^{-1} \tag{30}$$

and the formation rate of dtμ molecules

$$\lambda^0_{dt\mu} > 10^8 \text{ sec}^{-1}. \tag{31}$$

The value of λ^0_{dt} given in Eq. (30) is in good agreement with those calculated in [14]. For $\lambda_{dt\mu}$ we obtained only the lower limit (31). This is explained, in accordance with Eq. (28), by the insensitivity of the neutron yield from reaction (27) to $\lambda_{dt\mu}$ for higher values $\lambda^0_{dt\mu} C_D >> \lambda_0$.

The large value found for $\lambda_{dt\mu}$ substantially exceeds the known formation rates of other muonic molecules (ppμ, pdμ, and ddμ) and is in agreement with calculations [36] carried out on the basis of a consideration of the resonant mechanism of dtμ formation. Thus, the existence of this mechanism, which we had earlier established for ddμ molecules, is also confirmed for dtμ molecules.

On the basis of the resonant nature of the process of formation of the dtμ system, one would expect a considerable variation in the yield of neutrons from reaction (27) as a function of the temperature of the $D_2 + T_2$ mixture. The measured neutron yield, however, in fact does not vary (within the limits of the measuring error of ~10%) in the range 93-613°K investigated.

This fact can be explained as follows.

1. Even within the framework of a simple resonance dependence of the form (21) the value of $\lambda_{dt\mu}$, which varies with the temperature, can remain fairly large so that at all temperatures in the range 93-613°K we have $\lambda^{0}_{dt\mu\varphi}C_D \gg \lambda_0$. In this case (and with the condition that $\lambda^{0}_{dt\varphi}C_T \approx \lambda_0$) the yield of neutrons from reaction (27) is insensitive to $\lambda_{dt\mu}$ according to Eq. (28).

2. Muonic $t\mu$ atoms, obtained in the stripping process $d\mu + t \to t\mu + d$ (the dominant channel of their formation in a $D_2 + T_2$ mixture when $C_T \ll C_D$) with an initial energy of 19 eV, cannot manage to slow down to thermal energy during their short lifetime $\tau_{d\mu} \approx (\lambda^{0}_{dt\mu\varphi}C_D)^{-1} \ll \lambda_0^{-1}$. In this case resonant formation of $dt\mu$ molecules takes place from the intermediate energy of $t\mu$ atoms with excitation of different vibration levels of the [$dt\mu$, d, 2e] system and, obviously, is weakly sensitive to the temperature of the $D_2 + T_2$ mixture.

It is important to emphasize that in both cases the maximum value of $\lambda^{0}_{dt\mu}$ can substantially exceed the estimate (31).

Comparison of the experimental data with the predictions of the theory [35, 45] of the possibility of multiple catalysis of the d + t reaction (with a multiplicity of ~100) in a deuterium-tritium mixture shows that two of the three principal conditions necessary for this possibility to be realized are satisfied: λ^{0}_{dt} and $\lambda^{0}_{dt\mu}$ are indeed fairly large. It is extremely important to check the third condition, viz., to measure the coefficient of "sticking" of a muon to helium reaction (27b). The theory predicts that $\omega_s \approx 0.01$ [47]. Besides these main characteristics it is important also to determine other parameters of the process of μ catalysis in a $D_2 + T_2$ mixture [45], e.g., the rate of formation of $tt\mu$ molecules, the rate of the nuclear reaction $tt\mu \to {}^4He + 2n + \mu$, and the probability of a muon "sticking" to a ^4He nucleus in this reaction.

The authors express their profound gratitude to L. I. Ponomarev who read the manuscript of this paper and made a number of valuable comments.

Note Added in Proof. After the manuscript of this paper had been sent to the editors, the Third International Conference on Emerging Nuclear Systems was held in Helsinki (June 6-9, 1983) and new data [50] were presented there on the experimental investigation of μ catalysis.

A group of U.S. physicists at the Los Alamos meson factory investigated the process (27) of μ catalysis of the nuclear reaction d + t ^4He + n + 17.6 MeV in a deuterium-tritium mixture with a high density ($\varphi = 0.6$). During the experiment the temperature of the $D_2 + T_2$ mixture and the relative tritium content were varied over wide limits (T = 100-530°K and C_T = 0.1-0.9). As in our experiments [48], neutrons with an energy of 14.1 MeV were recorded. Analysis of the experimental data enabled the U.S. physicists to obtain the following principal results (the notation is the same as in the text proper):

$$\lambda^{0}_{dt} = (2.8 \pm 0.1)\cdot 10^{6}\,\text{sec}^{-1}; \tag{32}$$

$$\begin{aligned} \lambda^{0}_{dt\mu-d} &= (6.9 \pm 0.4)\cdot 10^{8}\,\text{sec}^{-1}\ (534\ ^\circ\text{K}), \\ \lambda^{0}_{dt\mu-t} &= (3.0 \pm 0.3)\cdot 10^{8}\ \text{sec}^{-1}\ (534\ ^\circ\text{K}), \\ \omega_s &= (7.6 \pm 0.5)\cdot 10^{-3}, \end{aligned} \tag{33}$$

where $\lambda_{dt\mu-d}$ and $\lambda_{dt\mu-t}$ denote the rate of formation of $dt\mu$ molecules in collisions of a $t\mu$ atom with D_2 and DT molecules, respectively.

As can be seen from a comparison of Eqs. (30)-(31) and (32)-(33) good agreement is observed between the results obtained earlier by our group [48] and the new, more exact data. The coefficient of muon sticking to helium (ω_s), which determines the maximum possible (average) number of cycles of the d + t reaction initiated by one muon, has been measured for the first time. The data from the Los Alamos experiment indicate that at T = 534°K and an optimal deuterium/tritium ratio ($C_D = C_T = 0.5$) one muon initiates an average of 90 ± 9 reactions (27).

A group at the B. P. Konstantinov Institute of Nuclear Physics of the Academy of Sciences of the USSR, Leningrad (LIYaF AN SSSR), has completed an experiment on catalysis of the d + d fusion reaction in gaseous deuterium at a pressure of 8.98 MPa and a temperature T ≈ 300°K. Charged products from the reaction (22) were detected. The group measured the ratio $\frac{W(dd \to {}^3\mathrm{He}\, n)}{W(dd \to tp)} = 1.39 \pm 0.04$, or the probabilities of reactions (22a) and (22b) in ddμ, the coefficient of muon sticking to a ^{3}He nucleus formed in reaction (22a) ($\omega_d = 0.126 \pm 0.004$), and the rate of formation of ddμ molecules [$\lambda^{\circ}_{dd\mu}$ (T ≈ 300°K) = 2.76 ± 0.09)·10^6 sec^{-1}]. In accordance with the data obtained earlier [20] as given by Eq. (26) and with the theoretical predictions made on the basis of a consideration of the resonant mechanism of ddμ formation, the rate of ddμ formation in gas at T ≈ 300°K measured by the LIYaF group turned out to be several times (roughly 30 times) that in liquid deuterium at T = 30°K [9]. The value of $\lambda^{\circ}_{dd\mu}$ measured by the group is more than three times the value we obtained (26) at the same temperature (300°K) but at half the pressure.

As for other data presented at the conference, we point out the results of an experiment carried out at the Swiss Institute of Nuclear Research (Villingen) by a group of physicists from the University of Vienna. On the basis of measurements of the yield of the reaction pdμ → ^{3}He + γ + 5.5 MeV in a mixture of liquid hydrogen and deuterium they were able to determine the rate of the process dμ (F = 3/2) + p → dμ (F = 1/2) + p [$\lambda^{\circ}_p = (4.7 \pm 0.2)\cdot 10^6$ sec^{-1}] and, in accordance with our data [19], to arrive at the conclusion that in a gaseous mixture of hydrogen and deuterium ($\varphi_H \lesssim 0.05$, $\varphi_D \lesssim 0.005$) the population of the spin states of dμ atoms should be nearly statistical.

LITERATURE CITED

1. L. Alvarez et al., Phys. Rev., 105, 1127 (1957).
2. F. Frank, Nature, 160, 525 (1947).
3. Ya. B. Zel'dovich, Dokl. Akad. Nauk SSSR, 95, 493 (1954).
4. Ya. B. Zel'dovich and S. S. Gershtein, Usp. Fiz. Nauk, 71, 581 (1960).
5. V. P. Dzhelepov et al., in: Proceedings Twelfth International Conference on High-Energy Physics, Moscow, (1966), p. 878; V. P. Dzhelepov et al., Zh. Eksp. Teor. Fiz., 50, 1235 (1966).
6. V. P. Dzhelepov, At. Energ., 14, No. 1, 27 (1963).
7. E. Bleser et al., Phys., Rev., 132, 2679 (1963).
8. S. Gerstein and L. Ponomarev, in: Muon Physics, Vol. III, Academic Press, New York (1975), p. 141.
9. J. Fetkovich et al., Phys. Rev. Lett., 4, 570 (1960); J. Doede, Phys. Rev., 132, 1782 (1963).
10. É. A. Vesman, Pis'ma Zh. Eksp. Teor. Fiz., 5, 113 (1967).
11. A. Bertin et al., Phys. Rev., 8D, 3774 (1973).
12. S. S. Gershtein, Zh. Eksp. Teor. Fiz., 40, 693 (1961).
13. A. V. Matveenko and L. I. Ponomarev, Zh. Eksp. Teor. Fiz., 59, 1593 (1970).
14. L. Ponomarev, in: Proceedings Seventh International Conference on Atomic Physics, Plenum Press, New York—London (1978), p. 182.
15. G. Conforto et al., Nuovo Cimento, 33, 1001 (1964).
16. S. I. Vinitskii et al., Zh. Eksp. Teor. Fiz., 79, 698 (1980).

17. V. M. Bystritskii et al., Zh. Eksp. Teor. Fiz., 70, 1167 (1976).
18. Yu. G. Budyashov et al., Preprint R15-3964, Joint Institute for Nuclear Physics, Dubna (1968).
19. V. M. Bystritskii et al., Zh. Eksp. Teor. Fiz., 71, 1680 (1976).
20. V. M. Bystritskii et al., Zh. Eksp. Teor. Fiz., 76, 460 (1979).
21. V. M. Bystritskii et al., Zh. Eksp. Teor. Fiz., 66, 61 (1974).
22. L. I. Ponomarev and M. P. Faifman, Zh. Eksp. Teor. Fiz., 71, 1689 (1976).
23. W. Breunlich et al., Ninth International Conference on High Energy Physics and Nuclear Structure, Versailles, July 6-10 (1981).
24. V. M. Bystritskii et al., Zh. Eksp. Teor. Fiz., 80, 840 (1981).
25. S. Gallone, G. Prosperi, and A. Scoffi, Nuovo Cimento, 6, 168 (1957).
26. V. A. Dzhrbashyan, Zh. Eksp. Teor. Fiz., 36, 277 (1959); I. Shmushkevich, Nucl. Phys., 11, 419 (1961); R. Mann and M. Rose, Phys., 121, 293 (1961); A. P. Bukhvostov, Yad. Fiz., 4, 83 (1966) and 9, 107 (1967).
27. A. P. Bukhovstov and N. P. Popov, Zh. Eksp. Teor. Fiz., 82, 23 (1982).
28. H. Uberall, Phys. Rev., 114, 1640 (1959); E. Lubkin, Phys. Rev., 119, 815 (1960).
29. A. A. Dzhuraev et al., Zh. Eksp. Teor. Fiz., 62, 1424 (1972).
30. S. S. Gershtein, Zh. Eksp. Teor. Fiz., 34, 463 (1958).
31. R. Klem, Nuovo Cimento, 48A, 743 (1967).
32. A. E. Ignatenko et al., Zh. Eksp. Teor. Fiz., 35, 894 (1958).
33. D. Buchke et al., Phys. Rev. Lett., 20, 705 (1968); M. Ezhkause et al., Nucl. Phys., 81, 575 (1966).
34. K. Arnold et al., SIN Newsletters, No. 11, 45 (1979).
35. S. Gershtein and L. Ponomarev, Phys. Lett., 72B, 80 (1977).
36. S. I. Vinitskii et al., Zh. Eksp. Teor. Fiz., 74, 839 (1978).
37. D. D. Bakalov, S. I. Vinitskii, and V. S. Melezhik, Zh. Eksp. Teor. Fiz., 79, 1629 (1980).
38. D. V. Balin et al., Preprint No. 715, B. P. Konstantinov Institute of Nuclear Physics (LIYaF), Academy of Sciences of the USSR, Leningrad (1981).
39. L. Bogdanova et al., Phys. Lett., 115B, 171 (1982).
40. V. S. Melezhik, Pis'ma Zh. Eksp. Teor. Fiz., 36, 101 (1982).
41. L. N. Bogdanova et al., Zh. Eksp. Teor. Fiz., 81, 829 (1981); Yad. Fiz., 34, 1191 (1981).
42. Yu. V. Petrov, Nature, 285, 466 (1980); Yu. V. Petrov, in: Proceedings Fourteenth Winter School [in Russian], B. P. Konstantinov Institute of Nuclear Physics (LIYaF), Academy of Sciences of the USSR, Leningrad (1979), p. 139; Yu. V. Petrov, Priroda, No. 4, 62 (1982); S. S. Gershtein, Inventor's Certificate No. 713373, Byull. Izobret., No. 10, 297 (1981).
43. L. I. Ponomarev, Priroda, No. 9, 8 (1979).
44. J. Rafelsky, International School of Physics of Exotic Atoms, Erice, March 25-April 5 (1979).
45. L. I. Ponomarev, Tenth European Conference on Controlled Fusion and Plasma Physics, September 14-19, Moscow (1981); Preprint R4-81-800, Joint Institute for Nuclear Physics, Dubna (1981).
46. L. Bracci and C. Fiorentini, Phys. Reports, 86, 170 (1982).
47. S. S. Gershtein et al., Zh. Eksp. Teor. Fiz., 80, 1690 (1981).
48. V. M. Bystritskii et al., Zh. Eksp. Teor. Fiz., 80, 1700 (1981).
49. S. S. Gershtein et al., Zh. Eksp. Teor. Fiz., 78, 2099 (1980).
50. S. Jones et al.; D. Balin et al.; W. Breunlich et al., Reports on the Muon Catalysis Section of the Third International Conference on Emerging Nuclear Systems, June 6-9, Helsinkii (1983).

VERSION OF A HYBRID REACTOR BASED ON MUON CATALYSIS OF THE D–T REACTION

V. V. Orlov, G. E. Shatalov, and K. B. Sherstnev

UDC 621.039.67

The regeneration of interest in the concept of a μ-meson catalysis (MC) of a nuclear fusion reaction in a "cold" D–T mixture is due to the papers of Gershtein and Ponomarev [1], who predicted a resonance mechanism for the formation of dtμ molecules. In [2], the high velocity of this process is verified experimentally, and in [3] Petrov, by means of estimate calculations showed the feasibility in principle of creating a system consisting of a hybrid MC-reactor and several nuclear reactors, and having approximately twice as good an energy balance by comparison with the similar electronuclear system. In this case, the design of a hybrid MC-reactor requires more detailed consideration.

It is well known that new power concepts must possess a considerable "margin of stability" because after the first usually idealized physical estimates they must first of all pass a successful approval at the stage of technical realization of the concept, and then demonstrate their economic applicability. Fast reactors, the margin of the breeding coefficient of which (about 2.5 according to ideal estimates) was found to be sufficient, can serve here as a positive example, whereby K_b should confidently exceed unity in technical achievement (1.2–1.3 for modern reactors). It is not difficult also to cite contrary examples.

Our problem consists in estimating the energy balance of a hybrid MC-reactor, taking account if only in general outline of a number of factors associated with the technical application of this system. In the estimates, we can draw on the data about fast nuclear reactors and on the results of a calculation of hybrid thermonuclear reactors.

Following [3], the scheme being considered can be represented as an electronuclear scheme (accelerator with a nucleon flux I, with their energy ~1 GeV, in conjunction with a uranium target and a ^{238}U blanket, where approximately $\eta_e = 50$ atoms of ^{239}Pu in the calculation, per nucleon are produced), with an MC-"attachment" in the form of a light target for the production of π^--mesons (0.25 π^-/nucleon)* and a magnetic trap in which $\pi^- \to \mu^-$-decay takes place. The muons are directed into a D–T-synthesizer, initiating Y reactions $D + T \to {}^4He + n$ in their lifetime (2.2×10^{-6} sec). The 14-MeV neutrons formed in this reaction enter the uranium blanket where $K_T > 1$ atoms of tritium and K_{Pu} atoms of plutonium are formed, and also approximately $K_{Pu}/2.5$ fission events in ^{238}U occur. The energy produced from this is converted to electrical energy with an efficiency of $\eta \approx 0.35$, and goes almost entirely into feeding the accelerator with an efficiency $\eta_a \approx 0.6$, and the plutonium goes into thermal nuclear reactors where, taking account of breeding, approximately 1.7 fission events per atom of plutonium makeup occur.

Figure 1 depicts the scheme described. The synthesizer is a tube with diameter ~20 cm, filled with D–T gas (optimum composition, according to the data of [4], corresponds to T:D = 2:1 or 0.75T by mass); density n, temperature T, and pressure p. The synthesizer is surrounded by a uranium and lithium blanket, and with a shield located inside a solenoid with a magnetic field of B ~ 10 T, which is necessary for confining the muons.

*This value is the maximum, corresponding to the collision of tritium nuclei with one another. In realistic cases (e.g., D–Li, etc.), it is appreciably less.

Translated from Atomnaya Énergiya, Vol. 55, No. 6, pp. 391-395, December, 1983. Original article submitted June 23, 1983.

0038-531X/83/5506-0843$07.50

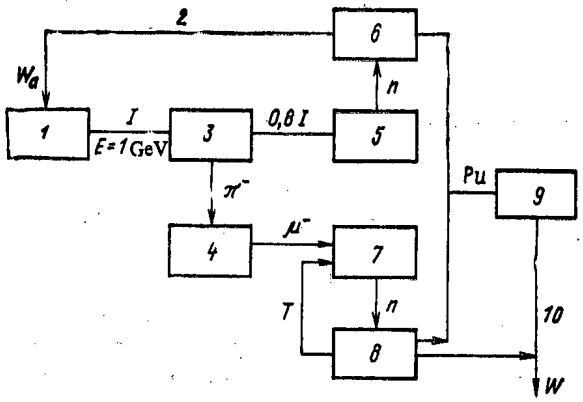

Fig. 1. Diagram of a system of MC-reactor + nuclear reactors: 1) accelerator; 2) accelerator feed; 3) light target; 4) π^- + μ^- converter; 5) target (^{238}U); 6) blanket (^{238}U); 7) D–T synthesizer; 8) blanket (^{238}U + Li); 9) nuclear reactors; 10) useful power.

According to [5], the energy of the muons amounts to 50-300 MeV. If we assume [6] that the mean free path of the muons is related with their energy by the relation

$$nl(E) \approx 60 \frac{(E/100)^2}{1+E/100}, \text{ g} \cdot \text{cm}^{-2} \qquad (1)$$

(here it is assumed that the muon is moving along a spiral trajectory with a longitudinal velocity component $v_z = v\sqrt{3}$, neglecting the spread of direction of the velocity), then the length of the synthesizer should amount to $nl \approx 140$ g·cm^{-2} and the mass of the D–T gas is 44 kg (mass of tritium M_s = 33 kg). In the absence of an MC-attachment, in a purely electronuclear scheme the power enhancement factor of the system amounts to

$$\frac{W}{W_a} = \frac{\eta_e \cdot 1.7 \cdot 200 \text{ MeV}}{1 \text{ GeV}} \eta \cdot \eta_a \approx 3.4,$$

i.e., the electronuclear method of production possesses a positive but quite meager energy balance which, taking account of the high cost of the accelerator and target, leads to a relatively low efficiency of this method. The MC-attachment improves the energy balance of the system by a factor of approximately ν, where

$$\nu \approx 1 + 0.2 \frac{YK_{Pu} - \eta_e}{\eta_e}. \qquad (2)$$

It is assumed here that the losses of π^--mesons in the trap and muons in the synthesizer amount to approximately 20%. If it is assumed, in accordance with [3], that Y = 100 and K_{Pu} = 2.4, then ν = 1.8, which also amounts to an idealized estimate of the hybrid MC-reactor.

In the following estimates, we shall start from values of the probability of formation of dtμ-molecules $\lambda_{dt\mu} = 10^9$ sec^{-1} and the probability of "attachment" of the muon to the atom, of ^{4}He: $\omega_s = 10^{-2}$ [1].

Tritium Charge, Synthesizer, and Accelerator Power. We shall assume that the energy released in the synthesizer per single D–T reaction (it consists of the energy of the α-particle, muon, and part of the energy of the neutron) is equal to approximately 5 MeV, so that per joule of energy released $\zeta \approx 0.63 \cdot 10^{-11}$ g·J^{-11} of tritium is burned.

The tritium balance in the system, developing with a rate of ω (we shall assume that ω = 3% per annum), taking account of its decay (λ_T = 0.056/yr) and breeding, is determined by the equation

$$\frac{dM}{dt} = \omega M = -\lambda_T M + (K_T - 1)\zeta\varphi W_s.$$

Hence, the power released in the synthesizer should amount to

$$W_s = \frac{\omega + \lambda_T}{\zeta\varphi\varepsilon (K_T - 1)} M_s, \qquad (3)$$

where $\varphi \approx 0.8$ is the power utilization factor of the system and $\varepsilon = M_s/M$ is the fraction of tritium located in the synthesizer from its total amount in the system (including the purification, cooling, blanket systems, and structural materials, etc.). We shall assume that ε = 0.7 (as will be seen later, this estimate is extremely optimistic). Then, the amount of tritium in the system is $M = M_s/\varepsilon$ = 47 kg, which is greater by an order of magnitude than in a thermonuclear reactor of comparable power. This also constitutes one of the principal difficulties on the path for the construction of a hybrid MC-reactor and generating many other problems about which more will be said later.

First and foremost, with a large loading, just as for fast reactors the problem arises of the tritium doubling time, equal in our case to $T_2 = \ln 2/\omega$ = 23 years. This means that in the initial (and quite long) period of development of these reactors, a considerable quantity of tritium would have to be produced in nuclear reactors (from this point of view, 50 kg of tritium is equivalent to 4 tons of plutonium) for their charges. It is true that with an output of the MC-attachment of 1 ton of plutonium per year, this amount of tritium could be recovered over approximately 5 years, but it must be stressed that the required period of repayment of the initial costs amounts to only 8-10 years and for the return of the capital investment (probably large, in consequence of the complexity of the system) there remains little time. In other words, the large quantity of tritium markedly worsens the technico-economic indices of the MC-hybrid reactor.

The large tritium charge also leads to a high power W_s of the synthesizer. A reduction of W_s is possible only because of an increase of K_T, but this leads to a reduction of the plutonium production (K_{Pu}). If we assume that K_T = 1.4 is the optimum estimate, then W_s = 63 MW and the intensity of the beam of nucleons at the accelerator outlet, proportional to W_s/Y, amounts to $W_s \geqslant 1.3$ GW for $Y \leqslant 65$ (see later), which corresponds to a nucleon flux $I \geqslant 1.3$ A. In designs of electronuclear systems, accelerators are being considered with a current of 200-300 μA, so that obviously a single synthesizer must be "served" by several accelerators.

Purification of Tritium from Helium. In the D–T gas, ^{4}He and ^{3}He are built up at the rate $M(\lambda_T + 1/\tau_{con})$ ($\tau_{con} = M/\psi\zeta W_s = (K_T - 1)/(\omega + \lambda_T) = 4.7$ years). The probability of capture of a muon by helium is close to the analogous value for hydrogen, and therefore the concentration of helium must be limited to the value $C \leqslant 10^{-3}$ (in a thermonuclear reactor the permissible concentration of helium amounts to ~10^{-1}). The flow of tritium in the purification system, where the helium concentration must be reduced to $C_1 = C - \Delta C$, is equal to

$$G = \frac{M}{\Delta C}\left(\frac{1}{\tau_B} + \lambda_T\right) \geqslant 13\frac{C}{\Delta C} \text{ ton/yr for } C = 10^{-3}.$$

In the case of extreme purification ($\Delta C \sim C$), the tritium circulation is found to be greater by a factor of approximately 40 than in a thermonuclear reactor of comparable power for a fuel burnup of 5%.

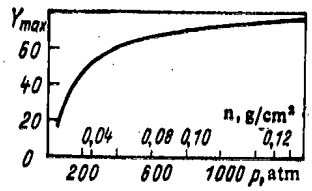

Fig. 2. Dependence of the number of fusion reactions per muon on the D–T gas pressure for T = 400°K ($\lambda_{dt\mu} = 10^9$ sec^{-1} and ω_s = 0.01).

It is assumed that on the purification of tritium from impurities up to a helium concentration of ~10^{-2}, ~10 h are expended (without taking account of the considerable delay due to the dissolution of tritium in the structural materials). If, in the case being considered, the tritium can be purified over the same time to $C_1 \approx 10^{-4}$, its amount in the purification system will be not less than $G(\tau) \approx 13$ kg. A sharp reduction of the tritium loss also is required.

Thus, in the achievement of a hybrid MC-reactor, a new technology for handling tritium is necessary, which will considerably increase the output of the purification system, increase its extent and shorten the holdup time of tritium in these systems and also its loss.

Temperature, Pressure, and Density of the D–T Mixture. The specific heat release in the synthesizer amounts to $w = (3/4)W_s/M_s = 1.4$ kW/g or, with a density of the mixture n = 0.07 g/cm³, $w_s = 0.1$ kW/cm³. This heat can be led off either to the heat exchanger, located on the periphery of the synthesizer or to an external heat exchanger which requires an increased amount of tritium. In the first case, the overall thermal loading on the wall of the synthesizer amounts to $q = \bar{w}_s (d/4) = 0.55$ kW/cm² = $4.7 \cdot 10^6$ kcal/m²·h. With strong turbulence of the gas on account of its pumping through with a velocity of ~50 m/sec, the heat-transfer coefficient can be raised to $\alpha \approx 5 \cdot 10^4$ kcal/m²·h·deg K, so that the temperature drop in the gas amounts to $\Delta\bar{T} = \bar{q}/\alpha = 100$°K, but the gas temperature in the synthesizer with cold water cooling is $\geqslant$400°K.

Using Van der Waals equations for the D–T gas [7] and the function Y(n) adopted from [3], the curve of Y versus the pressure of the gas mixture can be constructed as is shown in Fig. 2. The limiting value of Y = 80, corresponding to a density of the liquid D–T mixture n = 0.2 g/cm³, in practice is unattainable, but with a pressure of 500-1000 atm (1 atm = 101.325 kPa), Y = 60-70. Without doubt, the preferred value in this case is assumed to be p = 500 atm. Therefore, in our estimates the values of Y = 65 and n = 0.07 g/cm³ are assumed.

Neutron Flux, Primary Wall, Blanket. If w(z) is the heat release density along the length of the synthesizer, then neglecting the angular distribution of the muons, we have

$$w(z)\,dz \approx \chi(E_\mu)\,dE_\mu$$

or

$$w(z) \approx \frac{\chi[E_\mu(z)]}{dz/dE_\mu},$$

where $\chi(E_\mu)$ is the energy spectrum of the muons; $E_\mu(z)$ is their mean free path before retardation. The dependence of dz/dE_μ on the longitudinal coordinate leads to "peaking" of the distribution, but for simplicity we shall assume that the coefficient of nonuniformity w(z) is equal to the coefficient of nonuniformity of the muon spectrum in the range 50-300 MeV.

$$k = \frac{w_{max}}{\bar{w}} \approx 2.$$

In this case, the neuron loading on the wall of the synthesizer amounts to $\bar{q}_n = (4\bar{q})E_\alpha/E = 1.3$ kW/cm^2 = 13 MW/m^2, and $q_n^{max} = 26$ MW/m^2, which is a factor of 30 greater than the loading on the primary wall of a hybrid thermonuclear reactor [8]. This loading corresponds to a fast neutron flux density at the wall of

$$\bar{\Phi} \approx 1.3 \cdot 10^{16} \text{ neutrons/(cm}^2\cdot\text{sec)};$$
$$\Phi_{max} \approx 2.6 \cdot 10^{16} \text{ neutrons/(cm}^2\cdot\text{sec)}.$$

which is a factor of 30 higher than that for the hybrid thermonuclear reactor, and a factor of 3 higher than in the core of a fast reactor. (By comparison with a thermonuclear reactor, the operating conditions of the chamber material have been lightened somewhat due to the elimination of erosion under the action of the fast plasma particles but has been worsened sharply because of the increase of the neutron fluxes.)

In fast reactor conditions, the mechanical stresses in the structural materials of the core do not exceed $\sigma \approx 10$ kg/mm^2. If materials are successfully found for the wall of the synthesizer, which will tolerate $\sigma \approx 20$ kg/mm^2, then at a pressure of p = 500 atm = 5 kg/mm^2, the thickness of this wall will amount to

$$\delta = \frac{1}{2}\left\{\sqrt{\frac{1+p/\sigma}{1-p/\sigma}} - 1\right\} d = 3 \text{ cm}.$$

A wall of this thickness reduces the 14-MeV neutron flux in the uranium blanket and K_{Pu} by a factor of approximately 1.5. It may be found advantageous to transfer the high pressure vessel outside the blanket, but then its thickness increases considerably and the problem arises of injection of the muon beam into the synthesizer.

In the uranium blanket of a hybrid thermonuclear reactor, the specific power amounts to ~200 kW/liter, which allows metallic uranium and gas cooling to be used. In the blanket of the hybrid MC-reactor the specific power is increased to 3-5 MW/liter, which is a factor of 6-10 greater than the energy intensity of a fast reactor with oxide fuel. The transition from metallic uranium and gas to other fuel materials and coolants leads to a considerable worsening of the neutron balance and to a sharp drop in the values of K_T and K_{Pu}.

Neutron Balance. Idealized calculations of the 14-MeV neutron distribution in an infinite layer of ^{238}U give 1 fission event and 4.2 atoms of plutonium made per initial neutron. In the calculations of designs of thermonuclear hybrid reactors, the limiting thickness of the uranium blanket, the primary wall and structural materials depend upon a reduction of the stated values to approximately 0.6 fission event and $K_{Pu} + K_T \approx 2.6$-2.8 per initial 14-MeV neutron, using metallic uranium and gas cooling, and these values correspond to the initial stages of development and must be considered as optimistic. In order to explain the "structure" of the reduction of $K = K_{Pu} + K_T$ in the blanket of the hybrid MC-reactor, a series of calculations was undertaken with the following results:

Infinitely thick uranium blanket	4.2
Blanket with thickness 20 cm	4.0
Synthesizer with wall thickness 0.5 cm (without pressure)	3.7
Uranium blanket containing 20% of structural materials	3.0
Synthesizer with D–T gas (n = 0.07 g/cm^3)	2.8

It should be emphasized that an increase of $K_T(>1)$ can be achieved only by a reduction of the thickness of the uranium blanket, or even a combination of the uranium and lithium blankets. This leads to an additional reduction of the neutron multiplication factor and the total coefficient of production, which has not been taken into account in the calculations. Taking as an optimistic estimate K = 2.8, we obtain $K_{Pu} = 1.4$ for $K_T = 1.4$.

Conclusion. In order to achieve a nuclear fusion reaction in a "cold" D–T mixture based on muon catalysis, it is necessary to solve technical problems in many respects more complex by comparison with thermonuclear fusion. The achievement of a hybrid MC-reactor requires new materials and technical solutions to be found, which fall outside the scope of present-day reactor technology. However, even in the case of a successful solution of these problems without additional losses in the values of K_{Pu} and Y, the hybrid MC-reactor gives almost no advantage in energy balance by comparison with the purely electronuclear scheme with $\lambda_{dt\mu} \approx 10^9$ sec^{-1} and $\omega_s \approx 0.01$. In this case, according to an optimistic estimate, $Y \approx 65$ and $K_{Pu} \approx 1.4$, and $\nu \approx 1.1$. Only with the condition that the principal characteristics of muon catalysis ($\lambda_{dt\mu}$, ω_s, etc.) prove to be significantly better than is estimated now, can one count on a marked gain in the energy balance of the system "hybrid MC-reactor–electronuclear facility–nuclear reactors" by comparison with the purely electronuclear scheme ($\nu = 1.4$ with $Y \approx 100$). In this case, a more detailed development of this system and its economic assessment will be advantageous.

The present paper originated as the result of a number of discussions on muon catalysis with I. I. Gurevich, Yu. V. Petrov, and L. I. Ponomarev, to whom the authors express their appreciation.

LITERATURE CITED

1. S. Gershtein and L. Ponomarev, Phys. Lett., 72B, 80 (1977).
2. V. M. Bystritskii et al., Pis'ma Zh. Eksp. Teor. Fiz., 31, 249 (1980).
3. Yu. Petrov, Nature, 285, 466 (1980).
4. S. S. Gershtein et al., Zh. Eksp. Teor. Fiz., 78, 2099 (1980).
5. Yu. V. Petrov and Yu. M. Shabel'skii, Preprint No. 699, Leningrad Institute of Nuclear Physics, Leningrad (1981).
6. N. P. Kalashnikov, V. S. Remizovich, and M. I. Ryazanov, Collisions of Fast Charged Particles in Solid Bodies [in Russian], Atomizdat, Moscow (1980).
7. Tables of Physical Quantities (Handbook) [in Russian], I. K. Kikoin (ed.), Atomizdat, Moscow (1976).
8. E. P. Velikhov et al., At. Energ., 45, No. 1, 3 (1978).

CORRECTION TO THE READINGS OF A THERMOELECTRIC THERMOMETER IN REACTOR CONDITIONS

A. A. Greshilov, V. S. Terekhov, V. I. Nalivaev,
S. V. Priimak, and I. I. Fedik

UDC 536.51

When measuring temperature with thermoelectric thermometers in the core of a nuclear reactor, the resistance between the working junction of the thermoelectric transducer (TET) and the object being investigated, depending on the structure, materials, and method of installation of the latter, in conjunction with the radiation internal release in the structural elements of the TET, leads to the appearance of an additional error [1-3]. Numerical estimates of the corresponding corrections are mainly of an approximate nature [1], associated with the difficulty of taking account of the whole set of influencing factors.

Experimental investigations of the effect of internal energy release on the TET readings are conducted on mock-up irradiation facilities with the subsequent conversion of the results to realistic conditions, as it is not always possible to carry out control measurements in them [1, 4, 5]. Because of this, it is of practical interest to develop an experimental-numerical method of determining these corrections for realistic conditions of use of TET.

We shall consider the case when the TET junction is located in direct contact with the medium being measured. We shall suppose that all other corrections are known, and without altering the generality of the consideration, we shall assume them further to be equal to zero. We shall assume that in the temperature range being considered the system TET—object of temperature measurement is linear, and the temperature of all points of the working junction of the TET is identical. The correction $\delta T_q(t)$ of the TET readings due to the internal energy release acting in the junction in the time $0 \leqslant \tau \leqslant t$ is determined from the expression

$$\delta T_q(t) = \int_0^t K_q(t-\tau)\, q_V(\tau)\, d\tau, \tag{1}$$

where $K_q(t)$ is the pulse characteristics of the TET with respect to the energy release in its junction for the system TET—medium (object); and $q_V(t)$ is the specific volume energy release in the junction, W/m^3. The pulse characteristics $K_q(t)$ describe the change of the TET readings at any instant $t > 0$, by the action at the initial instant in the TET junction of a unit instantaneous volume source of heat (the temperature of the medium remains constant).

The correction to the TET readings due to the internal heat release in steady-state conditions (q_V = const) is independent of the nature of the outflow in it. This correction is equal to

$$\delta T_q = q_V \int_0^\infty K_q(\tau)\, d\tau. \tag{2}$$

Consequently, knowing the pulse characteristics of the TET with respect to the channel of internal energy release in the TET junction — the TET readings in realistic measurement conditions, we find this correction.

The pulse characteristics $K_q(t)$ can be determined from the results of measurement of the TET signal in working conditions, after heating its junction with an electric current pulse of small duration, simulating the δ-pulse of the internal energy release [6]. In fact, the pulse characteristics of the TET with respect to the internal heat release channel in the

Translated from Atomnaya Énergiya, Vol. 55, No. 6, pp. 395-399, December, 1983. Original article submitted September 13, 1982.

0038-531X/83/5506- 0849$07.50

TET junction—TET readings are calculated from the relation $K_q(t) = \Delta T(t)/Q$, where $\Delta T(t)$ are the TET readings and Q is the quantity of heat released in unit volume of the junction by the pulsed heating. Taking into account that $Q = C_V \Delta T(0)$, we obtain

$$K_q(t) = \frac{1}{C_V} \frac{\Delta T(t)}{\Delta T(0)} \quad \text{or} \quad K_q(t) = \frac{1}{C_V} h_T(t),$$

where $h_T(t) = \Delta T(t)/\Delta T(0)$ is the transitory characteristic of the TET with respect to the channel temperature of the medium—TET reading; C_V is the specific bulk heat capacity of the material of the working junction, $J/(m^3 \cdot \text{deg K})$ and $\Delta T(0)$ is the sudden change of the TET reading at the instant of action of the heat release pulse.

In realistic conditions, it is not always possible to effect a δ-pulse or stepwise heating up of the TET junction; however, knowing the law of change of energy release in this junction operative for the electrical heating, with an accuracy up to the constant [$q_{V\,el}(t) = \mu f(t)$], the pulse characteristics are found from the solution of the following integral equation:

$$v(t) = \int_0^t K_q(t-\tau)\, q_{V\,el}(\tau)\, d\tau = \mu \int_0^t K_q(t-\tau)\, f(\tau)\, d\tau. \tag{3}$$

Here $v_q(t)$ is the TET reading, counted from the initial value for $t = 0$, and μ is a constant determined from the condition

$$K_q(0) = \frac{1}{C_V} h_T(0) = \frac{1}{C_V};$$

f(t) is the nature of the dependence of the energy release in the TET junction on the time. The methods for solving the integral equations of the type of contraction (3) are explained in [7, 8].

With a simultaneous change of internal energy release in the TET junction and the temperature of the medium, i.e., in the case of nonsteady conditions, which occurs frequently in practice, the change of temperature of the medium Θ(t) relative to the initial temperature can be found for a known value of $h_T(t)$ from the solution of the integral equation

$$v_q(t) = \int_0^t K_q(t-\tau)\, \Delta q_V(\tau)\, d\tau + \int_0^t K_T(t-\tau)\, \theta(\tau)\, d\tau, \tag{4}$$

where $\Delta q_V(t)$ is the internal energy release in the TET junction, reckoned from the initial value with $t = 0$, and $K_T(t) = -dh_T(t)/dt$ is the pulse characteristics of the TET with respect to the channel temperature of the medium—TET reading, in the case of fulfillment of the normalization condition $\int_0^\infty K_T(\tau)\, d\tau = 1$.

When measuring a high temperature, TET frequently are used with the junction insulated from the housing or the transducer is installed in a shielded sheath. In this case, the presence of internal heat release in the shield construction leads to an additional error. Taking error of the additivity of the effect of the heat sources, the correction to the TET reading due to the energy release in its elements and shielding structure is determined from the expression

$$\delta T_q(t) = \sum_{i=1}^{N} \int_0^t K_{q_i}(t-\tau)\, q_{V_i}(\tau)\, d\tau, \tag{5}$$

where $K_{q_i}(t)$ is the pulse characteristics with respect to the energy release in the i-th element; and $q_{V_i}(t)$ is the specific bulk energy release in the i-th element.

Assuming that the internal radiation energy release in the structural materials at the site of location of the TET depends linearly on the reactor power P [9], i.e., $q_{V_i}(t) = \beta_i P(t)$, we find $q_{V_i}(t) = \alpha_i q_{V_p}(t)$, where $q_{V_p}(t)$ is the specific energy release in a certain p-th structural element of the TET, and $\alpha_i = \beta_i/\beta_p$, where β_i is the specific energy release in the i-th structural element for unit reactor power. Then, from Eq. (5) we obtain

$$\delta T_q(t) = \int_0^t \left[\sum_{i=1}^N \alpha_i K_{q_i}(t-\tau)\right] q_{V_p}(\tau)\, d\tau. \tag{6}$$

The sum $\sum_{i=1}^N \alpha_i K_{q_i}(t)$ can be considered as the effective pulse characteristic with respect to the energy release in the p-th element which we chose earlier, i.e., the integral equation (6) assumes the form

$$\delta T_q(t) = \int_0^t K_{q\text{eff}}(t-\tau)\, q_{V_p}(\tau)\, d\tau. \tag{7}$$

The transitory characteristic of the TET with respect to the temperature of the medium will be determined in this case by its reaction $v_q(t)$ to a stepwise change of the temperature difference between the medium and the TET with shielded construction to the value ΔT: $h_T(t) = v_q(t)/\Delta T$. We can consider the transitory characteristic $h_T(t)$ of the TET with respect to the temperature of the medium just like the reaction to the simultaneous action of instantaneous heat releases Q_i in each i-th element with $Q_i = C_{V_i}\Delta T$, J/m^3. Then, taking account of Eq. (5), we shall have

$$h_T(t) = \frac{v_q(t)}{\Delta T} = \frac{\sum_{i=1}^N K_{q_i}(t) Q_i}{\Delta T} = \sum_{i=1}^N C_{V_i} K_{q_i}(t). \tag{8}$$

The direct determination of $K_{q\text{eff}}(t)$ in realistic conditions of operation of the TET is difficult, as for this it is necessary to find either the values of $\alpha_i K_{q_i}(t)$, or to simulate the δ-pulse of the energy releases in all elements of the TET simultaneously with consideration of their actual values in each structural element. A change of radiation energy releases in the reactor core is accompanied, as a rule, by a simultaneous change of temperature of the medium. The change of the TET readings in this case will be determined by the equation

$$v_q(t) = \int_0^t K_{q\text{eff}}(t-\tau)\, q_{V_p}(\tau)\, d\tau + \int_0^t K_T(t-\tau)\, \theta(\tau)\, d\tau. \tag{9}$$

In order to find the temperature of the medium $\theta(t)$ from Eq. (9), it is necessary to know $v_q(t)$, $K_{q\text{eff}}(t)$, $q_{V_p}(t)$, and $h_T(t)$, and in order to determine $K_{q\text{eff}}(t)$ it is necessary to know $\theta(t)$. In reality, however, by carrying out intrareactor experiments we determine quite simply only $v_q(t)$ and $q_{V_p}(t)$. However, with constant parameters of the coolant at the inlet to the reactor, the relation between the temperature of the medium and its power, and hence also with the internal radiation energy releases, can be represented in the form

$$\theta(\tau) = \int_0^\tau K_\theta(\tau-\xi)\, q_{V_p}(\xi)\, d\xi, \tag{10}$$

where $K_\theta(\tau)$ is the pulse characteristic relative to the energy release channel in the p-th element of the TET—temperature of the medium being measured, and ξ is the integration variable.

TABLE 1. Correction to TET Readings in Steady-State Conditions

Type of TET	δT_{qst}, K		
	$q_V = 105$ W/(m³·10⁻⁶)	$q_V = 210$ W/(m³·10⁻⁶)	$q_V = 420$ W/(m³·10⁻⁶)
Junction insulated	16	33	66
Junction welded w/ TET sheath	5	10	19

Then the pulse characteristic of the TET with respect to the internal energy release channel in the p-th element of the TET—temperature of the medium—TET reading, will be determined by the expression

$$K_{q\,m}(\tau) = \int_0^\tau K_T(\tau - \xi)\, K_\theta(\xi)\, d\xi. \tag{11}$$

Consequently, Eq. (9) taking account of expressions (10) and (11) can be written in the form

$$v_q(t) = \int_0^t K_{q\,\text{eff}}(t-\tau)\, q_{V_p}(\tau)\, d\tau + \int_0^t K_{q\,m}(t-\tau)\, q_{V_p}(\tau)\, d\tau = \int_0^t [K_{q\,\text{eff}}(t-\tau) + K_{q\,m}(t-\tau)]\, q_{V_p}(\tau)\, d\tau. \tag{12}$$

In order to solve the integral equation (12), we shall introduce, using experimental data, additional limitations on the class of possible solutions.

For the purpose of determining the class of the functions by which $h_T(t)$ and correspondingly $K_{q\text{eff}}(t)$ are described, as they are linear combinations of one and the same $K_{q_1}(t)$, the following laboratory experiments were carried out. A VR 5/20 calibrated TET with a diameter of 1.6 mm of two types (with a welded junction, and a junction insulated from the housing) in a protective tube of molybdenum and without it, were tested in the following way: They were heated up in a tubular furnace and rapidly immersed in running water; the TET was heated in the running water with an electric current pulse with a duration of 0.10-0.15 sec; they were placed in an opening in a copper block and heated with a current pulse of the same duration. The signals were recorded by means of a cathode ray oscilloscope. The transitory characteristics obtained are shown in Fig. 1.

As the investigations showed, $h_T(t)$ is described with sufficiently good accuracy by the sum of the exponents, and the number of exponents coincides with the number of contact resistances in the TET structure. Thus, for example, for $h_T(t)$ of the TET in the protective tube, cooled by running water, the number of exponents is equal to two (see Fig. 1b, curve 2), and for the same TET located in the opening in the copper block, the number of exponents is equal to three. It follows from Fig. 1b that for the thermoelectric transducer with the insulated junction and without protective tube, $h_T(t)$ obtained with pulsed current heating, almost coincides with $h_T(t)$ obtained with external heating. On the contrary, for the same TET in the protective tube, $h_T(t)$ obtained with pulsed heating, just as in the first case, the rate of cooling will be determined mainly by the heat exchange conditions between the TET and the protective tube, but in the second case both between the TET and the protective tube and also between the protective tube and the running water.

Assuming that the VR 5/20 TET with the junction welded and insulated from the housing is in direct contact with the cooling water, i.e., the condition $K_q(t) = (1/C_V)h_T(t)$ is fulfilled for them, we obtain on the basis of the data shown in Fig. 1 the values of the corrections for steady-state conditions shown in Table 1 [it is assumed for the TET 5/20 junction that $C_V = 2.59 \cdot 10^6$ J/(m³·deg K)].

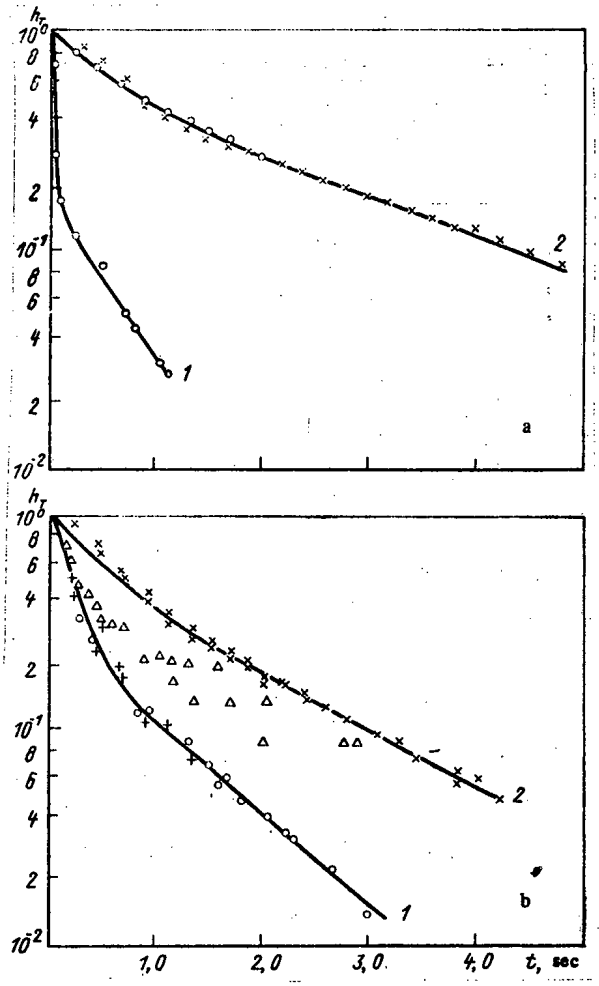

Fig. 1. Transitory characteristics of a VR 5/20 TET, cooled by running water: a) junction welded with the sheath of the TET: 1) external heating of the TET without protective tube, approximating function $h_T(t) = 0.82965e^{-45.07t} + 0.17e^{-1.68t}$, and $\delta T_q = 0.12q_V/C_V$; 2) external heating of the TET in the protective tube of molybdenum, approximating function $h_T(t) = 0.391e^{-2.118t} + 0.609e^{-0.4165t}$ and $\delta T_q = 1.647\ q_V/C_V$, O) heated with a current pulse; ×) externally heated; b) insulated junction: 1) TET without protective tube: O external heating; +) heated with a current pulse; approximating function $h_T(t) = 0.709e^{-6.46t} + 0.29e^{-0.977t}$, and $T_q = 0.407\ q_V/C_V$; 2) TET in protective tube of molybdenum: ×) external heating; Δ) heated with a current pulse, approximating function $h_T(t) = 0.367e^{-2.81t} + 0.633e^{-6.06t}$, and $\delta T_q = 1.174q_V/C_V$.

Taking into account that $K_{qeff}(t)$ is described by the same number of exponents as $h_T(t)$, and the correction of the TET readings for radiation energy release depends on $\int_0^\infty K_{q\,\mathrm{eff}}(\tau)\,d\tau$,

TABLE 2. Variation of $v_q(t)$ with Time

t, sec	0	0,05	1,0	1,5	2,0
$v_q(t)$, K	0	1,02	4,89	12,75	25,11

Continuation of Table 2

t, sec	2,5	3,0	3,5	4,0
$v_q(t)$, K	41,83	62,33	85,73	111,04

the authors of the present paper additionally conducted investigations which showed that $K_{qeff}(t)$ is described with an accuracy sufficient for practical purposes by the sum of two exponents. With further increase of the number of exponents, an increase of the error of the solution occurs in view of the inaccuracy of the problem of approximation of the experimental data by the sum of the exponents [8].

As an example, let us consider a numerical experiment. We take $K_{qeff}(t) = A_1 e^{-\lambda_1 t} + A_2 e^{-\lambda_2 t}$, and we approximate $K_{qm}(t)$ by a polynomial of the third order $\sum_{i=0}^{3} a_i t^i$. Based on a series of measurements of the temperature $v_q(t)$ with a change of internal energy release, we obtain a system of equations, for which we determine the coefficients A_1, A_2, λ_1, and λ_2, and the parameters of the polynomial. Using these coefficients and knowing $q_{V_p}(t)$, the correction to the TET readings can be obtained for its similar position in the reactor. Thus, for the law of change $\Delta q_V(t) = 25 \cdot 10^6 t$ W/m^3 and the value of $v_q(t)$ given in Table 2,

$$A_1 = 2.33 \cdot 10^{-7} \ (\text{m}^3 \cdot {}^\circ\text{K})/(\text{J} \cdot \text{sec}); \quad \lambda_1 = 6.5 \ \text{sec}^{-1};$$

$$A_2 = 9.6 \cdot 10^{-8} \ (\text{m}^3 \cdot {}^\circ\text{K})/(\text{J} \cdot \text{sec}); \quad \lambda_2 = 1.0 \ \text{sec}^{-1}.$$

The problem is also solvable in the case of breakdown of the conditions of linearity, on the basis of which expressions (10)-(12) were obtained; however, in this case, the integral $\int_0^t K_T(t-\tau)\theta(\tau)\,d\tau$ must be approximated by the polynomial and $K_{qeff}(t)$ is approximated by the sum of the exponents. With the known function $q_{Vp}(t)$ and measured values of $v_q(t)$, the system of equations can be compiled for determining the unknown parameters A_1, A_2, λ_1, λ_2, a_0, a_1, a_2, and a_3 [10].

In conclusion, we note that the procedure developed for determining the temperature correction, depending on the method of locating the thermoelectric thermometer, allows the accuracy of the measurements in reactors with a high nuclear radiation intensity to be increased.

LITERATURE CITED

1. B. V. Lysikov and V. K. Prozorov, Reactor Thermometry [in Russian], Atomizdat, Moscow (1980).
2. J. Bringley, Nucl. Sci. Eng., 23, No. 4, 313 (1965).
3. V. Singkh and A. Daibs, Teploperedacha, No. 3, 162 (1977).
4. U. E. Browning and H. L. Hemfill, in: Measurement of Temperature in Objects of New Technology [Russian translation], Mir, Moscow (1965), p. 66.
5. L. Hess, At. Tekh. Rubezhom, No. 1, 15 (1970).
6. M. M. Mal'gun and M. D. Sobolev, Prib. Tekh. Eksp., No. 3, 197 (1977).

7. V. N. Vapnik, Reconstruction of Functions from Empirical Data [in Russian], Nauka, Moscow (1979).
8. A. N. Tikhonov and V. Ya. Arsenin, Methods of Solving Incorrect Problems [in Russian], Nauka, Moscow (1979).
9. N. S. Shimanskaya, Calorimetry of Ionizing Radiations [in Russian], Atomizdat, Moscow (1973).
10. K. Lantsosh, Practical Methods of Applied Analysis [in Russian], Gos. Izd. Fiz-Mat. Lit., Moscow (1961).

EQUIVALENT DOSES OF DIFFERENT TYPES OF RADIATIONS

B. G. Dubovskii

UDC 539.12.04

It was concluded in [1] that radiation with a large linear energy transfer (LET) is more effective than radiation with a small LET in inducing neoplasms, but this effectiveness frequently changes with a change of dose. For radiation doses of 100 rad and more (1 rad = 0.01 Gy) the value of the relative biological effectiveness (RBE), and consequently the quality factor (Q), is frequently ~1 and increases for small doses. On this basis it was proposed in [2] to decrease the numerical value of the coefficient D_0 in the equation for Q as a function of the LET to D_0 = 0.35 Gy (35 rad). This value of D_0 for an absorbed dose D = 1 Gy (100 rad) corresponds to a quality factor Q = 1.5 for fast neutrons instead of Q = 10 for small doses. Since this value of D_0 is valid for large values of the LET, it is the upper limit for small values of the LET (L).

It is known that the duration of the physical stage of the effect of radiation – excitation of molecules, ionization, and the formation of primary free radicals – is 10^6-10^{10} sec; the chemical stage is completed in the first 10^{-6}-10^{-3} sec, followed by the biological stage which may last for years and even decades [3]. In the chemical stage, at least, the law of mass action is unconditionally valid. According to this law the rate of a chemical reaction is proportional to the product of the concentrations of the reacting molecules. These concentrations in turn are directly proportional to the number of ions formed as a result of irradiation, or L. Thus, it follows directly from the law of mass action that $Q \sim L^2$.

On the basis of the above it was proposed in [2] to determine the dependence of the equivalent radiation dose H in sieverts (rem) on the absorbed dose D in grays (rads) by the relation

$$H = DQ = D\left[1 + a^2L^2 \exp\left(-\frac{D}{D_0}\right)\right],$$

where $a^2 = (3/53)^2 = 3.2 \times 10^{-3}$ (μm/keV)^2.

Table 1 compares the data of NRB-76 [4] determining the stipulated dependence of Q on L, the values of Q calculated with the above formula, and the values recommended by the author, including those for L = 175 keV/μm. The calculated values confirm the validity of Q = 1.04 for x rays and γ rays, normalized to Q = 10 for fast neutrons.

The biological effect of different types of radiations is determined by the energy absorbed in tissue as a result of irradiation, but not by the radiation energy absorbed, since the latter determines the number of ions formed, which initiate a free-radical chain reaction.

In the first approximation the relation H(D) or Q(L) under discussion takes account of the energy absorbed in tissue, since it takes account of secondary reactions. However, at the same time it does not take account of the repair capabilities of the immune system of the irradiated organism, which determine the evolution of the radiation effect (injury) in time,

Translated from Atomnaya Énergiya, Vol. 55, No. 6, pp. 399-401, December, 1983. Original article submitted May 23, 1983.

0038-531X/83/5506-0855$07.50

TABLE 1. Stipulated, Calculated, and Recommended Values of the Quality Factor of Ionizing Radiations

Value of Q	LET, keV/μm				
	⩽ 3,5	7,0	23	53	⩾ 175
Stipulated	1	2	5	10	20
Calculated with Eq. (2)	1,04	1,16	2,7	10	100
Recommended	1	1,2	3	10	50

and influence the total biological effect. Also, the relation under consideration does not take into account the biological hierarchy of various systems and organs under irradiation.

Table 1 shows that quadratic extrapolation led to good agreement of the results in the range L = 3.5-53 keV/μm (for a change in the LET by a factor of 13) for which there are reliable data for comparing gamma and neutron radiations, taking account of the similarity of the spatial distributions of their interaction with tissue of the organism. Table 2 shows that 2-MeV α particles have an LET ≈ 175. Further extrapolation calculations in the range 53-175 keV/μm must be performed particularly carefully, if only because the preceding interval was reliably based on a large amount of experimental data. It is also necessary to take account of the existence of a saturation effect of the biological action with increasing ionization density, since for a certain critical value of the LET a cell dies.

To understand the reasons for the increased radiation hazard of alpha particles at low radiation doses, it should be recalled that a DNA molcule consists of two twisted polynucleotide helixes (i.e., a double helix), and also that as a result of radiation injury single and double breaks of one or two strands of the double helix occur. It is known that repair phenomena at the cellular level promote the recombination of breaks in the DNA helix, and that the recombination is much less probable for double than for single breaks [5].

The high capability of alpha particles to produce double breaks can be illustrated in Table 2 which lists data from [6]. A comparison of data in the last column for a 1-nm track length (a value which is characteristic for diameters and cross sectional dimensions of protein molecules which form various cellular substructures) for α particles and fast electrons shows that α particles can produce double breaks in DNA helixes which cause a new qualitative increase of the degree of radiation injury produced by them. The character of the Bragg curves for α particles with approximately a threefold increase in ionization density at the maximum over its average value, and the rectilinearity of each α-particle track only strengthen this conclusion. These considerations confirm the advisability of a substantial increase in the value of Q for α particles. Moreover, taking account of the metabolic instability of DNA, it can be assumed that the main contribution to the part of the damaging effect of all types of radiation which cannot be reduced by repair is made by double breaks, so that the absorbed dose D_0 = 35 rad, which we introduced earlier into the formula, acquires the meaning of the threshold value of the contribution of double breaks to radiation injury. The authors Yu. I. Moskalev and V. N. Strel'tsova came to this same conclusion independently.

Many scientific organizations, including the Scientific Committee on the Effect of Nuclear Radiation (SCENR), came to a similar conclusion. Thus, in a book edited by Academician A. P. Aleksandrov [7] it was noted that "In a number of experiments and observations a relatively high effectiveness of small doses of alpha radiation was detected, but these data indicate a higher RBE of small doses of alpha radiation than now assumed (Q_α = 20)." In July 1981 the physics group at the 30th session of the SCENR indicated a 50-100% increase in dose as a result of the inhalation of radionuclides in the atmosphere in uranium mining and processing. The standardized expected equivalent dose for the population attributable to the production of nuclear power is determined on the basis of the inhalation of radon, and the contribution of this element will increase steadily as a result of its liberation from tailings of uranium ores [8]. This conclusion was also confirmed at the 31st session of the SCENR in March 1982 [9], and in many papers including [10-12].

TABLE 2. LET, Range, and Number of Primary Ionizations (P.I.) Formed by α Particles and Electrons per nm of Tissue

Energy*	LET, keV/μm	Range μm	P.I./nm
	Alpha particles		
1	264	5,3	6,2
2	176	10,1	2,9
3	135	16,8	2,0
4	110	25,1	1,6
5	94	35	1,3
	Electrons		
0,1	33,2	0,003	1,7
0,2	28,7	0,006	1,0
0,3	24	0,010	0,7
0,4	21	0,014	0,6

*Energy values for α-particles are given in meV, for electrons, in keV.

These considerations and the references confirm qualitatively the value Q = 100 calculated for α radiation. Moreover, only further experimental research can reliably determine the critical value of L for which a saturation effect in the function Q(L) occurs, and with a further increase in the ionization density even a decrease in Q. Taking all these factors into account, it is advisable to take provisionally Q = 50 for the quality factor of 1-MeV α radiation.*

An appreciable increase in Q leads to a realization of the increasing hazard of the radiation effect of α radiation, and certainly requires taking measures to reduce the entrance of α-radioactive nuclides (principally radon) into the atmosphere.

The cardinal solution of the problem of reducing the hazard created by α-active radionuclides for large groups of workers employed in the mining industry and the public, is to speed up in every possible way the conversion to a closed fuel cycle (NFC) with fast reactors of the BN-600 type, including the recirculation of plutonium. The use of such nuclear power plants would decrease the requirement for natural uranium by about a factor of 40, decrease the collective radiation dose, and practically eliminate the ever increasing danger for future generations of people due to the emission of radon from tailings of uranium ores [13]. In doing this, account must be taken of the main difficulty of further improvement of radiation safety in the mining of uranium ore and the extraction of uranium from it because of the large volumes of processed rock and the large contingent of miners. Such difficulties do not exist at plants providing for the recirculation of plutonium, thanks to the introduction of automation, robotization, the development of ecologically optimized processes, and many fewer workers.

The considerations presented are valid also for power generation based on the coal fuel cycle (CFC). A comparison of the amount of radon emitted in the mining of the amounts of coal and uranium necessary to generate 1 GW(el)·yr shows that uranium miners are irradiated about a fifth as much as coal miners. A comparison of the emission of α-active nuclides, primarily uranium and radium, from CFC and NFC power plants shows that the hazard is ten times smaller at NFC plants. Thus, the realization of a plutonium NFC in the long run will lead to an appreciable decrease in the emission of uranium and radium at plants with a CFC by curtailing the volume of coal mining [7]. Nevertheless, there is need for an appreciable increase in coal mining in the next decade.

*Editor's Note. In the monograph by Yu. I. Moskalev and V. N. Strel'tsova, "Radiation Carcinogenesis in the Problem of Radiation Protection" [in Russian], Energoizdat, Moscow (1982), it was shown that in their ability to induce malignant bone and lung tumors the RBE of the α-emitting nuclides ^{239}Pu, ^{241}Am, ^{237}Np, and ^{252}Cf as compared with the β emitters ^{90}Sr and ^{144}Ce, which have a small LET, may reach 50.

LITERATURE CITED

1. Dokl. NKDAR OON, Part 3, "Radiation carcinogenesis in experiment," Sec. 6, Results and Conclusions, Paragraph 330 (1977).
2. B. G. Dubovskii, At. Energ., 51, 235 (1981).
3. Yu. B. Kudryashov and V. S. Berenfel'd, Fundamentals of Radiation Biophysics [in Russian], Moscow State Univ. (1982).
4. NRB-76, Atomizdat, Moscow (1978).
5. S. P. Yarmonenko, Radiobiology of Man and Animals [in Russian], Vysshaya Shkola, Moscow (1977), pp. 76, 216.
6. D. E. Lea, Action of Radiations on Living Cells, Macmillan, New York (1955).
7. N. S. Babaev et al., Nuclear Power, Man, and the Environment [in Russian], Énergoizdat, Moscow (1981).
8. A. A. Moiseev, At. Energ., 51, 349 (1981).
9. A. A. Moiseev, At. Energ., 53, 419 (1982).
10. K. Morgan, in: Safety of Nuclear Power [Russian translation], Atomizdat, Moscow (1980), p. 60.
11. R. M. Aleksakhin, Nuclear Energy and the Biosphere [in Russian], Énergoizdat, Moscow (1982), p. 166.
12. R. M. Aleksakhin, At. Energ., 54, 150 (1983).
13. O. D. Kazachkovskii et al., At. Energ., 54, 262 (1983).

LETTERS TO THE EDITOR

BREEDING CHARACTERISTICS OF A FAST NEUTRON REACTOR IN A TRANSIENT FUEL CYCLE

V. A. Chirkov

UDC 621.039.526

The breeding characteristics of a fast neutron reactor are determined either from the neutron balance [1] or from the fuel balance [2]. When calculating these characteristics, the fuel cycle is assumed to be open, in which the composition of the fuel charged into the reactor and discharged from it is unchanged with time. In a closed cycle, however, the discharged fuel after reprocessing again enters the reactor, and therefore the fuel composition is changing continuously during operation of the reactor. This leads to the necessity for correcting the procedure for the calculation of the breeding characteristics.

We shall suppose that the reactor operates in a continuous recharging cycle, for which the operative margin or reactivity is equal to zero. Of the different fuel cycles of operation of the reactor, we shall consider a transient fuel cycle which is achieved in the closed fuel cycle. In this case, the composition of the fuel charged into the reactor in the (n + 1)-th cycle is equal to the composition of the fuel discharged from the reactor in the n-th cycle, but is not equal to the composition of the fuel charged into the reactor in the n-th cycle. In the present paper, a procedure is considered for the calculation of the physical characteristics of a reactor operating in the transient fuel cycle.

We define the coefficient B, introduced in [2], as the coefficient of fuel growth:

$$KI(n) = \frac{\text{Quantity of fuel discharged from reactor in unit time in the n-th cycle}}{\text{Quantity of fuel charged into reactor in unit time in the (n + 1)-th cycle}} = \frac{P'(n)}{P^0(n+1)} = \frac{\sum_{i=239}^{242} w_i P_i'(n)}{\sum_{i=239}^{242} w_i P_i^0(n+1)} \quad (1)$$

where

$$P_i' = \int_{r \in V_r} \frac{\mu(r)}{T(r)} \rho_i'(r)\, dr; \quad P_i^0 = \int_{r \in V_r} \frac{\mu(r)}{T(r)} \rho_i^0(r)\, dr -$$

are, respectively, the rate of discharging and charging of the i-th isotope; $\mu(r)$ and $T(r)$, mass of heavy atoms and the time of their delay at the point r; $\rho_i'(r)$ and $\rho_i^0(r)$, relative concentrations of the i-th plutonium isotope at the point r; $P' = \sum_{i=239}^{242} w_i P_i'$, $P^0 = \sum_{i=239}^{242} w_i P_i^0$, quantity of equivalent plutonium discharged from the reactor and charged into it; V_r, reactor volume; and w_i, relative worth of the i-th isotope by comparison with ^{239}Pu; the value of w_i are chosen by the researcher.

The coefficient of fuel growth does not give a complete representation of the reactor breeding characteristics, as two reactors with identical coefficients of fuel growth can have a different critical mass or quantity of fuel in the cycle. Therefore, a more important characteristic of the reactor is the rate of breeding of fuel:

Translated from Atomnaya Énergiya, Vol. 55, No. 6, pp. 402-403, December, 1983. Original article submitted December 20, 1982.

0038-531X/83/5506-0859$07.50

TABLE 1. Weight Factors $w_{i,k}$

Isotope i	Variant k								
	1	2	3	4	5	6	7	8	9
239	1	0	0	0	1	1	1	1	1
240	0	1	0	0	1	0	0,15	0,57	0,51
241	0	0	1	0	1	1	1,50	1,1	1,13
242	0	0	0	1	1	0	0,11	0,47	−0,1

$$RB(n) = \left(\begin{array}{c}\text{Quantity of fuel discharged from reactor in unit time in the n-th cycle}\end{array}\right) - \left(\begin{array}{c}\text{Quantity of fuel charged into reactor in unit time in the } (n-1)\text{-th cycle}\end{array}\right)$$

$$\text{Quantity of fuel in the } (n+1)\text{-th cycle}$$

$$= \frac{P'(n) - P^0(n+1)}{G(n+1)} = \frac{r(n)}{G(n+1)} = \frac{\sum_{i=239}^{242} w_i |P'_i(n) - P^0_i(n+1)|}{\sum_{i=239}^{242} w_i G_i(n+1)}, \quad (2)$$

where

$$G_i = \int_{V_r} \mu(r) \left[\bar{\rho}_i(r) + \rho^0_i(r) \frac{\varphi t_{xn}}{T(r)}\right] dr;$$

$\bar{\rho}_i(r)$ is the average relative concentration of the i-th plutonium isotope; t_{xn}, holding time of the plutonium during chemical reprocessing; φ, coefficient of utilization of the nominal power of the nuclear power station; $G = \sum_{i=239}^{242} w_i G_i$, quantity of equivalent plutonium in the cycle; and r(n), annual surplus amount of plutonium.

If $t_{xn} \to 0$, then the quantity of fuel in the cycle tends to the critical mass of the reactor, $G \to M^r_{cr}$. If $t_{xn} \to 0$ and integration is performed with respect to that volume of the reactor where P^0 is different from zero (core), then the quantity of fuel in the cycle tends to the critical mass of the core, $G \to M^{core}_{cr}$.

We shall investigate the change of the parameters characterizing the breeding in open and closed fuel cycles, for certain sets of weight factors $w_{i,k}$ (see Table 1). The first four variants allow the behavior of the individual plutonium isotopes to be considered, the fifth characterizes the changes of plutonium as a chemical element, the sixth — the behavior of the fissile isotopes, the seventh — the equivalent plutonium with respect to the contribution to the critical mass, the eighth — the equivalent plutonium with respect to production of secondary neutrons ($w_{i,8} = \eta_i/\eta_{239}$), and the ninth — the equivalent plutonium with respect to the contribution to the fuel breeding in the natural fuel cycle [3]. The values of $w_{i,9}$ were calculated by the improved method of [2].

Figures 1-3 show the change of the fuel growth coefficient, the fuel breeding rate, and the equivalent excess plutonium in the open and closed fuel cycles in transient conditions, with different weight factors $w_{i,k}$. The parameters T(r), $\rho'_i(r)$, and $\rho^0_i(r)$ were calculated by the procedure proposed in [2]. In the open fuel cycle, in the case of transient fuel conditions, the fuel growth coefficient depends in a significant way on the choice of the weight factors $w_{i,k}$, whereas in the closed fuel cycle it has one and the same value for any weight

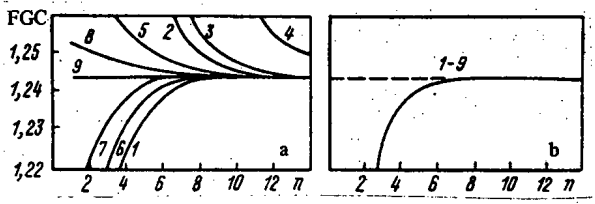

Fig. 1. Dependence of the fuel growth coefficient in the open (a) and closed (b) fuel cycles on n, for different weight factors $w_{i,k}$. Here and in Figs. 2 and 3, the numbers of the curves correspond to the numbers of the variants in Table 1.

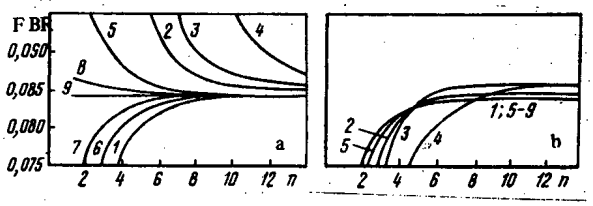

Fig. 2. Dependence of the fuel breeding rate in the open(a) and closed(b) fuel cycles, for different weight factors $w_{i,k}$.

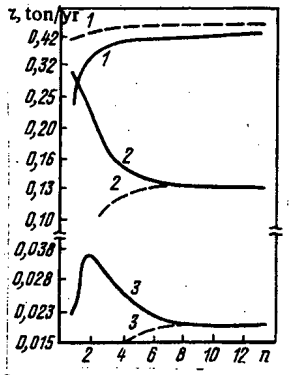

Fig. 3. Curves of the annual surplus quantity of plutonium in the open (——) and closed (— — —) fuel cycles, for different weight factors $w_{i,k}$.

factors. The fuel breeding rate for the transient fuel cycle in the closed fuel cycle depends slightly on the choice of the weight factor $w_{i,k}$, whereas in the open fuel cycle it varies just as strongly as the fuel growth coefficient.

In the transient fuel cycle the breeding characteristics calculated for a closed fuel cycle differ in a significant way from the characteristics calculated for an open fuel cycle as, in the latter case, the composition of the charged and discharged fuel is different. It is only in the natural fuel cycle, when the isotopic compositions of the discharged and charged fuel are identical, that the results of the calculation are independent of the type of fuel conditions, the type of fuel cycle, and the choice of the weight factors $w_{i,k}$.

Thus, when calculating the breeding characteristics in an open fuel cycle, it is recommended that the weight factors $w_{i,9}$ be used, by means of which in transient conditions in the open fuel cycle, the values of the fuel growth coefficient and the breeding rates which are characteristic for the natural fuel cycle can be obtained. In order to estimate the breeding

characteristics of the closed fuel cycle, in the case of transient conditions, from the results of calculations of the open fuel cycle, it is advantageous to use the weight factors $w_{i,\gamma}$.

In conclusion, the author thanks G. B. Usynin for critical comments and discussion of the results of the work.

LITERATURE CITED

1. V. S. Kagramanyan, V. B. Lytkin, and M. F. Troyanov, At. Energ., 46, No. 4, 232 (1979).
2. G. B. Usynin and V. A. Chirkov, At. Energ., 48, No. 6, 357 (1980).
3. N. Hanan, R. Borg, and K. Ott, Am. Nucl. Soc., 28, 286 (1978).

EFFECT OF INTERMOLECULAR INTERACTION IN GASEOUS NITROGEN ON THE SCATTERING CROSS SECTION OF COLD NEUTRONS

S. B. Stepanov, V. E. Zhitarev,
A. M. Motorin, and Yu. V. Sharanin

UDC 539.125.5.162.2

Nitrogen is one of the very few gases for which calculation of the scattering cross section of slow neutrons is possible, including taking exact quantum-mechanical account of the contribution of the rotational motion of the molecules [1]. But a system of free molecules was considered in this case. In its turn the experimental data of [2, 3] have not permitted, due to a certain limitedness, estimating the adequacy of the theoretical model and the reliability of the computational scheme. For neutrons with a wavelength $\lambda \lesssim 0.5$ nm the agreement of the data was good (Fig. 1), but at a longer wavelength the experimental data of [3] differed strongly from the calculation. The gas pressure was not varied in [2, 3]. The scattering cross section in nitrogen at a gas pressure of 4-60 bar (1 bar = 10^5 Pa) and a neutron wavelength of 1.3-1.9 nm has been investigated previously [4]. In accordance with the "quasiideal" approximation of [5], the scattering cross section of slow neutrons in a real gas should be proportional to the ratio of its density ρ to the density of an ideal gas ρ_0. For nitrogen $\rho/\rho_0 \approx 1$ over a wide range of state parameters. Actually, in contrast to the results for water and benzene vapors [4], an almost constant scattering cross section was observed at a nitrogen pressure up to approximately 40 bar. However, at a still greater pressure some decrease of the cross section was recorded, and the effect exceeded the experimental error. The difference from the computational results of [1] was very large.

The purpose of this paper is to obtain results over a wider range of conditions (neutron energy, gas pressure) in order to fill the gap in the experimental data in comparison with the calculations and to reliably establish the effect of gas pressure on the scattering cross section of neutrons.

The interaction cross section of nitrogen was determined at a temperature of 288 ± 3°K and a pressure of 30-132 bar for neutrons with a wavelength of 0.6-1.7 nm. The transmission of the gas samples was measured by a crystal spectrometer with a curved neutron guide and a monochromator made out of fluorophlogopite. The apparatus, similar in type to those described in [6], operates on the beam of the IRT-2000 of the Moscow Physics Engineering Institute; its characteristics are: a spectrum with a short-wavelength limit $\lambda_{lim} = 5$ nm and a maximum at $\lambda_{max} = 1.1$ nm; resolution $\Delta\lambda/\lambda \lesssim 0.04$; and a counting rate of monochromatic neutrons of 70-800 sec^{-1}. The aluminum alloy containers for the gas had two chambers each equipped with lead-ins for a thermocouple and a manometer and with an "inflow—outflow" valve which are in communication with each other through a valve. The division of the gas chamber into two

Translated from Atomnaya Énergiya, Vol. 55, No. 6, pp. 403-405, December, 1983. Original article submitted March 11, 1983.

 0038-531X/83/5506-0862$07.50

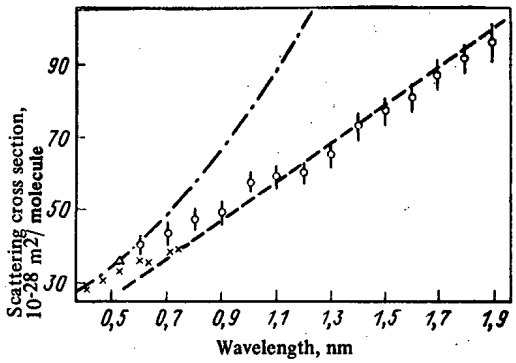

Fig. 1. Scattering cross section of cold neutrons by a nitrogen molecule: ○) experiment of this paper (p = 30 bar); – – – and –·–) calculation according to the relationship in [9] and [1]; Δ, ×) experiment of [2] and [3] at p = 8.5 bar.

parts permitted more convenient and rapid measurement of the passage of the gas from maximum values of pressure and volume to minimum values with subsequent scouring and bypassing of the gas. The absence of an effect of multiple scattering was simultaneously checked: The interaction cross section at a single value of the pressure did not depend on sample thickness. The transmission of the gas in the tests was 0.5-0.8 and of the empty container — 0.4-0.7. The pressure was measured with an error of 0.5-3%; the density was determined on the basis of data of [7] with an overall error of 1-4%. The error in determining the thickness of the gas layer (25-60 mm) was no more than 1%. The measurements were made for ten values of the nitrogen pressure in three independent series, including using different containers. The results for each value of the pressure are averaged. The total error of the calculated values of the interaction cross section was 2-7%. In calculating the cross section of scattering by a nitrogen atom the absorption cross section $\sigma_a \sim \lambda$: $(1.85 \pm 0.05) \times 10^{-28}$ m^2 at $\lambda = 0.18$ nm [8] was subtracted from its total interaction cross section.

The results of the research showed that the macroscopic cross section of cold neutrons in nitrogen decreases as the gas pressure increases, and this variation falls outside the limits of experimental error in the $p \gtrsim 40$-50 bar pressure region. Figure 2 illustrates this result for neutrons with wavelength 0.6, 1.3, and 1.7 nm. A sharp increase of the effect at large values of the wavelength is observed: The variation of the total scattering cross section reaches 20%, and $\partial\sigma_s/\partial p$ varies appreciably (from 0.01 to 0.15×10^{-28} m^2/bar with a linear approximation in the 30-130 bar region).

Previously published computational [1] and experimental [2, 3] data as well as results which we obtained at a nitrogen pressure of 30 bar are shown in Fig. 1. The variation in the scattering cross section does not exceed 6% in the 4-30 bar pressure region according to our data, so that the result of a comparison of all the data is completely indicative. The large discrepancy of the calculated cross section [1] measured experimentally in the region of cold neutrons is confirmed. This can be more easily explained by errors in the computational scheme which implements the theoretical model with its potential for miscalculation than by any inadequacy of the model itself: Such errors can be large for such a small energy of the neutrons. The calculation which we made on the basis of the limiting relationship of [9] for a small neutron energy, which is obtained in a model of an ideal monatomic gas with a molecular mass equal to 28 neutron masses, gave an appreciably better result (see Fig. 1). This indicates in particular an inappreciable contribution of rotation of the nitrogen molecules to the scattering cross section.

One can qualitatively explain the detected dependence of the total scattering cross section on gas pressure on the basis of the characteristics of the phenomenon observed earlier of the effect of the dynamics of molecules on the scattering of slow neutrons. Thus it proved successful in [10] to record the broadening of a quasielastic scattering line in gaseous hydrogen upon a lowering of its pressure, which is characteristic of a weakening of the degree of chemical binding of the molecules and a slowing down of their motion. The authors of [10]

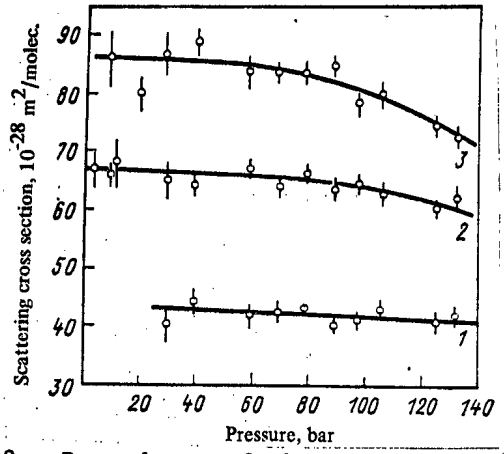

Fig. 2. Dependence of the scattering cross section of neutrons in nitrogen at (1) λ = 0.6, (2) 1.3, and (3) 1.7 nm on its pressure: $p \geqslant 30$ bar — this paper; $p < 30$ bar — [4].

have explained the effect as the action of collisions of the molecules on their translational motion. At the same time it has been shown for a broad class of condensed and gaseous materials that as the overall mobility of the particles scattering the neutrons decreases, the degree of slowing down of their motion increases, and the effective mass increases the total scattering cross section of cold neutrons decreases by virtue of the inelastic component [4, 9]. And so as long as the gas pressure is so low that the molecules on the average are located at distances greater than the effective action radius of intermolecular forces and the neutron wavelength, and molecular collision events are rare relative to the interaction time of cold neutrons with molecules, the scattering of neutrons occurs primarily the same as in a gas of free particles. As the gas pressure increases, the collision frequency of molecules increases and the average distance between them decreases. A neutron interacts now with molecules which are to this or that extent under the influence of their nearest neighbors, which increases the effective mass of the scattering particle. Upon a change in pressure from 4 to 132 bar the distance between nitrogen molecules varies from 2.2 to 0.65 nm, and the time between their collisions varies from 30 to 2 psec. The time for a neutron with wavelength 1 nm to traverse the region occupied by a nitrogen molecule is ~1 psec. It is natural to assume that it is precisely intermolecular collisions and interaction which determine the observed dependence of the scattering cross section on gas pressure. Estimating according to the relationship mentioned [9] the variation of the effective mass of the gas particles upon a change in pressure on the basis of the cross sections measured in this paper, we obtain that the mass increases by 10 and 50% in the 30-130 bar range for neutrons with wavelengths of 0.7 and 1.7, respectively.

Thus the data obtained in this paper on the scattering cross section of cold neutrons in nitrogen have for the first time permitted making a reliable confirmation of the existing computational results within the framework of ideal gas models in the energy range up to approximately 10^{-4} eV. A dependence of the microscopic scattering cross section of neutrons on gas pressure has been discovered which is qualitatively explained by the effect of intermolecular collisions. The possibility of experimental confirmation of dynamic scattering models which would take account of intermolecular interaction in the gas is shown.

LITERATURE CITED

1. J. Løvseth, Kjeller Report, No. 26 (1962).
2. E. Fermi and L. Marshall, Phys. Rev., 75, 578 (1949).
3. V. P. Vertebnyi et al. At. Energ., 18, No. 5, 452 (1965).
4. V. E. Zhitarev, Candidate's Dissertation, MIFI, Moscow (1980).
5. A. Fulinski, Acta Phys. Polon., 34, No. 1, 119 (1968).
6. S. B. Stepanov et al., in: Neutron Physics [in Russian], Izd. FÉI, Obninsk (1974), p. 257.
7. A. A. Vasserman et al., Thermophysical Properties of Air and Its Constituents [in Russian], Nauka, Moscow (1966).

8. Neutron Cross Sections, Vol. 1, Ses. ed. Supp. No. 2, BNL-325 (1964).
9. E. Yanik and A. Koval'skaya, in: The Scattering of Thermal Neutrons [in Russian], Atomizdat, Moscow (1970), p. 377.
10. Y. Lefevre et al., in: Neutron Inel. Scatt., Vienna (1972), p. 445.

COMPOSITION OF THE GASEOUS PHASE AND THE BEHAVIOR OF XENON AND KRYPTON IN IRRADIATED FUEL ELEMENTS OF A BOR-60 REACTOR

A. P. Kirillovich, Yu. I. Pimonov,
Yu. G. Lavrinovich, and O. S. Boiko

UDC 621.039.546

The gaseous phase in irradiated fuel elements is a complex multicomponent system consisting of a filler gas (He, Ar, and others), gaseous fission products (GFP), and nonfragmentary (process) gases desorbed from the fuel [1]. The investigation of the amount and composition of this phase has great meaning for raising the efficiency of the fuel elements and ensuring the safety of the reactor as well as for accomplishing the subsequent regeneration of the depleted fuel. Only a few publications [2-4] are devoted to the investigation of the composition of the gaseous phase in irradiated fuel elements and to the behavior of GFP at different stages of the fuel cycle, which is evidently associated with systematic and technological difficulties.

The aim of this article is to develop a procedure for the sampling and mass spectrometric analysis of the chemical and isotopic composition of the gaseous phase in irradiated fuel elements as well as to investigate the composition of the gases in regular and experimental heat-generating assemblies (HGA) of a BOR-60 reactor and the behavior of Kr and Xe in the stage of thermal opening (fusing) of the fuel element casing.

Procedure of the Investigation. In working out a procedure of quantitative mass spectrometric analysis of complex gas mixtures the coefficients of relative sensitivity of the gas constituents being analyzed and the intake pressure region in which these coefficients remain constant were determined, and operating regimes of the mass spectrometer ion source which provide maximum sensitivity to the gases being determined were selected.

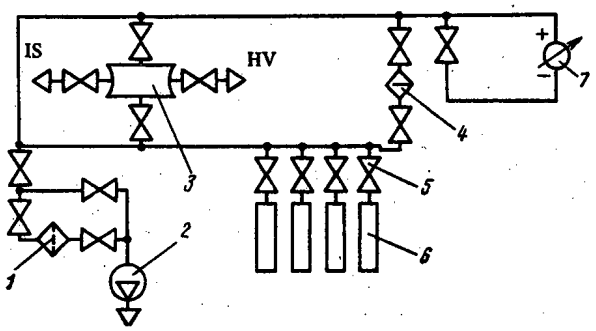

Fig. 1. Intake system: 1) sorption trap; 2) vacuum pump; 3) intake tank; 4) mixer; 5) valve; 6) sampler ampul; 7) manometer; IS) to the ion source; HV) to the high vacuum.

Translated from Atomnaya Énergiya, Vol. 55, No. 6, pp. 405-407, December, 1983. Original article submitted April 18, 1983.

0038-531X/83/5506-0865$07.50

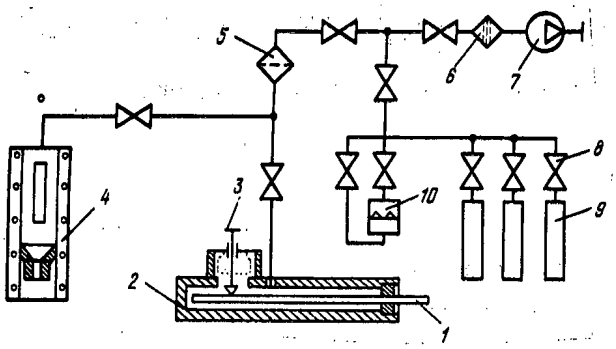

Fig. 2. Layout of the sampler: 1) fuel element; 2) mechanism for puncturing the fuel elements; 3) needle; 4) apparatus for thermal opening (fusing) of the casing; 5) filter; 6) absorbing column; 7) vacuum pump; 8) valve; 9) sampling ampul; 10) manometer.

TABLE 1. Main Characteristics of the Investigated Fuel Elements

Characteristics and parameters of HGA irradiation	Regular HGA	Exptl. HGA
Fuel comp.	UO_2 (90% enrichment in ^{235}U)	80% UO_2 (90% enrichment in ^{235}U) + 20% PuO_2
Av. depletion of heavy atom, %	11	
Holding time after irradiation, months	4	7

TABLE 2. Amount and Composition of the Gaseous Phase under the Casing of Some Fuel Elements of a BOR-60 Reactor

No. of fuel elements investigated	HGA	Amt. of gas, cm^3/fuel element	Content, vol. %							
			H_2	He	N_2	O_2	Ar	CO_2	Kr	Xe
5	Regular	93±14	0,09±0,010	4,30±0,26	0,16±0,02	0,040±0,003	0,040±0,003	0,009±0,002	14,0±0,3	81,4±0,8
4	Exptl.	257±8	0,07±0,05	2,6±1,3	1,15±0,69	0,29±0,21	0,46±0,23	0,054±0,010	12,5±0,2	82,8±0,8

TABLE 3. Release of Xe and Kr from the Fuel upon Its Heating and the Fusing of the Fuel Element Casing, cm^3/fuel elements

Temperature in fusing furnace, °C	Kr	Xe
	Regular HGA	
25—900	0,1	0,325
900—1300	2,56	7,69
2300—1650	1,5	8,36
	Experimental HGA	
25—800	0,071	0,77
800—900	0,0094	0,048

TABLE 4. Yield of Xe and Kr from the Irradiated Uranium and Uranium–Plutonium Fuel of a BOR-60 Reactor

Engineering operations	Xe		Kr	
	UO_2	UO_2-PuO_2	UO_2	UO_2-PuO_2
Puncture of the fuel element casing	0,059±0,008 / 81,9	0,1141±0,0041 / 98,5	0,0064±0,0009 / 76,2	0,0110±0,0004 / 99,1
Fusing of the fuel element casing	0,013±0,002 / 18,1	0,0017±0,0003 / 1,45	0,0020±0,0004 / 23,8	0,00010±0,00002 / 0,9
Total measured amt. of gas	0,072±0,010 / 100	0,1158±0,0044 / 100	0,0084±0,0013 / 100	0,01110±0,00042 / 100

Remark: The yield of the elements, g/g of the depleted fuel, is indicated in the numerator, and the percentage of the total measured amount of Xe and Kr is indicated in the denominator.

The measurements were made with an MI-1201 mass spectrometer additionally equipped with a gas intake system (Fig. 1) according to the procedure of [5]. We used the method of comparing the sample being analyzed with a control gas mixture prepared from certified gases, i.e., gases which have been additionally checked for purity (the instrument was not calibrated for tritium, since the sensitivity of the mass spectrometer to hydrogen – protium, deuterium, and tritium – is identical [6]), in investigating the composition of the gaseous phase. In order to raise the sensitivity when determining a small amount of tritium (T_2) and hydrogen, an ampul with the gas mixture to be analyzed was connected directly to the ion source through a membrane with a 50-μm hole and cooled to the boiling temperature of liquid nitrogen. The ion source operated in the maximum sensitivity regime of the instrument for hydrogen (10^{-10} g (10^{-6}%)). No special measures were adopted to concentrate tritiated water (T_2O) and other tritium compounds. The relative mean square deviation in the determination of Xe and Kr was 1 and 2%, respectively, and it did not exceed 15% for the remaining constituents of the gas mixture (He, Ar, N_2, O_2, CO, and CO_2) when their volume content ranged from 0.01 to 100%.

Sampling of the gases from under the casings of irradiated fuel elements and from the apparatus for thermal opening of the fuel element casing by fusing was done with the help of a sampler system (Fig. 2) located in a protective chamber. The ampuls and sampler system were put under a vacuum in advance to a pressure of 6.6 and 13.3 Pa and checked for inleakage. The residual background in nitrogen and oxygen in the ampuls did not exceed 1×10^{-13} and 5×10^{-14} A, respectively. Calculation of the amount of gas released from the fuel under the fuel casing was done from the measured pressure (the accuracy class of the instrument was 1.5) and the known volume of the sampling system (see [5] for more detail).

Results of the Experiments and Discussion of Them. The characteristics and parameters of the irradiation of the investigated fuel elements of regular and experimental HGA of a BOR-60 reactor are given in Table 1, and the results of measurement of the amount and composition of the gaseous phase are given in Table 2. As follows from the latter, Kr and Xe, whose average content varied from 8 to 14 and from 81.4 to 89.59% for various types of fuel elements, are the main constituents of the gaseous phase of irradiated fuel elements with uranium oxide and uranium–plutonium fuel. In addition to Kr and Xe, H_2, He, N_2, CO, O_2, Ar, and CO_2 were detected under the casing of fuel elements. The presence of "nonfragmentary" gases can be explained by the fabrication technology of the fuel and fuel elements and by other factors (for example, by radiolysis of moisture, release or absorption of oxygen as a result of the chemical interaction of the fuel with constituents of the gaseous phase and the casing, and so on).

Elemental tritium (T_2) has not been detected in the gaseous phase of irradiated fuel elements of regular and experimental HGA at the maximum sensitivity of the method. The observed variations in the amount of gas (here and later the measurement data are given in cm^3 at normal conditions) in individual fuel elements of regular HGA (from 77 to 112 cm^3) exceed the error in determining the volume of released gas and can be explained by small differences in the fuel charging and in the conditions of fabrication of the individual fuel elements and their irradiation in the reactor. It turned out (see Table 2) that the amount of gas released from uranium–plutonium fuel under the fuel element casing exceeds by approximately a

TABLE 5. Isotopic Composition of Xe and Kr in the Fuel Elements of the BOR-60 Reactor

HGA	Xe				Kr			
	131	132	134	136	83	84	85	86
Regular	14,2±0,2	22,8±0,4	34,8±0,4	28,2±0,4	15,4±0,2	28,4±0,4	6,57±0,13	49,83±0,3
Exptl.	15,0±0,2	22,8±0,4	33,8±0,4	28,4±0,4	15,9±0,2	28,3±0,4	6,63±0,13	49,17±0,30

factor of two the volume of gases in irradiated fuel elements with uranium fuel. This may be a consequence of a larger fuel charge in the fuel elements and (or) a higher depletion of the uranium–plutonium fuel and specific linear loading during irradiation of the HGA in the reactor (see Table 1).

We investigated the behavior of Xe and Kr upon heating of the fuel elements to 700°C in the puncturing mechanism (see Fig. 2) and upon thermal fusing of their casings. It was established that when the fuel is heated part of the Xe and Kr is additionally released from it. This release is described by the following empirical equations for uranium–plutonium fuel in the 20-700°C temperature range:

$$v_{Xe} = 212{,}8 + 0{,}0010t;$$
$$v_{Kr} = 32.12 + 0.00009t,$$

where t is the temperature, °C, and v is the amount of gas (Xe, Kr), cm^3/fuel element.

Data on the release of Xe and Kr upon the heating of fuel elements in the thermal opening apparatus (see Fig. 2) are presented in Table 3. The total amount of Xe and Kr measured in the gaseous phase under the casing of fuel elements and when it is fused is given in Table 4. The relationship of Xe and Kr is not identical for the different types of fuel elements, which indicates a difference in the nature of the release of these GFP from the fuel both in the course of its irradiation in the reactor (which is evidently associated with the different irradiation regimes) and in the subsequent heating of the irradiated fuel elements and fusing of the casing. Thus for uranium–plutonium fuel the Xe and Kr yield from under the casing were 98.5 and 99.1%, respectively, of the total measured amount, whereas for fuel elements with uranium fuel it is equal to 81.9 and 76.2% (see Table 4). Part of the Xe and Kr remains in the fuel after fusing of the fuel element casing (1650°C) and may be released from it during chemical regeneration, for example.

A procedure is being developed at the present time for measurement of the amount of Xe and Kr released during chemical regeneration of depleted fuel which will permit accomplishing a balance in the GFP. The isotopic composition of xenon and krypton in the investigated fuel elements with UO_2 and UO_2–PuO_2 fuel irradiated in a BOR-60 reactor differs inappreciably (Table 5).

The experimental data obtained on the composition of the gaseous phase in irradiated fuel elements of a BOR-60 reactor with uranium and uranium–plutonium fuel and on the behavior of Xe at the stage of preparation of fuel elements for regeneration can be used for physical and engineering calculations in the design and operation of nuclear and radiochemical fuel regeneration facilities.

LITERATURE CITED

1. B. V. Samsonov and V. Sh. Sulaberidze, Gas Release from Oxidized Nuclear Fuel. Analytical Review NIIAR V-16 [in Russian], Dimitrovgrad (1977).
2. A. T. Ageenkov et al., At. Energ., 40, No. 3, 203 (1976).
3. A. T. Ageenkov et al., At. Energ., 41, No. 1, 23 (1976).
4. A. T. Ageenkov and E. M. Valuev, At. Energ., 41, No. 2, 141 (1976).
5. A. P. Kirillovich et al., Preprint NIIAR-31 (439), Dimitrovgrad (1980), p. 27.
6. M. Goldblatt and W. Gones, Anal. Chem. 36, 431 (1964).

BASICS OF PULSED NEUTRON LOGGING WHEN STRONG ABSORBERS ARE ESTABLISHED

D. K. Galimbekov, I. T. Ilamanova,
B. E. Lukhminskii, and A. I. Pshenichnyuk

UDC 550.83

The space–time distribution of neutrons and γ radiation from radiative capture has been theoretically treated in [1, 2] in relation to problems of pulsed neutron logging. Some useful qualitative conclusions in the theory of pulsed neutron logging have been drawn in [2] on the basis of numerical results obtained for a homogeneous infinite medium with a uniformly distributed absorber. Particularly, the authors of [3] have reported on experimental work in which the possibilities of various techniques of pulsed neutron logging were evaluated for establishing strong absorbers of neutrons. The investigations have confirmed that the pulse techniques are more sensitive than the stationary techniques as far as the concentration of neutron absorbers is concerned.

But a number of theoretical problems have not been solved: the possibilities of pulsed neutron logging techniques with short delay times; precise quantitative estimates of the influence which imply changes in the borehole diameter and the position of the instrument in the borehole; influence of the spectral composition of the γ radiation from radiative capture upon the readings of pulsed neutron γ logging; and the possibilities of techniques based on measurements of emission spectra.

These problems were solved with the Monte Carlo method. The features of the program are as follows: the geometry of the problem assumes a water-filled borehole; the pulsed neutron-logging instrument comprises a neutron generator (energy 14.1 MeV); the ore layer is modeled by sand (SiO_2) containing cinnabar (HgS; isotropic elastic scattering, radiative capture, and resonance capture of fast and epithermal neutrons and radiative capture in the thermal range were taken into account; the program portion modeling the transfer and the recording of γ quanta was taken from [4].

The analysis of the results of the calculations made it possible to assess the time in which the nonstationary distribution of the thermal neutrons and of the γ radiation from radiative capture becomes exponential, i.e., when the space–time dependencies are locally multiplicative. In the case of a pulsed neutron logging instrument with a long probe (thickness of the shield between the target of the generator and the detector) of 5-30 cm, the distribution of thermal neutrons is locally multiplicative in logging work in boreholes with a diameter of 59-76 mm, provided that the delay time after a pulse exceeds 300-400 μsec for the enclosing rock, and in practically the entire time interval in the case of rock with a cinnabar volume concentration q = 1%.

Recommendations can be derived from the calculations for selecting the measurement conditions in pulsed neutron–neutron logging work when neutrons are recorded in three time "windows" with center positions of 150, 350, and 800 μsec. The neutron fluxes which can be recorded in the windows then fall on the exponential portions which correspond to rock rich in mercury, poor in mercury, or enclosing rock. The window width required for reaching the necessary statistical accuracy is experimentally determined. The dependence of the attenuation decrement λ_n, measured on the exponential portion, upon the lifetime τ_n of the thermal neutrons in the layer (or upon the cinnabar concentration) is shown in Fig. 1. It follows from the figure, which may serve as a nomogram for determining the cinnabar concentration from λ_n, that in a borehole with a diameter of 59 mm, the differentiation by way of the decrement for rocks with a cinnabar concentration between 0 and 1% amounts to 10 and does not depend upon the position of the instrument in the borehole. In a borehole with a diameter of 76 mm, the differentiation on the basis of λ_n decreases to 5 and thereafter drops off sharply with increasing borehole diameter.

Translated from Atomnaya Énergiya, Vol. 55, No. 6, pp. 407-409, December, 1983. Original article submitted May 16, 1983.

0038-531X/83/5506-0869$07.50

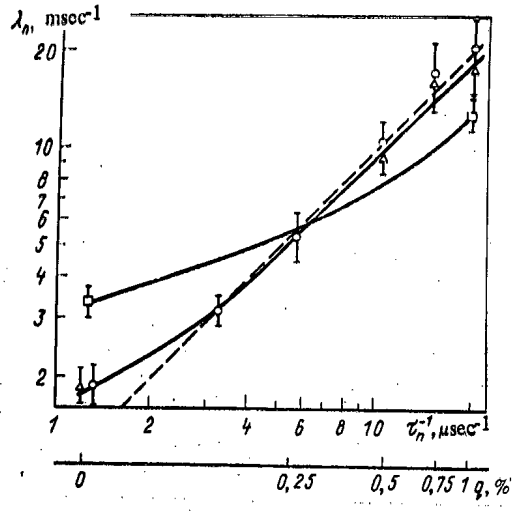

Fig. 1. Theoretical chart for interpreting pulsed neutron—neutron logging in boreholes (diameter of the instrument 42 mm); □ refers to a borehole diameter of 76 mm (instrument in the center); ○ and △) 59 mm (instrument in the center and at the wall, respectively); – – – –) dependence for an infinite homogeneous medium.

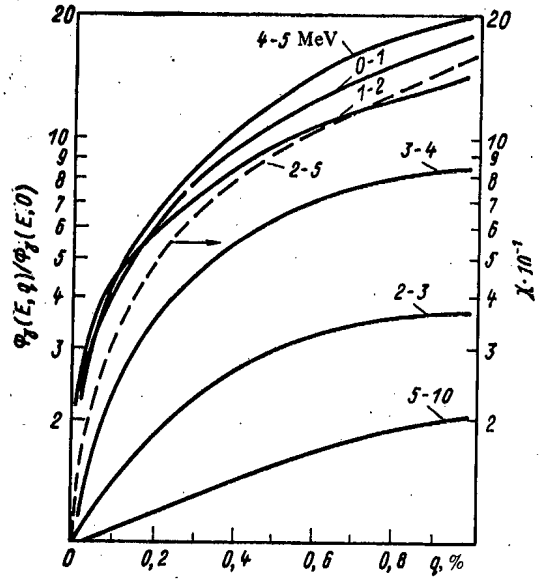

Fig. 2. Dependence of the flux $\Phi_\gamma(E, q)$ (——) and of χ(– – –) upon the volume concentration of cinnabar.

The field of the γ radiation from radiative capture is basically given by the neutron field. But the field is characterized by spectral features resulting from the material composition of the rock. An analysis of the dependency of the distribution has shown that the recommendations made for the measurement conditions in pulsed neutron—neutron logging are applicable to pulsed neutron γ logging with integral recording of the γ radiation from radiative capture. The rock differentiation through the attenuation decrement λ_γ is 12-13, i.e., it is higher than in pulsed neutron—neutron logging because the borehole has a lesser influence upon the readings of pulsed neutron γ logging. The rock differentiation through the flux $\Phi_\gamma(q)$ of the γ radiation measured with a small delay time (e.g., 0-25 μsec) is the same as in the λ_γ measurements. Though the amplitude characteristic of Φ_γ is less affected by

disturbances in the case of short times than the attenuation decrement (the influence of a hydrogen-containing layer, changes in borehole diameter, instability of the neutron yield), the spectral version of the technique has certain advantages over measurements of the decrement: higher sensitivity to the absorber concentration and absence of the disturbing background of the natural radioactivity of rocks.

Figure 2 depicts the dependence of the flux $\Phi_\gamma(E, q)$ of γ radiation from radiative capture (flux normalized to the flux $\Phi_\gamma(E, 0)$ in the enclosing rock) in the time interval 0-25 μsec for various energy intervals (see numbers at the curves). The highest sensitivity to changes in q is observed at 4-5 MeV. The low sensitivity at 5-10 MeV is explained by the missing mercury emission in this interval. Figure 2 includes the quantity

$$\chi = \frac{\Phi_\gamma(E, q)}{\Phi_\gamma(E, 0)} \frac{\tau_e(0)}{\tau_e(q)}$$

for 2-5 MeV. The quantities $\tau_e(0)$ and $\tau_e(q)$ are inverse quantities of the decrement λ for the enclosing rock and the ore, respectively. The quantity χ varies by more than two orders of magnitude in the energy interval under consideration.

Thus, based on the results of the calculations, the laws governing the time distribution of the thermal neutron field and the γ radiation field from radiative capture were determined for short delay times. The influence which changes in the borehole diameter and the eccentricity of the instrument have upon the readings of pulsed neutron logging has been determined with great precision. It has been shown that the pulsed neutron γ logging technique with short delay times is promising. Furthermore, it has been shown that it is possible to increase the efficiency of pulsed neutron γ logging when the spectral version of the technique is employed.

LITERATURE CITED

1. A. L. Polyachenko and N. S. Erichman (Érikhman), Fiz. Zemli, No. 8, 106 (1971).
2. V. F. Zakharchenko, Izv. Akad. Nauk SSSR, Ser. Geofiz., No. 10, 1522 (1963).
3. D. K. Galimbekov, in: Mathematical Modeling in Nuclear Geophysics [in Russian], Bashkir Branch, Academy of Sciences of the USSR, Ufa (1979), p. 66.
4. Nuclear Physics Techniques of Elementary Analysis and of Geophysical Sounding [in Russian], Nedra, Moscow (1972).

NUCLEAR-PETROPHYSICAL BASICS OF NEUTRON MEASUREMENTS IN ROCKS

A. I. Pshenichnyuk

UDC 539.125.523:550.832.5

The modern orientation of nuclear geophysics toward indirect measurements of neutron characteristics of rocks [1] requires the compilation and analysis of a set of characteristics for solving the corresponding direct and inverse problems. Since the number of parameters in the set coincides with the number of independent characteristics of the radiation field, the set determines the maximum information content of the technique of the measurements. Numerical calculations of neutron characteristics are important for the nuclear-petrophysical foundations of research in geophysics.

The high requirements to the solution of the problem manifest themselves through the measurement conditions: wide variability range of the hydrogen concentration; high neutron energy (14 MeV) at which inelastic scattering, angular anisotropy, and neutron absorption in reactions with emission of charged particles take place; and measurements at distances from the source which are characterized by a flux attenuation of 3-4 orders of magnitude so that the angular distribution of the radiation must be taken into account.

These requirements are met by the method developed in [2, 3] for solving the transfer equation. The method is based on a modified transport approximation and the technique of spectral approximations. The collision density of neutrons provided by a two-dimensional isotropic monoenergetic source in a medium of some composition is of the form

$$\Psi_0(z, u)=\frac{h(0)}{2\pi}\int_{-\infty}^{\infty}\frac{\operatorname{arctg} x\lambda(0)}{x\lambda(0)}\frac{\tilde{h}(x, u)}{h(u)\tilde{M}(x, u)}\exp\left[ixz-\int_0^u\frac{\tilde{g}(x, u')}{\tilde{M}(x, u')}du'\right]dx \tag{1}$$

(the notation is the same as in [2, 3]). Let us approximate the transformation function in Eq. (1) by the formula

$$\overline{\Psi}_0^*(x, u)=A(u)\frac{\exp\left[-B(u)\sqrt{1+C(u)x^2}\right]}{\sqrt{1+C(u)x^2}},$$

which preserves the essential features of a precise transformation and which allows an analytic treatment. The free parameters A, B, and C are obtained from the condition that the first three spatial moments coincide. Then

$$\Psi_0^*(z, u)=\frac{1}{\pi}\Psi(u)e^{\alpha(u)}\left(\frac{\alpha(u)+1}{2\tau(u)}\right)^{1/2}K_0\left[\alpha(u)\sqrt{1+\frac{\alpha(u)+1}{\alpha^2(u)}\frac{z^2}{2\tau(u)}}\right], \tag{2}$$

where

$$\alpha(u)+1=2\left[\sqrt{1+\frac{4}{3}Ex(u)-1}\right]^{-1}; \tag{3}$$

$$Ex(u)=6\tau_4(u)/\tau^2(u). \tag{4}$$

The notation is interpreted as follows: $K_0(x)$, a Bessel function; $\Psi(u)$, neutron spectrum; $\tau(u)$, age of the neutrons; and $Ex(u)$, excess of the distribution of Eq. (1). The

Translated from Atomnaya Énergiya, Vol. 55, No. 6, pp. 409-410, December, 1983. Original article submitted May 30, 1983.

 0038-531X/83/5506-0872$07.50

spectrum, the age, and $\tau(u)$ are defined by the formulas

$$\Psi(u)=\frac{h(0)}{M(u)}\exp\left[-\int_0^u\frac{g(u')}{M(u')}du'\right]; \tag{5}$$

$$3\tau(u)=\lambda^2(0)+\int_0^u h(u')\,l^2(u')\,[1-g(u')\,\theta(u')]\,\frac{du'}{M(u')}+l^2(u)\,[1-h(u)\,\theta(u)]; \tag{6}$$

$$5\tau_4(u)=\frac{13}{18}\,\lambda^4(0)+\int_0^u h(u')\,l^4(u')\times$$

$$\times\left\{[1-g(u')\,\theta(u')]\left[1+\frac{5}{9}\,h(u')\,\theta(u')\right]+\frac{5}{9}\,h(u')\,g(u')\,\frac{\beta_2(u')}{M(u')}\right\}\frac{du'}{M(u')}+$$

$$+l^4(u)\left\{[1+h(u)\,\theta(u)]\left[\frac{13}{18}+\frac{5}{18}\,h(u)\,\theta(u)\right]-\frac{5}{9}\,h^2(u)\,\frac{\beta_2(u)}{M(u)}\right\}, \tag{7}$$

where we have introduced, for the sake of brevity, the notation

$$l^2(u)=\frac{\lambda^2(u)}{1-h(u)\,\bar{\mu}_0(u)};\quad \theta(u)=M^{-1}(u)\,[\beta_1(u)+2g(u)\,\beta_2(u)].$$

The structure of Eq. (2) resembles that of the formula obtained in the P_2 approximation of the theory of continuous moderation [4]. The parameter M(u) is given by the type of the spectral approximation [3]. We observe a difference of at most 10% between the spatial distribution (calculated with Eq. (2)) of 1.46-eV neutrons in water (neutrons emitted from a two-dimensional isotropic ^{235}U fission source) and the experimental results of [5] in the distance interval which is characterized by a flux-density attenuation of three orders of magnitude. At a lower hydrogen concentration (water-saturated quartz sand) the comparison with the results of the Monte Carlo method shows full agreement within the error limits. The age figures for iron–water and aluminum–water mixtures and graphite differ from the experimental results of [5-7] by at most 5%.

The space–time and the energy distributions of moderated neutrons were calculated on the basis of the properties of the space–time multiplicativity of the distribution function [1]. The time distribution is given by the total moderation time $t_s(u)$ and the dispersion D[t(u)] of the pulse of moderated neutrons [8].

A program making use of the ENDL-2 library was compiled for routine calculations of the neutron parameters (Eqs. (5)-(7)) and of $t_s(u)$ and D[t(u)]. Inelastic scattering, absorption, and anisotropy of the scattering in the center-of-mass system were taken into account up to the fourth order. Equations (5)-(7), supplemented by equations for the moderation time and the dispersion of the pulse, determine the unknown set of neutron characteristics of the moderator and define the field of epithermal neutrons with a precision which is adequate for applications in nuclear geophysics.

LITERATURE CITED

1. D. A. Kozhevnikov, Neutron Characteristics of Rock and Their Use in the Geology of the Oil and Gas Industry [in Russian], Nedra, Moscow (1982).
2. D. A. Kozhevnikov and A. I. Pshenichnyuk, At. Energ., 51, No. 6, 366 (1981).
3. D. A. Kozhevnikov and A. I. Pshenichnyuk, At. Energ., 51, No. 6, 370 (1981).
4. I. A. Kozachok, V. V. Kulik, and V. I. Pirogov, At. Energ., 38, No. 3, 167 (1975).
5. R. Paschall, Nucl. Sci. Eng., 20, 451 (1964).
6. P. Palmedo, Nucl. Sci. Eng., 32, 302 (1968).
7. R. Paschall, J. Nucl. Energy, Part A, 20, 57 (1966).
8. D. A. Kozhevnikov, At. Energ., 40, No. 5, 338 (1976).

OPTIMIZATION OF RECTIFICATION AND EXCHANGE PILOT PLANTS FOR ISOTOPE PRODUCTION

V. A. Kaminskii, G. A. Tevzadze,
V. M. Vetsko, O. A. Devdariani,
and G. A. Sulaberidze

UDC 621.039.3

The difficulty of separation and the high cost of isotope-enriched compounds make it necessary to optimize the separating installations of all levels of output by using as many process and apparatus parameters as possible; the most common characteristic reflecting the efficiency and economy of a process is the cost of the enriched product.

It should be noted that the determination of an explicit cost function is impossible unless we take account of the design solution of the installation. In the general approach to optimization described in our previous article [1], two main design variants are possible. The first, described in [1], assumed that in approximating an ideal cascade by a cascade of rectangularly sectioned form we use a parallel and series set of columns of the same diameter and height with individual phase-conversion devices. This variant is intended for industrial large-scale production of isotopes.

For installations of pilot-plant scale, it is advisable to use one column of different diameter in each section. These columns are connected according to a scheme in which the flow of liquid in the following section is part of the flow in the preceding one, and the gas flow in the following section is fed directly to the preceding one. At the joints between the sections there is only partial phase conversion. Unlike the first design variant, in the present case each section is characterized not only by different values of the diameter of the columns with stage height H_n but also by the relative density of the flow, γ_n, and in the general case it contains packing with elements of different dimensions. The sections of such a cascade are usually placed vertically one under the other, and the stripping section constitutes a single whole with the column of the first section. Therefore, it is desirable to introduce into the optimization conditions either a limitation on the height of the installation, if the latter is situated in a definite room,

$$\sum_n S_n H_n \leqslant Z_{\max}, \tag{1}$$

or a cost coefficient characterizing the capital expenditures per unit height of the room, a_{cz}.

In using inequality (1), we must bear in mind that for given conditions there exists not only a minimum possible number of stages

$$S_{\min} = \frac{1}{\varepsilon} \ln \frac{c_P (1 - c_W)}{c_W (1 - c_P)}, \tag{2}$$

but also a minimum value of the stage height itself, which is determined by the competing effects of the vapor velocity and the number of stagnation zones on this quantity. Therefore in some cases conditions (1) may not be satisfied, and then we must discard the variant in which the columns of the cascade are all arranged vertically. However, even if condition (1) is satisfied, it must be borne in mind that it may have a marked effect on the result of the optimization, tending to reduce the relative load and increase the flow in the first section. This leads, respectively, to a reduction of the value for the height of a stage and to a reduction in the required number of stages. It must also be borne in mind that for technical reasons, the diameter of the columns and the dimensions of the packing elements must not be too small, i.e.,

Translated from Atomnaya Énergiya, Vol. 55, No. 6, pp. 410-412, December, 1983.
Original article submitted May 25, 1983.

 0038-531X/83/5506-0874$07.50

$$D_n \geqslant D_{\min}; \tag{3}$$

$$l_n \geqslant l_{\min}. \tag{4}$$

Moreover, these parameters are related by the formula

$$l_n(N) \leqslant \frac{1}{6} D_n, \tag{5}$$

which reflects the condition that the packing elements must be close against the column walls.

In the second design variant the pressure drops arising in each column of the cascade are added together. In this case, when rectification takes place along the cascade, there is an increase in the temperature of the process, and, as a rule, the separation coefficient decreases. The variation of H and ε along the length of the installation makes it impossible to use the concept of ideal cascade, so that the only possible method consists in the direct determination of the optimum volume of a real cascade within the framework of the general problem of optimization. Then the cost function can be written as follows:

$$C_0 = \frac{t_r}{Pt_a(t_r - t_p)}\left(V_p \sum_i a_{\text{capvi}} + L_1 \sum_i a_{\text{capLi}} + n \sum_i a_{\text{capmi}} + F \sum_i a_{Fi}\right) + \frac{t_r}{P(t_p - t_p)} \times$$

$$\times \left(L_1 \sum_i a_{\text{Op Li}} + F \sum_i a_{\text{Op Fi}} + a_{\text{Wg}} + a_{\text{s.e}}\right), \tag{6}$$

where

$$F = P\frac{c_P - c_W}{c_F - c_W}. \tag{7}$$

The cost function directly involves such optimization parameters as the flow L_1 in the first section and the tailings concentration c_W. The other parameters (the number N of packing elements per unit volume, the relative load γ, the flows L_n in the subsequent sections, the number n of such sections, and also the temperature and pressure of the process) are used in calculating the values of V_{plant} and t_p, which occur in the cost formula.

The values of Q*, Re_g, r_o, q_{cap}, q_{ts}, Γ, m, h, and H are determined from the formula given in [1], S_n and S_W from the formulas of [2], and λ and t_p by the methods described in [3] and [4], respectively. According to [5], the pressure drop per unit column length is equal to

$$\Psi_z = \frac{V_{o.g}^2 a_{\text{cap}} \rho_g \chi_c}{8(F_{\text{fr}} - \varphi_{\text{st}} - \varphi_d - \varphi_p)^3 (4V_{o.g}\rho_g/\mu_g a_{\text{cap}})^n}, \tag{8}$$

where $V_{o.g}$ for the case of rectification is given by the formula

$$V_{o.g} = \frac{\gamma Q_l^* \rho_l RT(p)}{60Mp}; \tag{9}$$

$$\rho_g = Mp/RT(p). \tag{10}$$

In laminar flow (when $\text{Re}_{d\ op} \leqslant 120$) $\chi_{sl} = 130$; $n_{lam} = 0.64$; in turbulent flow $\chi_{st} = 28$ and $n_{turb} = 0.33$. The value of T(p) is given by an empirical formula for the saturated vapor pressure of the working substance as a function of the temperature, the density of the volumetric flow of liquid is expressed in ml/(cm²·min), and R is the gas constant. The variation of the pressure as a function of the column length can be determined from the equation

$$p(z) = p_{\text{up}} + \Psi_z(p, T)z, \tag{11}$$

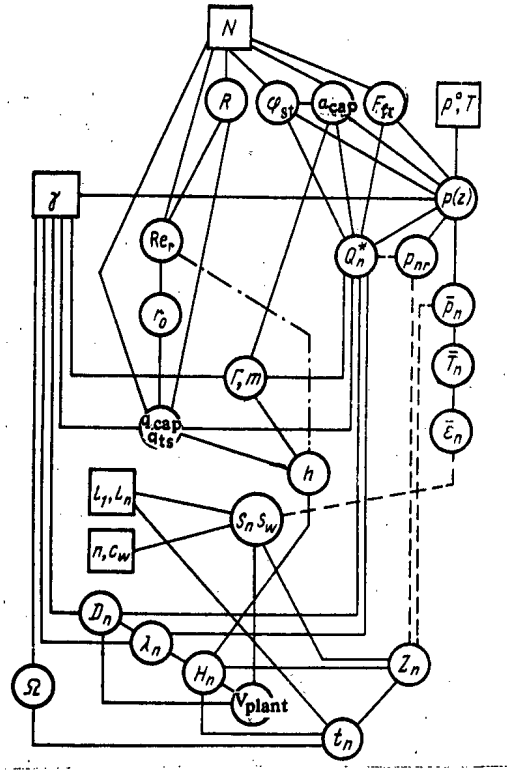

Fig. 1. Scheme for the calculation of the parameters of the cost function for a pilot-plant scale of isotope production.

where p_{up} is the pressure in the upper part of the cascade and z is the vertical coordinate measured from its top. For the other parameters the following relations obviously hold:

$$D_n = (4L_n/\pi\gamma Q_1^*)^{1/2}; \tag{12}$$

$$Z_n = S_n H_n; \tag{13}$$

$$V_{plant} = \frac{\pi}{4}\left(\sum_n D_n^2 S_n H_n + D_1^2 H_1 S_W\right). \tag{14}$$

The order of calculation of the parameters occurring in the cost function, and also of the optimal characteristics of the design and the technological regime, are shown in Fig. 1, where the circles indicate the parameters that can be determined during the calculation process, the rectangles indicate the parameters of optimization, and the dashed lines indicate the connections which take account of the variation in the enrichment coefficient, as well as the limiting transmissivity of each section because of the summation of the pressure drops along the cascade. It should be noted that the latter quantity can be estimated fairly accurately, since it is determined by the pressure and temperature at the upper cross section of the section (where the pressure is minimal); at the same time, the value of the pressure on the value of ε can be taken into account only approximately by using the average values $\bar{p}_n$ and $\bar{T}_n$ in each section.

As a first approximation, the pressure and temperature in the entire cascade are considered constant and equal to the values p° and T° which prevail at all times at the head of the cascade and are optimization parameters. The section length Z_n calculated with this approximation, using formula (9), enables us to determine the average values of the pressure and temperature in each section. At the same time, we can determine the pressure at the head of the sections that is necessary for finding more precisely the value of Q_n^* and the whole set of physical parameters corresponding to the average values $\bar{p}_n$ and $\bar{T}_n$. Taking account of the aforementioned parameters, as well as of the average values of the enrichment coefficients, $\bar{\varepsilon}_n$, we continue the calculation in the second approximation, as a result of which we determine the values of V_{plant} and t_n occurring in the cost function.

TABLE 1. Optimal Parameters of Separating Installations for Producing ^{13}C by the Method of Rectification of CO

Productivity of the installation and design features	Diam. of columns, mm	Characteristic dimension of packing element, mm	No. of enrichment sections	No. of parallel columns in the sections	Length of sections, m	Flow in first section, g CO/min	Rel. load	Height of stage (HETP)	Concn. of ^{13}C in tailings, %
3 kg carbon per year with ^{13}C in tailings, %	26 26	2,4	3	8 1	20,8±14,2 16,2	146	0,9	3,1	0,40
No limit on height of installation	14			1	18,5				
Same, but with limitation on height: $Z \leqslant 50$	40 40 20	2,4	3	8 1 1	14,3+9,6 13,6 12,5	152	0,4	2,3	0,43

It should be noted that in practice we may encounter a variety of the second design variant which consists in constructing the initial sections in the form of a parallel set of columns of equal diameter without individual phase-conversion devices at the joints between the sections [6]. As was shown in [7], in the parallel combination it is necessary in practice to have the exact distribution of the total reflux flow between the columns. This can easily be attained at the head of the cascade by using a special condenser design (in which the condenser sections are the continuation of each of the columns), but serious difficulties are encountered as soon as we reach the joint between the first and second sections. Therefore in the second section it is advisable to use a single column (whose diameter is small in installations of pilot-plant size) and to choose a diameter for the columns of the parallel set of the first and stripping sections that is equal to the diameter of the column in the second section, so as to maintain uniformity. Constructing the stripping section and the first section in the form of a parallel set of columns does not lead in this case to a change either in the form of the cost function or in the scheme for calculating its parameters; we need only only introduce the additional condition $D_W = D_1 = D_2$.

The proposed method was illustrated by using the example of an installation for producing 3 kg/yr of carbon with a ^{13}C concentration of 95%, constructed in the form of the second modified design variant. The optimal parameters of the installation, shown in Table 1, make it clear that the introduction of a limitation on the height led to a reduction in the relative load, thanks to which the value of an HETP was reduced by a factor of 1.35 even though the diameter of the columns was increased. The second method of reducing the length of the installation, which involves a reduction in the number of stages at the cost of an increase in the circulation flow, was found to be inefficient because of the large amount added to the cost by the expenditure for the cooling agent.

In the process of optimization the temperature in the upper part of the installation was varied between 72 and 84°K, which corresponded to condenser pressure values of $4.0 \cdot 10^4$ to $1.3 \cdot 10^5$ Pa. Taking account of the pressure drop in the columns, the range of variation of the enrichment coefficient was 0.006-0.009. In this temperature range we found a shallow minimum of the cost function at T = 77°K and p = $6.3 \cdot 10^4$ Pa.

LITERATURE CITED

1. V. A. Kaminskii et al., At. Energ., 53, No. 3, 174 (1982).
2. K. Cohen, The Theory of Isotope Separation as Applied to the Large-Scale Production of ^{235}U, McGraw-Hill, New York (1951).
3. V. A. Kaminskii et al., Teor. Osn. Khim. Tekhnol., 11, No. 6, 872 (1977).
4. N. I. Laguntsov, E. V. Levin, and G. A. Sulaberidze, Inzh.-Fiz. Zh., 21, No. 3, 506 (1976).
5. V. A. Kaminskii and N. A. Giorgadze, Kernenergie, 14, No. 6, 194 (1971).
6. P. Ya. Asatiani, "Investigation and apparatus-technological development of processes of separation of isotopes of carbon, nitrogen, and oxygen by the method of low-temperature rectification," Candidate's Dissertation, D. I. Mendeleev Chemical Technology Institute, Moscow (1981).
7. N. A. Giorgadze, G. L. Partsakhashvili, and V. A. Kaminskii, Izv. Akad. Nauk GSSR, Ser. Khim., 4, No. 2, 155 (1978).

ANGULAR DISTRIBUTIONS OF FLUXES OF CHARGED PARTICLES FROM A THICK TARGET BOMBARDED WITH BEAMS OF PROTONS, α PARTICLES, AND ^{12}C NUCLEI WITH ENERGIES OF 3.65 GeV/NUCLEON

V. E. Aleinikov and G. N. Timoshenko

UDC 539.17.015

We report on a study of the angular distributions of fluxes of charged particles emerging from a thick target bombarded with relativistic nuclei. The measurements were performed in the course of several sessions on beams of protons, alpha particles, and ^{12}C nuclei with energies of 3.65 GeV/nucleon from the slow extraction channel of the JINR High Energy Laboratory synchrophasotron. The target was a copper cylinder 100 mm in diameter and 130 mm thick along the beam placed at the beam focus. The beam was monitored with a sensitive ionization chamber (MC) placed in the beam at the ion pipe exit, and in certain sessions also by counter telescopes S_{M_1} and S_{M_2} directed toward the target at an angle of 90° with the direction of the beam (Fig. 1). The thickness of the chamber along the beam was 5.1×10^{-2} g/cm^2. The MC was calibrated in relativistic ^{12}C nuclei and α particle beams by a counting method using a fast counter telescope mounted in the beam behind the MC with a lowered intensity of the extracted beam and in the absence of the target. Activation detectors were used to calibrate the MC in beams of α particles and protons with an intensity of more than 10^5 particles/cycle to test the linearity of the chamber readings over a wide range of beam intensities. The error of the measurements of the flux of nuclei incident on the target was less than 5% for ^{12}C, ~7% for protons, and less than 10% for α particles resulted from the fact that the MC and counter telescope readings in the beam of α particles were normalized by using activation detectors; the counter telescope was not used in the proton beam, and the chamber was calibrated with activation detectors only. Thus, the accuracy of the MC calibration for protons and α particles was determined mainly by the accuracy of the measurement of the activity of the activation detectors.

The yields of secondary charged particles from the target for the angular range 10-105° relative to the direction of the beam were measured with three counter telescopes S_1, S_2, and S_3 with an angular resolution of 0.6°. The energy thresholds of the counter telescopes for secondary p, π, d, t, and α were 42, 18, 57, 68, and 168 MeV, respectively. The results of the measurements, normalized to one particle incident on the target, are shown in Fig. 2. The angular distributions are well approximated by the following exponential relations in the angular range 25-105° obtained from the experimental data by the method of least squares (θ is in degrees):

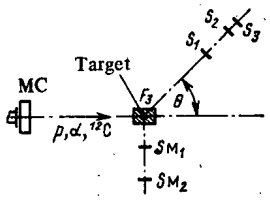

Fig. 1. Geometry of the experiment; MC) beam monitor chamber; S_{M_1}, S_{M_2} and S_1, S_2, S_3) monitor and counter telescopes, respectively.

Translated from Atomnaya Énergiya, Vol. 55, No. 6, pp. 412-414, December, 1983. Original article submitted June 9, 1983.

 0038-531X/83/5506-0878$07.50

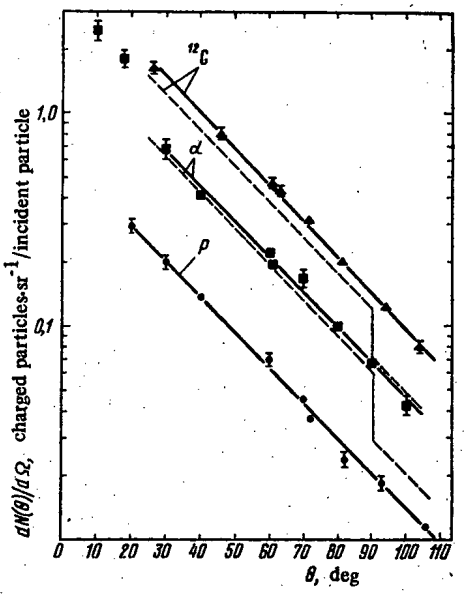

Fig. 2. Angular distributions of fluxes of charged particles from a target bombarded with with ^{12}C nuclei, α particles, and protons: ——) experiment; – – –) calculated with the equivalent proton model for the angular ranges 0–π/2 and π/2–π.

$$dN_C(\theta)/d\Omega = 5.32 \exp(-4.0 \cdot 10^{-2}\theta);$$
$$dN_\alpha(\theta)/d\Omega = 2.08 \exp(-3.8 \cdot 10^{-2}\theta); \quad (1)$$
$$dN_p(\theta)/d\Omega = 0.65 \exp(-3.9 \cdot 10^{-2}\theta).$$

The results of the present work was used to estimate the degree of correctness of the basic assumption of the equivalent proton method discussed in [1] where a simple approach was proposed for determining the characteristics of the secondary radiation fields from targets bombarded with relativistic nuclei in the energy range 100 MeV-10 GeV. The estimate of the radiation environment near the targets includes the contribution from structural elements of the accelerator which are bombarded with nuclei in the acceleration process. By a thick target we mean a target in which an internuclear cascade begins to play an important role in the formation of the secondary radiation field from it. The method of [1] was assumed to apply in making a sufficiently accurate expeditious estimate of certain dosimetric parameters of the radiation fields both near the target and beyond the shield of the heavy ion accelerator. The essence of the method of equivalent protons [1] reduces to the following. It is assumed that the characteristics of the distribution of secondary hadrons K_i emerging from a given target when bombarded with nuclei of energy E per nucleon of the nucleus are related to the analogous characteristics of the distribution of secondary hadrons K_p from the same target when bombarded with protons of the same energy E by the simple relation

$$K_i = N_{ip} K_p, \quad (2)$$

where N_{ip} is a proportionality factor which depends on the target material and the type of bombarding ion. The proportionality factors for comparing the angular distributions of fluxes of charged particles were calculated with the following formulas [1]:

$$N_{ip}=\begin{cases} 0{,}51A_i^{1/2}\,(1+0{,}29\ln A_{Cu})\times \\ \times[1-\exp(-\sigma_{in}^{i}nd)]/[1-\exp(-\sigma_{in}^{p}nd)] \\ \theta=0-\pi/2; \\ 0{,}09A_i^{1/2}\,(1+1{,}2\ln A_{Cu})\times \\ \times[1-\exp(-\sigma_{in}^{i}nd)]/[1-\exp(-\sigma_{in}^{p}nd)] \\ \theta=\pi/2-\pi. \end{cases} \qquad (3)$$

Here A_i and A_{Cu} are the atomic masses of the projectile and target nuclei, n is the number of nuclei per cm^3 of the target, d is the thickness of the target along the beam, σ_{in}^{i} and σ_{in}^{p} are the cross sections for the inelastic interaction of the projectile nucleus and a proton with the target material; σ_{in}^{i} was calculated with the formula in [2], and σ_{in}^{p} was taken equal to 0.72×10^{-24} cm^2. The values of N_{ip} obtained with the above formulas are 6.0, 3.58 and 3.1, 1.5 for ^{12}C nuclei and α particles in the angular ranges 0-π/2 and π/2-π, respectively.

The dashed curves in Fig. 2 show the calculated angular distributions in the angular ranges 25-90° and 90-105° obtained with the model of equivalent protons. The very small differences in the exponents of the exponentials approximating the experimental data (1) show that the assumption of similar shapes of the angular distributions from protons, α particles, and ^{12}C nuclei is quite correct. The ratio of the yields of charged particles in the angular range 25-90° for the measured angular distributions from ^{12}C nuclei and α particles to the analogous yield from protons is 7.69 and 3.32, respectively, which indicates satisfactory agreement of the proposed model with the experimental data. The model described did not take account of the yield of charged particles from the interaction of fragments of the projectile nucleus with the target; taking account of this factor clearly leads to better agreement of the calculated and experimental data. It should be noted that since the adsorbed and equivalent doses in a radiation field are determined not only by the flux of particles, but also by their energy, it is very important in estimating the applicability of the method of equivalent protons to have confirmation of the adequacy of the calculated and experimental spectral and angular distributions of secondary hadrons from a target bombarded with different ions.

The authors thank M. M. Komochkov for helpful discussions, and V. P. Bamblevskii for supplying data on the activation detectors.

LITERATURE CITED

1. M. M. Komochkov, Preprint JINR R16-82-432, Dubna (1982).
2. V. S. Stavinskii, Preprint JINR 2-80-66, Dubna (1980).

EXPERIMENTAL AND COMPUTATION–THEORETICAL STUDIES OF THE DEVELOPMENT OF THE NEUTRON SPECTRUM IN SUBCRITICAL ASSEMBLIES WITH HETEROGENEOUS REACTOR-ENRICHED FUEL

A. V. Bushuev, S. A. Bychkov, V. M. Duvanov,
A. Yu. Davydov, and V. I. Naumov

UDC 621.039.519.24

Experimental data which correspond to an asymptotic neutron spectrum in a particular fertile medium are used to check computational methods and the basis of the neutron-physical reactor parameters in trial and design calculations. Part of the required information can be obtained from experiments made on small subcritical assemblies with a sufficiently powerful external neutron source. It is then necessary to prove that a region with an asymptotic spectrum is present in the subcritical assembly. This implies special experimental and computational studies.

The development of the asymptotic neutron spectrum can be influenced by various factors: size of the assembly, its structure, position of the external neutron source and its spectrum, etc. The experience gathered in experiments on various types of assemblies is therefore of particular interest. The authors of [1], have compiled data on the asymptotic spectrum in heterogeneous uranium–graphite assemblies. We describe in the present paper experimental and computational studies of the development of the spectrum in small assemblies filled with spherical heterogeneous reactor-enriched fuel (HREF).

The theoretical analysis of the neutron spectra of such assemblies is difficult for two reasons: The fuel elements are porous, depending upon their packing; and the shape of the boundaries of the fuel elements is complicated. Since an adequate mathematical model for a quantitative analysis of the neutron distribution in space and over the energy in small HREF assemblies does not exist, the corresponding information had to be obtained in experiments. On the other hand, computational studies making use of an idealized homogeneous model made it possible to observe certain qualitative laws in the development of the neutron spectrum.

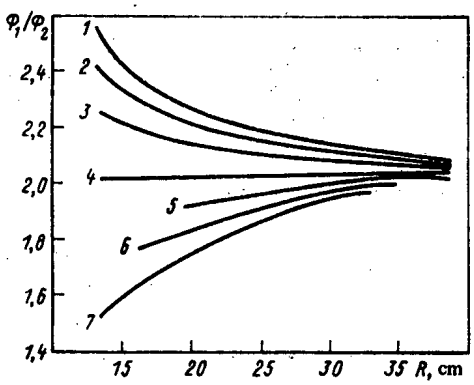

Fig. 1. Dependence of the hardness of the neutron spectrum upon the radius of the assembly: 1) without reflector; 2) with 4-cm thick lead reflector, and with graphite reflector of thickness: 3) 2 cm; 4) 4 cm; 5) 6 cm; 6) 8 cm; and 7) 10 cm.

Translated from Atomnaya Énergiya, Vol. 55, No. 6, pp. 414-415, December, 1983. Original article submitted June 2, 1983.

0038-531X/83/5506-0881$07.50

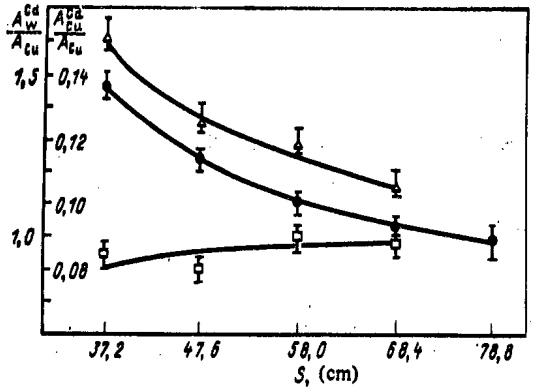

Fig. 2. Dependence of the ratio of the reaction rates upon the cross section of the assembly (S denotes the size under the wrench): Δ and ●) A_{Cu}^{Cd}/A_{Cu} and A_{W}^{Cd}/A_{Cu}, respectively (in assemblies without reflector); □) A_{W}^{Cd}/A_{Cu} (in assemblies with a graphite reflector.

The computational–theoretical analysis of the neutron distributions in space and over the energy was made under the assumption that in a sufficiently high cylindrical subcritical assembly, which is located far from the neutron source, an exponential distribution develops and that the Fick law is valid for the neutron flux in the axial direction. Under this assumption, the neutron-transfer equation in the subcritical assembly can be reduced to its one-dimensional form. The equation was solved in the two-group approximation by the collision method which avoided the main assumption of the material-parameter theory, namely that a unique extrapolation limit exists for neutrons of different energies.

The ratio $\gamma = \Phi_1/\Phi_2$ of the fluxes of moderated neutrons and thermal neutrons at the center of the assembly was calculated in dependence upon the radius of the assembly. The calculations were made for an assembly without reflector as well as for assemblies with reflectors of various compositions and thicknesses. Figure 1 illustrates the results of the calculations. It follows from the data displayed that the Φ_1/Φ_2 ratio, which is usually termed the hardness of the spectrum, decreases with increasing radius in an assembly without reflector and approaches an asymptotic value. When a reflector is introduced, the form of the Φ_1/Φ_2 dependence upon the radius of the assembly changes: The hardness of the spectrum increases with increasing radius and approaches an asymptotic value; when a reflector is introduced, the change in the sign of $\gamma - \gamma_{as}$ allows an experimental evaluation of the degree to which the neutron spectrum resembles the asymptotic spectrum; by optimizing both the thickness and the composition of the reflector, the asymptotic spectrum can be attained more rapidly.

Experiments were made on assemblies which consisted of 2-m-high hexahedral prisms filled with spherical VGR-50 fuel elements [2]. The size under the wrench was varied between 37.2 and 78.8 cm. Owing to their special arrangement, the spherical fuel elements formed two types of lattices with a porosity of 0.26 and 0.4, respectively; the effective thickness of the graphite reflector used in several of the experiments was 22 cm.

The assemblies were mounted under the vertical neutron beam which with a cross section of 300 × 300 mm is emitted from the F-1 reactor core of the I. V. Kurchatov Institute of Atomic Energy. The ratio of the capture rates of supercadmium neutrons in tungsten (resonance energy 18.7 eV) and in copper to the total neutron capture in copper, A_{W}^{Cd}/A_{Cu} and A_{Cu}^{Cd}/A_{Cu}, was selected as the characteristic quantity of the neutron spectrum in the assemblies. The change of these ratios is an indication of the variation of the neutron spectrum in the energy range encompassing the range of HREF neutron thermalization. During the irradiation, foils were disposed along the axis of the experimental assemblies and over their radius. The activity of the foils was measured with a scintillation spectrometer; the ^{186}W γ radiation

and the annihilation radiation accompanying the β^+ decay of ^{64}Cu were recorded. Figure 2 illustrates the results of measurements of the A_W^{Cd}/A_{Cu} and A_{Cu}^{Cd}/A_{Cu} ratios observed in regions of the assemblies where the external neutron source does not affect the neutron spectrum.

The results lead to the following conclusions: The minimum cross section which in an assembly with spherical fuel elements provides an asymptotic neutron spectrum has been experimentally determined; for developing the asymptotic spectrum, the size under the wrench must amount to at least 1.3 neutron path lengths in the system in the case of a hexahedron; when a graphite reflector is inserted, the size under the wrench can be reduced to about one neutron path length; when the porosity of the assembly is increased, its transverse dimensions must be accordingly increased to obtain the asymptotic spectrum; and the results of the experiments are in sufficiently good agreement with the computational results and can be used for improving computational models of the neutron transfer in such media.

The authors thank in conclusion V. V. Khromov, V. I. Savander, N. I. Belousov, A. N. Protsenko, E. S. Glushkov, V. G. Kosovskii, V. F. Tsibul'skii, Yu. V. Silaev, A. E. Savost'yanov, and V. V. Khmyzov for useful discussions and help in the experiments.

LITERATURE CITED

1. L. N. Yurova et al., At. Energ., 40, No. 5, 384 (1976).
2. N. N. Ponomarev-Stepnoi et al., Problems of Atomic Science and Technology, Series "Atomic-Hydrogen Power Generation and Technology" [in Russian], No. 1 (4), 40 (1978).

Declassified and Approved For Release 2013/02/21 : CIA-RDP10-02196R000300030004-5

INDEX

SOVIET ATOMIC ENERGY

Volumes 54-55, 1983

SOVIET ATOMIC ENERGY
Volumes 54-55, 1983

(A translation of Atomnaya Énergiya)

F

G

H

I

K

L

M

N

O

P

R

S

T

U

V

Y

Z

TABLES OF CONTENTS

SOVIET ATOMIC ENERGY

Volumes 54-55, 1983

(A translation of Atomnaya Énergiya)

Volume 54, Number 1 January, 1983

Volume 54, Number 2 February, 1983

Volume 54, Number 3 March, 1983

ARTICLES

Volume 54, Number 4 April, 1983

Volume 54, Number 6 June, 1983

ARTICLES

LETTERS TO THE EDITOR

Volume 55, Number 1 July, 1983

Volume 55, Number 2 August, 1983

Volume 55, Number 3 September, 1983

Volume 55, Number 4 October, 1983

Volume 55, Number 5 November, 1983

Engl./Russ.

Volume 55, Number 6 December, 1983

How To Comply With The New Copyright Law

Participation in the Copyright Clearance Center (CCC) assures you of legal photocopying at the moment of need.

Libraries everywhere have found the easy way to fill photocopy requests legally and instantly, without the need to seek permissions, from more than 3000 key publications in business, science, humanities, and social science. You can:

Fill requests for multiple copies, interlibrary loan (beyond the CONTU guidelines), and reserve desk without fear of copyright infringement.

Supply copies from CCC-registered publications simply and easily.

The Copyright Clearance Center is your one-stop place for on-the-spot clearance to photocopy for internal use.

Its flexible reporting system accepts photocopying reports and returns an itemized invoice. You send only one convenient payment. CCC distributes it to the many publishers whose works you need.

And, you need not keep any records, the CCC computer will do it for you. Register now with the CCC and you will never again have to decline a photocopy request or wonder about compliance with the law for any publication participating in the CCC.

To register or for more information, just contact:

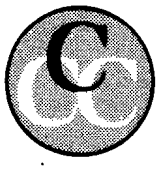

Copyright Clearance Center
21 Congress Street
Salem, Massachusetts 01970
(617) 744-3350

a not-for-profit corporation

NAME _____ TITLE _____

ORGANIZATION _____

ADDRESS _____

CITY _____ STATE _____ ZIP _____

COUNTRY _____ TELEPHONE _____

CHANGING YOUR ADDRESS?

In order to receive your journal without interruption, please complete this change of address notice and forward to the Publisher, 60 days in advance, if possible.

(Please Print)

Old Address:

name

address

city

state (or country) zip code

New Address

name

address

city

state (or country) zip code

date new address effective

name of journal

THE LANGUAGE OF SCIENCE
Plenum
PUBLISHING CORPORATION

233 Spring Street, New York, New York 10013

MEASUREMENT TECHNIQUES
Izmeritel'naya Tekhnika
Vol. 27, 1984 (12 issues) $520

MECHANICS OF COMPOSITE MATERIALS
Mekhanika Kompozitnykh Materialov
Vol. 20, 1984 (6 issues) $430

METAL SCIENCE AND HEAT TREATMENT
Metallovedenie i Termicheskaya Obrabotka Metallov
Vol. 26, 1984 (12 issues) $540

METALLURGIST
Metallurg
Vol. 28, 1984 (12 issues) $555

PROBLEMS OF INFORMATION TRANSMISSION
Problemy Peredachi Informatsii
Vol. 20, 1984 (4 issues) $420

PROGRAMMING AND COMPUTER SOFTWARE
Programmirovanie
Vol. 10, 1984 (6 issues) $175

PROTECTION OF METALS
Zashchita Metallov
Vol. 20, 1984 (6 issues) $480

RADIOPHYSICS AND QUANTUM ELECTRONICS
Izvestiya Vysshikh Uchebnykh Zavedenii, Radiofizika
Vol. 27, 1984 (12 issues) $520

REFRACTORIES
Ogneupory
Vol. 25, 1984 (12 issues) $480

SIBERIAN MATHEMATICAL JOURNAL
Sibirskii Matematicheskii Zhurnal
Vol. 25, 1984 (6 issues) $625

SOIL MECHANICS AND FOUNDATION ENGINEERING
Osnovaniya, Fundamenty i Mekhanika Gruntov
Vol. 21, 1984 (6 issues) $500

SOLAR SYSTEM RESEARCH
Astronomicheskii Vestnik
Vol. 18, 1984 (6 issues) $365

SOVIET APPLIED MECHANICS
Prikladnaya Mekhanika
Vol. 20, 1984 (12 issues) $520

SOVIET ATOMIC ENERGY
Atomnaya Énergiya
Vols. 56-57, 1984 (12 issues) $560

SOVIET JOURNAL OF GLASS PHYSICS AND CHEMISTRY
Fizika i Khimiya Stekla
Vol. 10, 1984 (6 issues) $235

SOVIET JOURNAL OF NONDESTRUCTIVE TESTING
Defektoskopiya
Vol. 20, 1984 (12 issues) $615

SOVIET MATERIALS SCIENCE
Fiziko-khimicheskaya Mekhanika Materialov
Vol. 20, 1984 (6 issues) $445

SOVIET MICROELECTRONICS
Mikroélektronika
Vol. 13, 1984 (6 issues) $255

SOVIET MINING SCIENCE
Fiziko-tekhnicheskie Problemy Razrabotki Poleznykh Iskopaemykh
Vol. 20, 1984 (6 issues) $540

SOVIET PHYSICS JOURNAL
Izvestiya Vysshikh Uchebnykh Zavedenii, Fizika
Vol. 27, 1984 (12 issues) $520

SOVIET POWDER METALLURGY AND METAL CERAMICS
Poroshkovaya Metallurgiya
Vol. 23, 1984 (12 issues) $555

STRENGTH OF MATERIALS
Problemy Prochnosti
Vol. 16, 1984 (12 issues) $625

THEORETICAL AND MATHEMATICAL PHYSICS
Teoreticheskaya i Matematicheskaya Fizika
Vol. 58-61, 1984 (12 issues) $500

UKRAINIAN MATHEMATICAL JOURNAL
Ukrainskii Matematicheskii Zhurnal
Vol. 36, 1984 (6 issues) $500

Send for Your Free Examination Copy

Plenum Publishing Corporation, 233 Spring St., New York, N.Y. 10013
In United Kingdom: 88/90 Middlesex St., London E1 7EZ, England
Prices slightly higher outside the U.S. Prices subject to change without notice.

RUSS[redacted] THE PHYSICAL A[redacted]L SCIENCES

PEEL HERE

AVAILABLE IN ENGLISH TRANSLATION

ALGEBRA AND LOGIC
Algebra i Logika
Vol. 23, 1984 (6 issues) $360

ASTROPHYSICS
Astrofizika
Vol. 20, 1984 (4 issues) $420

AUTOMATION AND REMOTE CONTROL
Avtomatika i Telemekhanika
Vol. 45, 1984 (24 issues) $625

COMBUSTION, EXPLOSION, AND SHOCK WAVES
Fizika Goreniya i Vzryva
Vol. 20, 1984 (6 issues) $445

COSMIC RESEARCH
Kosmicheskie Issledovaniya
Vol. 22, 1984 (6 issues) $545

CYBERNETICS
Kibernetika
Vol. 20, 1984 (6 issues) $445

DIFFERENTIAL EQUATIONS
Differentsial'nye Uravneniya
Vol. 20, 1984 (12 issues) $505

DOKLADY BIOPHYSICS
Doklady Akademii Nauk SSSR
Vols. 274-279, 1984 (2 issues) $145

FLUID DYNAMICS
Izvestiya Akademii Nauk SSSR, Mekhanika Zhidkosti i Gaza
Vol. 19, 1984 (6 issues) $500

FUNCTIONAL ANALYSIS AND ITS APPLICATIONS
Funktsional'nyi Analiz i Ego Prilozheniya
Vol. 18, 1984 (4 issues) $410

GLASS AND CERAMICS
Steklo i Keramika
Vol. 41, 1984 (6 issues) $590

HIGH TEMPERATURE
Teplofizika Vysokikh Temperatur
Vol. 22, 1984 (6 issues) $520

HYDROTECHNICAL CONSTRUCTION
Gidrotekhnicheskoe Stroitel'stvo
Vol. 18, 1984 (12 issues) $385

INDUSTRIAL LABORATORY
Zavodskaya Laboratoriya
Vol. 50, 1984 (12 issues) $520

INSTRUMENTS AND EXPERIMENTAL TECHNIQUES
Pribory i Tekhnika Eksperimenta
Vol. 27, 1984 (12 issues) $590

JOURNAL OF APPLIED MECHANICS AND TECHNICAL PHYSICS
Zhurnal Prikladnoi Mekhaniki i Tekhnicheskoi Fiziki
Vol. 25, 1984 (6 issues) $540

JOURNAL OF APPLIED SPECTROSCOPY
Zhurnal Prikladnoi Spektroskopii
Vols. 40-41, 1984 (12 issues) $540

JOURNAL OF ENGINEERING PHYSICS
Inzhenerno-fizicheskii Zhurnal
Vols. 46-47, 1984 (12 issues) $540

JOURNAL OF SOVIET LASER RESEARCH
A translation of articles based on the best Soviet research in the field of lasers
Vol. 5, 1984 (6 issues) $180

JOURNAL OF SOVIET MATHEMATICS
A translation of Itogi Nauki i Tekhniki and *Zapiski Nauchnykh Seminarov Leningradskogo Otdeleniya Matematicheskogo Instituta im. V. A. Steklova AN SSSR*
Vols. 24-27, 1984 (24 issues) $1035

LITHOLOGY AND MINERAL RESOURCES
Litologiya i Poleznye Iskopaemye
Vol. 19, 1984 (6 issues) $540

LITHUANIAN MATHEMATICAL JOURNAL
Litovskii Matematicheskii Sbornik
Vol. 24, 1984 (4 issues) $255

MAGNETOHYDRODYNAMICS
Magnitnaya Gidrodinamika
Vol. 20, 1984 (4 issues) $415

MATHEMATICAL NOTES
Matematicheskie Zametki
Vols. 35-36, 1984 (12 issues) $520

continued on inside back cover